The multipole method for the on-the-fly computation of the temperature dependency of nuclear cross-sections

Thomas Freiman

Thèse de doctorat

NNT : 2020UPASS004

université PARIS-SACLAY

The multipole method for the on-the-fly computation of the temperature dependency of nuclear cross-sections.

Thèse de doctorat de l'université Paris-Saclay

École doctorale n°576 : Particules, Hadrons, Énergie, Noyau, Instrumentation, Image, Cosmos et Simulation (PHENIICS).
Spécialité de doctorat : Énergie nucléaire.
Unité de recherche : Université Paris-Saclay, CEA, Service d'étude des réacteurs et de mathématiques appliquées, 91191, Gif-sur-Yvette, France.
Référent : Faculté des Sciences.

Thèse présentée et soutenue à Saclay, le 08/01/2020, par

Thomas FREIMAN

Composition du Jury

Cheikh M'Backé DIOP Directeur de recherche, CEA Paris-Saclay	Président
Dimitri ROCHMAN Ingénieur-chercheur, Paul Scherrer Institut (Suisse)	Rapporteur & Examinateur
Cyrille DE SAINT JEAN Ingénieur-chercheur (HDR), CEA/DIF	Rapporteur & Examinateur
Luiz LEAL Ingénieur-chercheur (HDR), IRSN	Examinateur
Frédéric NATAF Professeur, Paris-Sorbonne Université	Examinateur
Olivier SEROT Ingénieur-chercheur (HDR), CEA/CAD	Examinateur
Andrea ZOIA Ingénieur-chercheur (HDR), CEA Paris-Saclay	Directeur de thèse
François-Xavier HUGOT Ingénieur-chercheur, CEA Paris-Saclay	Co-Encadrant & Examinateur
Mireille COSTE-DELCLAUX Ingénieur-chercheur, CEA Paris-Saclay	Invitée

Acknowledgements

Voici venu le moment d'affronter le périlleux exercice des remerciements : si les listes exhaustives ne se prêtent pas au jeu de l'oral, il me semble que les oublis n'en sont que plus remarquables à l'écrit !

Je remercie tout d'abord Dimitri Rochman et Cyrille de Saint Jean d'avoir accepté le rôle de rapporteur de ma thèse et de l'intérêt qu'ils ont porté à mes travaux. Je remercie aussi Luiz Leal, Frédéric Nataf et Olivier Serot d'avoir participé au jury de soutenance en tant qu'examinateurs. Enfin je remercie chaleureusement Cheikh M'Backé Diop d'avoir assumé le rôle de président de jury.

Sur un plan personnel je tiens à remercier ma mère et mon père pour leur présence lors de ma soutenance mais aussi et surtout pour leur soutien tout au long de mes études. Je remercie encore une fois mon frère Mathieu qui est mon premier confident et a toujours été présent pour moi.

Je suis heureux du groupe de jeunes que nous avons formé et qui a rendu nos déjeuners et - nombreuses - pauses très agréables. Je me dois bien sûr de citer nommément deux condisciples, Laura et Margaux, avec qui j'ai pu vivre toutes les joies et les peines des études de doctorat. Je suis ému d'avoir pu partager cette expérience avec elles. Évidemment je me dois aussi de parler de Wesley, mon cher co-bureau, dont les progrès en français ont été inversement proportionnels aux progrès en anglais du reste des thésards (un peu par ma faute il faut bien le dire). Sur un ton plus sérieux, je suis honoré d'avoir pu partager ces trois années en sa compagnie. Si je devais me risquer à une prédiction d'un optimisme qui ne me ressemble pas, je dirais même que nous avons bâti ensemble les fondations d'une très grande amitié !

Je remercie toutes les personnes que j'ai croisées au SERMA et qui en ont fait un lieu de travail accueillant et chaleureux. Je tiens à remercier Émeric Brun pour le temps qu'il m'a consacré sur des questions de mise en oeuvre informatique même si je n'ai finalement pas poursuivi ces aspects là. Je remercie aussi Claude Mounier pour son temps concernant certains détails de la méthode sigma-1. Je remercie Davide Mancusi pour ses excellentes suggestions de cauchemars sur l'utilisation du C++. Je remercie Fausto Malvagi, mon chef de laboratoire, pour ses conseils et suggestions tout au long de la thèse. Enfin je remercie Cédric Jouanne pour son aide concernant le traitement des données nucléaires.

Je remercie Andrea Zoia, mon directeur de thèse, pour sa disponibilité sans faille malgré un emploi du temps souvent chargé. Merci du temps passé à corriger un manuscrit parfois

dur à lire. L'étendue de ses connaissances suscite chez moi une admiration sans réserve mais c'est son exigence soutenue qui m'a toujours le plus impressionné.

Je remercie François-Xavier Hugot, mon encadrant, pour avoir proposé le sujet de stage qui m'a fait découvrir le SERMA et ce qui allait devenir ma future thèse. Merci d'être venu me chercher et d'avoir cru au projet le premier. Merci aussi d'avoir été disponible pour des discussions scientifiques plus générales et les nombreux livres conseillés.

Enfin, je tiens à remercier du fond du coeur Mireille Coste-Delclaux dont l'aide immense m'a permis d'achever mes travaux et ce manuscrit. Il y a des formules et compliments que l'on se doit de réserver pour des rencontres particulières. Je me permets naturellement de les utiliser ici, tant sa générosité et sa gentillesse m'ont touché durant ces derniers mois de thèse. Je n'ai peut-être que le regret de ne pas avoir pu travailler davantage en sa compagnie. J'espère sincèrement avoir été à la hauteur de son investissement et avoir su lui montrer à quel point sa présence avait compté pour moi.

Contents

Chapter 1

Introduction

Numerical simulations play a major role in the design and use of complex industrial systems. Nuclear reactors are no exception, as design choices are important for both safety concerns and optimization. There are several disciplines involved in their analysis, encompassing mechanics, thermal-hydraulics and neutronics [1]. The Commissariat à l'Énergie Atomique et aux Énergies Alternatives (CEA) takes interest in all the research and development aspects of these physics. Specifically, the Service d'Études des Réacteurs et de Mathématiques Appliquées (SERMA), where this PhD work has been done, is devoted to the development of codes to simulate the transport of neutrons in reactor cores.

Neutrons are the main vector of the fission chain reaction, that is the source of energy in the aptly named fission nuclear reactors. The knowledge of the population of neutrons is thus of primary importance in the study of reactor designs. The equation that governs the transport of these neutrons is the Boltzmann transport equation. A simplified stationary form of this balance equation reads :

$$\left(\hat{\mathbf{\Omega}} \cdot \boldsymbol{\nabla} + \Sigma_t(\boldsymbol{r}, E)\right) \psi(\boldsymbol{r}, E, \hat{\mathbf{\Omega}}) = \int_{4\pi} d\hat{\mathbf{\Omega}}' \int_0^\infty dE'\, \Sigma_s(\mathbf{r}, E' \to E, \hat{\mathbf{\Omega}}' \to \hat{\mathbf{\Omega}}) \psi(\boldsymbol{r}, E', \hat{\mathbf{\Omega}}') + S(\boldsymbol{r}, E, \hat{\mathbf{\Omega}}). \quad (1.1)$$

The unknown function ψ denotes the angular neutron flux, characterizing the average population of neutrons in the phase space. The terms Σ_x are called macroscopic cross-sections for nuclear reactions of kind x. I will describe them shortly thereafter. The quantity S gathers general source terms, possibly depending on the flux ψ itself, as in the case of fission contributions.

There exist two main approaches to the numerical simulation of this equation. On one hand, deterministic methods, which rely on a discretization of the spatial ($\boldsymbol{r}$), angular ($\hat{\mathbf{\Omega}}$) and energy (E) variables in this equation [2]. On the other hand, stochastic methods, and specifically Monte Carlo methods, which sample the 'history' of individual neutrons to form a statistics describing the population [3]. The latter methods have found many applications in the study of different topics in physics, mathematics and finance, although they were actually first used with the precise goal of studying population of neutrons [4].

The properties of the medium through which the neutrons propagate are described by the macroscopic cross-sections noted Σ_x in equation (1.1). They characterize the probability of a generic interaction x of the neutrons with their environment. Their knowledge is of critical importance for an accurate simulation of the neutron transport. Macroscopic cross-sections are related to more fundamental physical quantities called microscopic nuclear cross-sections by

$$\Sigma_x(\boldsymbol{r}, E) = \sum_i N_i(\boldsymbol{r}) \sigma_x^{(i)}\big(E, T(\boldsymbol{r})\big). \tag{1.2}$$

The summation is on the different nuclei composing the medium. The quantities N_i are their corresponding density and $\sigma_x^{(i)}$ is the physical quantity describing the probability of the considered interaction with a single nucleus of type i. The variable T designates the temperature of the medium.

Relation (1.2) aims at separating geometrical properties, i.e. the local concentrations of nuclei, from physical properties, i.e. the interaction probabilities between neutrons and matter. This separation is not total since microscopic cross-sections still have a temperature dependency, which pertains to local property of the medium. This PhD work is focused on some aspects of the study of these cross-sections.

1.1 Cross-section study

The reactions to be taken into account in the Boltzmann equation result from short-distance nuclear interactions between neutrons and nuclei. There are various possible such interactions according to, among other factors, the energy of the incident neutron. Their study is a very active topic of research and involves many fields of physics.

From a nuclear reactor standpoint however, we take particular interest only in some reactions and energy ranges. Specifically for the latter, we are mainly concerned with neutrons with energies between 10^{-5} eV and 20 MeV. In this energy range, the prominent interactions are elastic and inelastic scattering, fission and radiative capture (emission of one or multiple photons after capture of a neutron by a nucleus). Without giving a very extensive list of all possible interactions, we can also cite more complicated ones such as the n-2n reaction (where a neutron frees a pair of neutron after a collision) or the n-alpha reaction (where an entire alpha nucleus is emitted from the nucleus).

1.1.1 R-matrix theory

In reactor physics, cross-section profiles may or may not be resonant according to the considered nucleus or the energy range. A tabulated data description of the former is much more difficult to obtain than that of a smooth profile. Hence, physicists set out to find a model to give an analytical expression of the resonant cross-sections. These would involve a set of so-called resonance parameters, to be later fitted based on experimental measurements.

For this purpose, E. Wigner and L. Eisenbud developed the R-matrix theory [5, 6], which is a subset of what is known today as quantum scattering theory. The idea stems from the fact that, at the scale of nucleons, particles have to be considered as quantum probability waves. The framework then chosen was that of the first quantization. On one hand, the nucleons composing the nucleus are all described by probability wave functions. On the other hand, their interactions are described by scalar potentials representing the nuclear and Coulombian forces. The R-matrix theory uses the short distance nature of nuclear interactions to simplify the study of the Schrödinger equation describing the evolution of the wave function of the whole system.

The R-matrix theory was further developed by A.M. Lane and R.G. Thomas in a very extensive article published in 1958 [7]. In it, they described more precisely the inclusion of interactions such as the radiative capture which require elements of quantum field theory. They also discussed the treatment of inelastic reactions in the R-matrix theory.

In parallel, D.L. Hill and J.A. Wheeler discussed and proposed a model for the fission reaction, which involves a priori rather different physical phenomena [8]. These theoretical elements are gathered in the excellent book by J.E. Lynn published in 1968 [9]. Two articles by F. Fröhner also offer an interesting overview of the R-matrix theory [10, 11].

1.1.2 Cross-section representation formalisms

The formulae for the cross-sections and the associated sets of resonance parameters involved in the full R-matrix theory do not lend themselves easily to fitting with experimental measurements. As such, further approximations of the theory were needed. The first one was proposed by G. Breit and E. Wigner [12]. The resonance peaks in the cross-sections profiles are modelled by a sum of terms that describe each resonance separately. Although quite simplistic, this model proved itself quite good as a first step for the representation of cross-sections. It lacked, however, precision for the elastic cross-section, where interference phenomena between resonances must be taken into account for more accurate results. The extended Multi-Level Breit-Wigner formalism became more widely used to tackle these issues.

Later, with the progress of computer capabilities, a new formalism was proposed by C.W. Reich and M.S. Moore [13]. Its use was motivated by the lack of accuracy of previous formalisms for the fission process and cross-sections presenting very close resonance peaks. Some of such nuclei are of paramount importance in nuclear reactor applications : U235, U238 and Pu239. Through the years, more and more nuclei cross-sections have been described with the use of this formalism, as the previous concerns about computing cost became largely irrelevant. For this same reason, a new formalism called R-matrix limited format is set to replace the use of these older formalisms in the coming years [14].

1.1.3 The multipole and other alternative cross-section representations

The choice and use of the different formalisms were initially driven by the limited computing capabilities. Consequently, physicists took interest in finding alternative mathematical forms of the complicated cross-sections formulae. These ideas stemmed from the original A.M. Lane and R.G. Thomas paper [7], which remarked some of the meromorphic properties of the elements of the R-matrix theory. This was further discussed by G. Saussure and R.B. Perez in their rationale published in 1969 [15]. Their idea was that cross-sections formulae derived from the R-matrix theory could likely be seen as rational functions of the energy.

D.B. Adler and F.T. Adler built on this idea to define a new alternative formulation of the cross-sections [16]. R.N. Hwang later proposed the so-called multipole representation that made an even larger use of these mathematical properties [17, 18]. He surmised that some of the 0K cross-sections that admit a description with resonance parameters could be written

$$\sigma_{nx}(E) \propto \frac{1}{E}\Re\left(\sum_p \frac{a_p + b_p \exp(-2i\phi_p(E))}{\sqrt{E} - z_p}\right). \tag{1.3}$$

This is almost what is known to mathematicians as a partial fraction decomposition. The denominator variables z_p are complex numbers known as poles, while the numerator variables a_p and b_p are complex numbers known as residues. The function ϕ_p differentiates it slightly from being exactly a partial fraction decomposition. However, the main idea of writing the cross-sections as a sum of so-called pole terms is still valid. We will see shortly thereafter that this formulation is far-reaching for computing the temperature dependency of the cross-sections. This idea was successfully applied by R.N. Hwang to both the Reich-Moore formalism [18] and the Multi-Level Breit-Wigner formalism [19]. He developed a code named WHOPPER to perform the conversion from standard resonance parameters to these multipole parameters, which is still in use at MIT [20].

1.1.4 Doppler broadening of the cross-sections

All the aforementioned models describe interactions between a neutron and a single motionless target nucleus. Actually, in nuclear reactor applications, and even in the experimental measurements of cross-sections, the target nuclei are not motionless : the neutrons 'see' moving targets as per the well-known Doppler effect [21]. Hence, the cross-sections have to be Doppler-broadened in accordance with the distribution of motion of the targets for a given temperature. This distribution is usually chosen to be that of the free gas model, also known as the Maxwell-Boltzmann distribution [22],

$$p(\boldsymbol{w})d\boldsymbol{w} = \frac{1}{\pi^{3/2}w_T^3}\exp\left(-\frac{\|\boldsymbol{w}\|^2}{w_T^2}\right)d\boldsymbol{w} \text{ with } \frac{Mw_T^2}{2} = k_B T. \tag{1.4}$$

The cross-sections are then broadened with the following formula :

$$\sigma\left(E,T\right) = + \frac{1}{\sqrt{4\pi}E}\int_{E=0}^{\infty}\frac{\sqrt{E'}}{\sqrt{E_T}}\sigma\left(E',0\right)\exp\left(-\frac{(\sqrt{E}-\sqrt{E'})^2}{E_T}\right)dE' \\ - \frac{1}{\sqrt{4\pi}E}\int_{E=0}^{\infty}\frac{\sqrt{E'}}{\sqrt{E_T}}\sigma\left(E',0\right)\exp\left(-\frac{(\sqrt{E}+\sqrt{E'})^2}{E_T}\right)dE'. \tag{1.5}$$

with $E_T = \frac{mw_T^2}{2} = \frac{m}{M}k_BT$. The letters m and M denote respectively the mass of the neutron and the mass of the target nucleus. The Boltzmann constant is noted k_B and the temperature of the medium is noted T.

The particular kernel appearing when gathering these integrals, with the particular Maxwell-Boltzmann distribution, is known as the Solbrig kernel [23].

1.2 Nuclear data evaluation and processing

The ENDF collaboration [14] aims at gathering nuclear data for different nuclei. Among these data, cross-sections for different nuclear interactions are available. Either tabulated values or sets of resonance parameters are provided. The latter are used to reconstruct the 0K cross-sections with specific formulae for each different formalism. The choice of this formalism is up to the evaluator who performs the measurement of the cross-sections. These evaluations are obtained by codes such as SAMMY [24] and CONRAD [25]. More insight about the choice of formalisms and the fits can be found in their respective documentations.

These data are finally gathered in files that are then processed by different software such as NJOY [26], PREPRO [27] and GALILÉE-1 [28] to reconstruct, among other quantities of interest, the 0K cross-sections. The codes then perform the Doppler broadening to obtain the cross-sections at the desired temperatures. This is done typically with variations of the so-called sigma-1 algorithm [21], which is based on a linearization of the 0K cross-sections and a broadening of this approximated profile with analytical tools.

Other approaches have been studied to broaden the cross-sections. G. Ferran [29] has worked on a Fourier-transform-based method to compute the integrals of formula (1.5). Finite difference methods have also been investigated to compute these same integrals [30, 31].

1.3 On the temperature dependency of cross-sections

1.3.1 Multi-physics simulation challenges

The temperature dependency of the cross-sections is one of the main coupling effect of thermal-hydraulics with respect to neutron transport. It is a key issue in multi-physics

simulations involving feedbacks. The usual approach of Monte Carlo simulation is to store in memory the required cross-section data at all temperatures and energies of interest. These cross-sections are generated before running the simulation by the codes previously cited.

The nature of the Monte Carlo method implies storing a continuous energy, i.e. finely tabulated profile of these cross-sections. The sheer amount of data to store is a limitation to the problems that can be studied. Indeed, a single temperature cross-section profile can take up to the order of a megabyte of data for a nucleus with numerous resonances, such as the isotopes of Uranium or Plutonium. Hence, storing the cross-sections of a hundred nuclei for various reactions and a handful of temperatures can easily occupy the order of the gigabytes in memory.

Moreover, the access itself to the memory during simulations can become a limiting factor to the performance of codes. Efforts have been recently made to alleviate this issue, notably by the implementation of methods accelerating the lookup in the stored tabulated cross-sections [32, 33, 34].

These limitations in memory availability and access speed suggest looking at on-the-fly approaches, where some data is computed as needed (instead of being stored in advance). Particular interest for on-the-fly computation of the temperature dependency has surged in the recent years. The idea is to store only a limited amount of cross-section data, corresponding to one or few temperatures. The desired cross-sections at the required temperature are then computed as needed during the simulation.

1.3.2 Overview of the "on-the-fly" methods

Monte Carlo codes have adopted distinct approaches to this on-the-fly temperature dependency calculation [35]. I list here four of them that are of current interest :

- the so-called sigma-1 method, which consists in storing linearized 0K cross-section profiles. The cross-section at a desired energy and temperature is then computed at each collision by the exact same algorithm as it would be before launching the simulation by software as NJOY [26] or GALILÉE-1 [28]. The numerical integration scheme of these linearized profiles is described by Cullen in [21].
- a target motion sampling algorithm [36, 37]. As the name suggests, the cross-sections are not averaged with respect to the target nuclei motion distribution. Rather, the motion of the target nuclei is sampled at each collision according to expression (1.4).
- an interpolation scheme between a set of cross-sections at carefully chosen temperatures over a pre-defined energy grid [38].
- an on-the-fly multipole Doppler broadening. Only the equivalent multipole representation of the 0K cross-sections is stored.

There exist multiple implementations of the methods listed here. In this work we have chosen to focus on the last approach.

1.3.3 Focus on the multipole representation

The additive nature of the multipole representation, combined with the linear nature of the Doppler broadening, can be successfully used to compute the broadened cross-sections. Indeed, from these two properties, the broadening of a cross-section can be written as the sum of the broadening of each pole term in expression (1.3). The broadening of each pole term is done via an integral that can be analytically expressed in terms of a special function known as the Faddeeva function [39].

The Faddeeva function [39] is of particular interest in the field of spectroscopy and plasma physics, and has been studied extensively. It is closely related to the so-called complex error function. Numerical algorithms to compute these special functions can be found in [40] and [41]. An overview and comparison of different approaches for the particular Faddeeva function are provided in [42]. An implementation used by the code ABINIT [43] done by the MIT is available online.

In recent years, the group of B. Forget at MIT has investigated the possibility of using the multipole representation for the on-the-fly Doppler broadening [20], especially in connection with their Monte Carlo code OpenMC [33].

Two main challenges have been encountered. On the one hand, not all cross-sections for all nuclei admit a multipole representation. This is due to both theoretical and practical reasons that I will discuss later in this report. On the other hand, on-the-fly computation cost with the multipole representation can be significantly larger than that of the sigma-1 approach mentioned above. Indeed, the accurate computation of the Faddeeva function can be quite challenging. Efforts have been made to tackle both issues.

Concerning the computing cost, C. Josey has developed an algorithm, called the "windowed" multipole method, to reduce the number of poles to be taken into account at a given energy [44, 45]. It builds on the idea of R.N. Hwang that poles far away from a given energy can be approximated by fewer so-called pseudo-poles [18, 19].

Concerning the non-universality of the multipole representation of cross-sections, vector fitting techniques have been directly applied to the cross-section profiles [46, 47, 48]. The goal is to ensure a multipole representation even for those cross-sections that lack a theoretical justification for a multipole representation. It is hoped that a systematic treatment of all cross-sections for all nuclei will ultimately be possible.

The CEA has also taken interest in on-the-fly approaches for its own Monte Carlo transport codes TRIPOLI-4® [49] and PATMOS [50]. As of today, the former uses only the method of stochastic interpolation (also used by MCNP [51]). The sigma-1 approach has been implemented in the latter. The multipole representation offers yet another approach for an on-the-fly Doppler broadening and is as such of great interest. Additionally, it provides an alternative way of reconstructing and working with the 0K cross-sections. These two aspects were the prime motivations for this PhD work.

1.4 Plan of this report

As outlined in the introduction, in my thesis, I have taken interest in the theoretical and numerical aspects of the multipole representation of the cross-sections. One of the goals was to assert mathematically, and possibly improve, the results of R.N. Hwang concerning this alternative representation. Another was to provide algorithms and their computer implementations to convert the usual ENDF resonance parameters into multipole parameters.

The first part of this manuscript provides a general setup concerning cross-section reconstruction, as well as a set of mathematical properties that will be relevant for the rest of my work.

- Chapter 1 is a very brief summary of the R-matrix theory and of the basic cross-section formulae. It presents the different algebraic elements that will appear throughout the manuscript.
- Chapter 2 outlines the relevant details of the implementation of the cross-section reconstruction in the frame of the ENDF collaboration.
- Chapter 3 gives the useful mathematical tools that I have used during my PhD work. These include a list of properties of rational functions, which are at the heart of the multipole representation. I also expose here some elements of the key issue of finding the roots of polynomials, as well as the solutions I have adopted to tackle these issues.

The second part of this thesis is devoted to an in-depth theoretical investigation of the multipole representation. There are currently two main reconstruction formalisms used for representing cross-sections. We will see that they involve rather different challenges as far as the multipole representation is concerned. We will finally discuss some qualitative aspects of this representation of the cross-sections.

- Chapter 1 focuses on the conversion of the Multi-Level Breit-Wigner resonance parameters to multipole parameters. This chapter involves a careful mathematical investigation of the energy dependency of some of the resonance parameters. I will show that a multipole representation with fewer poles than previously thought is possible. This will provide some insights related to the idea presented by C. Jammes and R.N. Hwang in [19], as well as an algorithm to find these new parameters.
- Chapter 2 focuses on the conversion of the Reich-Moore resonance parameters to multipole parameters. This chapter involves heavy algebraic manipulations of the cross-section formulae. The root-finding issue will be more central than in the previous chapter. A fast and robust algorithm is proposed in order to find a new multipole representation with fewer poles than the previously established results [18, 20].
- In Chapter 3, I provide some insights about the nature of the poles and the qualitative differences in their contribution to the cross-sections profile. I wish to show here that, once the multipole parameters are computed, the interpretation of the poles is largely independent of the formalism from which they were obtained.

The third part of this thesis is devoted to some applications of the multipole representation. I have implemented a code performing the conversion of standard resonance parameters to multipole parameters. These are used for two purposes :

- In Chapter 1, I show that these parameters can be used to reconstruct the 0K cross-sections for a large number of nuclei. This confirms the validity of the extensive mathematical study I have done in the second part of my work. I present numerical results for some nuclei of interest.
- In Chapter 2, I discuss some theoretical aspects of the Doppler broadening with the multipole representation, notably concerning the use of the Faddeeva function. I also give some encouraging numerical results of the Doppler broadening with my newly computed multipole parameters.

I will finally draw some conclusions and discuss perspectives concerning the applications and limitations of the multipole representation.

Part I

Background and context

Chapter 1

From the R-matrix theory to the cross-section reconstruction formalisms

1.1 General concepts of the R-matrix theory

The R-matrix theory aims at modelling the interactions between particles composed of nucleons in the framework of the first quantization of quantum mechanics. The very extensive details required to properly explain it are far outside the scope of this report. They can be found in the seminal article of A.M. Lane and R.G. Thomas [7]. I will only present here the elements that are relevant to the definition and manipulation of cross-sections.

1.1.1 Definition of the channels

The system composed of N nucleons is described by a probability wave function of 3N spatial dimensions. To be able to study such a complex wave function, the variable space is separated in an external and an internal region. The external region is restricted to configurations where the nucleons composing the system are gathered in exactly two particles. It is further separated in so-called channels. These are characterized by :

- a pair of particles a and A of respective spins i and I. These particles and their internal states are gathered in a single notation α,
- an orbital quantum number noted l,
- a channel spin noted s,
- a total angular momentum and its parity noted J^π. Often the parity is implicitly included in the notation J.
- the projection of the total angular momentum on a quantification axis m_J

The orbital quantum number l can take any non negative integer value and corresponds to a

spherical harmonics decomposition whose description is outside the scope of this manuscript. The channel spin s can take values between $|I-i|$ and $|I+i|$ as per usual spin sum rules. The total angular momentum J can take value between $|l-s|$ and $|l+s|$. Finally, the parity is computed as the product of the parity of a, the parity of A and $(-1)^l$. A fundamental property of nuclear reactions is the conservation of the total angular momentum and parity.

Additionally, in relation with the aforementioned quantities characterizing a channel, we define :

- a channel radius a_c beyond which the two particles of the channel have no nuclear interactions,
- a wave number k_c or conversely a De Broglie wave length $\lambda\!\!\!^{-}_c$ that characterizes the relative motion of the two particles,

$$\frac{1}{k_c} = \lambda\!\!\!^{-}_c = \frac{\hbar}{\sqrt{2\mu_c E}}, \tag{1.1}$$

  where $\hbar$ is the reduced Planck constant and μ_c the reduced mass of the two particles a and A,
- a statistical factor g_c that is concerned with spin properties and possible degeneracies of the solutions of the channels. These are linked notably to the projection number m_J, that will not appear in later formulae. Its expression is

$$g_c = \frac{(2J+1)}{(2i+1)(2I+1)}. \tag{1.2}$$

The definition of the channels is such that the space of waves solutions of the Schrödinger equation is exactly two-dimensional. A basis can be chosen with an incoming wave noted I_c and an outgoing wave noted O_c. A global solution of the Schrödinger equation is entirely described by its decomposition on the two wave basis of each channel. Not all such decompositions are possible. They are constrained so that prescribing the decomposition on the incoming waves imposes the rest of the decomposition on the outgoing waves. This relation is linear and it is possible to define a matrix encoding it. Namely if x_c and y_c are the coefficients of the decomposition on the O_c and I_c, there exists a relation of the form

$$x_c = -\sum_{c'} U_{cc'} y_{c'}. \tag{1.3}$$

where U is the so-called collision matrix. The cross-sections will be naturally defined from this matrix. If the I_c and O_c are properly normalized, the matrix U will be unitary. Finally, from the conservation of J^π, all elements of this collision matrix between channels of different total angular momentum and parity are null.

1.1.2 The R-matrix parametrization

The R-matrix theory provides a way to indirectly parametrize the collision matrix. The aforementioned constraining relation between incoming and outgoing waves is found by working with an internal region. It is defined to connect the otherwise disjoint channels of the

external region, and allow for nuclear reactions between the pair of particles. The conservation of J^π is particularly crucial in this internal region. Hence, only channels of common such value are really connected with each other through this region. Moreover, this means that even if the Hamiltonian of the complete system cannot be easily separated in the internal region : there is still a separation possible between the different J^π values. At a fixed value of the total angular momentum and parity, the R-matrix theory states that we can relate the value of the wave function on each concerned channel surface with the value of its derivative on these surfaces. The matrix R does so and is defined by

$$R_{cc'} := \sum_\lambda \frac{\gamma_{\lambda c}\gamma_{\lambda c'}}{E_\lambda - E}\delta^{\pi\pi'}_{JJ'}. \tag{1.4}$$

where the E_λ and the $\gamma_{\lambda c}$ are real numbers notably independent of the energy E of the system. The Kronecker symbol δ asserts that this R-matrix only relates channels of common J^π. This description is obtained by considering the Schrödinger equation at fixed total angular momentum and parity, restrained to the internal region, with the addition of some real boundary conditions. These are prescribed on each channel surface and impose the ratio, noted B_c, between solution derivatives and solution values. Following the R-matrix theory, this yields a set of eigenvalues E_λ and real valued eigenvectors ψ_λ that constitute a basis of wave functions in the internal region (of corresponding J^π value, this index being omitted here and in the following). The parameters $\gamma_{\lambda c}$ are projections of ψ_λ on channel surface c.

1.1.3 Continuity between the internal and external regions

Just on the other side of the channel surfaces, in the channel themselves, the value of the wave function and its derivative have well known analytical expressions. The following diagonal matrices contain these properties :

$$L_{cc} = \left(\frac{r_c}{O_c}\frac{\partial O_c}{\partial r_c}\right)_{r_c=a_c}, \tag{1.5}$$

$$S_{cc} = \Re(L_{cc}), \tag{1.6}$$

$$P_{cc} = \Im(L_{cc}), \tag{1.7}$$

$$\Omega_{cc} = \exp(-i\phi_c) \quad \text{with} \quad \phi_c = \arg(O_c(a_c)). \tag{1.8}$$

In this formulae, the symbols $\Re$ and $\Im$ denote respectively the real and imaginary parts of a complex number. The elements of S_{cc} are called level-shift factors and will, as their name suggests, shift the levels E_λ. The elements of P_{cc} are called penetration factors. They occur in the definition of the width of a channel c for level λ :

$$\Gamma_{\lambda c} := 2\gamma^2_{\lambda c}P_{cc}. \tag{1.9}$$

Finally, the elements ϕ_c are called phase-shift factors. I will provide more details about these three factors later on, as they are of central importance to my work.

From the definition of R and the different factors I just presented, it is then possible to give a relation between the matrix U, that relates the incoming and outgoing waves,

to the matrix R, which relates the properties of the wave function on the surface between internal and external region. The following expression can be derived after many algebraic manipulations :

$$U = \Omega P^{1/2}\big(Id - R(L-B)\big)^{-1}\big(Id - R(L^*-B)\big)P^{-1/2}\Omega. \tag{1.10}$$

where the matrix L^* is the conjugate transpose of L and Id is the identity matrix. This relation is central to the R-matrix theory. On one hand, the cross-sections are naturally defined from the matrix U. On the other hand, the matrix R can be represented with a convenient set of parameters (to be experimentally fitted). We have bridged these two definitions which will now allow defining the cross-sections.

1.2 Intermediary algebraic elements to define the cross-sections

1.2.1 Auxiliary matrices X and ρ

So as to alleviate a bit the notations of (1.10), it is usual to define the X matrix as,

$$X = P^{1/2}(Id - R(L-B))^{-1}RP^{1/2}, \tag{1.11}$$

or the ρ matrix which is very similar,

$$\rho = -iX. \tag{1.12}$$

Then the fundamental relation (1.10) between U and R can be written in terms of X or ρ :

$$\begin{aligned}
U &= \Omega P^{1/2}\big(Id - R(L-B)\big)^{-1}\big(Id - R(L^*-B)\big)P^{-1/2}\Omega \\
&= \Omega P^{1/2}\big(Id - R(L-B)\big)^{-1} \\
&\qquad \big(Id - R(L-B) + R(L-B) - R(L^*-B)\big)P^{-1/2}\Omega \\
&= \Omega P^{1/2}\left(Id + \big(Id - R(L-B)\big)^{-1}R(L-L^*)\right)P^{-1/2}\Omega \\
&= \Omega\left(Id + 2iP^{1/2}\big(Id - R(L-B)\big)^{-1}RP^{1/2}\right)\Omega \\
&= \Omega\left(Id + 2iX\right)\Omega \\
&= \Omega\left(Id - 2\rho\right)\Omega.
\end{aligned} \tag{1.13}$$

1.2.2 Cross-sections in function of the collision matrix U

We admit that the cross-sections of the reaction producing a state described by the channel c' from a state described by the channel c is

$$\sigma_{cc'} = \pi \lambda_c^2 g_c \left|\delta_{cc'} - U_{cc'}\right|^2 \delta^{\pi\pi'}_{JJ'}. \tag{1.14}$$

The multiplicative term $\delta^{\pi\pi'}_{JJ'}$ will be dropped going further as it is often equivalently included in the definition of the collision matrix U. From now on, it will be implicit that terms concerning channels of different J^π will be null.

The total cross-section of a channel c is obtained by summing over c' all the terms $\sigma_{cc'}$:

$$\begin{aligned}
\sigma_{c,total} &= \sum_{c'} \sigma_{cc'} = \sum_{c'} \pi \lambda\!\!\!^{-2}_c g_c |\delta_{cc'} - U_{cc'}|^2 \\
&= \pi \lambda\!\!\!^{-2}_c g_c \sum_{c'} |\delta_{cc'} - U_{cc'}|^2 \\
&= \pi \lambda\!\!\!^{-2}_c g_c \left(|1 - U_{cc}|^2 + \sum_{c' \neq c} |U_{cc'}|^2 \right) \\
&= \pi \lambda\!\!\!^{-2}_c g_c \Big(1 - 2\Re\big(U_{cc}\big) + |U_{cc}|^2 + \sum_{c' \neq c} |U_{cc'}|^2 \Big) \\
&= \pi \lambda\!\!\!^{-2}_c g_c \Big(1 - 2\Re\big(U_{cc}\big) + 1 \Big) \\
&= 2\pi \lambda\!\!\!^{-2}_c g_c \Big(1 - \Re\big(U_{cc}\big) \Big).
\end{aligned} \tag{1.15}$$

The key property here is the unitarity of the matrix U.

1.2.3 Cross-sections in function of the matrix ρ

The relation (1.13) between U and ρ with explicit indices c and c' reads,

$$U_{cc'} = \exp(-i(\phi_c + \phi_{c'}))\,(\delta_{cc'} - 2\rho_{cc'})\,, \tag{1.16}$$

so the cross-section formulae in function of ρ are, for $c \neq c'$,

$$\sigma_{cc'} = 4\pi \lambda\!\!\!^{-2}_c g_c |\rho_{cc'}|^2, \tag{1.17}$$

and for $c = c'$,

$$\sigma_{cc} = 4\pi \lambda\!\!\!^{-2}_c g_c \left[\sin^2(\phi_c)\big(1 - 2\Re(\rho_{cc})\big) + \sin(2\phi_c)\Im(\rho_{cc}) + |\rho_{cc}|^2 \right]. \tag{1.18}$$

1.3 Approximations to the R-matrix theory

Although the general expression of the R-matrix given in expression (1.4) is somewhat elegant, further approximations of this model are necessary for practical applications. I am going to give a very quick summary of the two main approximations of the R-matrix currently in use for cross-section reconstruction.

The developments I will make in this section give a very schematic overview of the necessary algebraic manipulations. My aim here is simply to expose some of these elements that will be of use later.

1.3.1 Definition of the level matrix A

The fundamental idea is to define, implicitly, the so-called level matrix A :

$$\gamma^T A \gamma = \big(Id - R(L-B)\big)^{-1} R, \tag{1.19}$$

where the γ matrix is the matrix whose elements are the $\gamma_{\lambda c}$. The previously defined R, X and ρ matrices all describe relations between channels. This newly defined A matrix describes relations between levels.

It is possible to show that, from this implicit definition, A^{-1} actually admits an explicit definition :

$$A^{-1}_{\lambda\mu} = (E_\lambda - E)\delta_{\lambda\mu} - \sum_c \gamma_{\lambda c}(L_{cc} - B_{cc})\gamma_{\mu c}. \tag{1.20}$$

Although the manipulation of infinite dimension matrices may lack a rigorous mathematical framework, the idea of switching from channel-based expressions to level-based ones is far-reaching. Most approximations, among which are the two I am about to present, have been naturally derived from the latter perspective.

Finally, with the implicit definition of A, let us also note that,

$$\rho = -iP^{1/2}\gamma^T A \gamma P^{1/2}. \tag{1.21}$$

1.3.2 The Multi-Level Breit-Wigner formalism

We assume that the matrix A^{-1} is diagonal, therefore,

$$A_{\lambda\mu} = \frac{1}{(E_\lambda - E) - \sum_c \gamma^2_{\lambda c}(L_{cc} - B_{cc})}\delta_{\lambda\mu}. \tag{1.22}$$

By definition, $L_{cc} = S_{cc} + iP_{cc}$. We can rewrite the denominator of $A_{\lambda\mu}$:

$$(E_\lambda - E) - \sum_c \gamma^2_{\lambda c}(L_{cc} - B_{cc}) = E_\lambda - \sum_c \gamma^2_{\lambda c}(S_{cc} - B_{cc}) - E - i\sum_c \gamma^2_{\lambda c} P_{cc}. \tag{1.23}$$

The total width of the level λ is defined by

$$\Gamma_\lambda := \sum_c \Gamma_{\lambda c} \tag{1.24}$$

$$= \sum_c 2\gamma^2_{\lambda c} P_{cc} \text{ by definition of } \Gamma_{\lambda c}. \tag{1.25}$$

The shifted energy level is defined as

$$E'_\lambda := E_\lambda - \sum_c \gamma^2_{\lambda c}(S_{cc} - B_{cc}). \tag{1.26}$$

With these two new definitions :

$$A_{\lambda\lambda} = \frac{-1}{E - E'_\lambda + i\Gamma_\lambda/2}. \tag{1.27}$$

The formulae for the cross-sections are then, for $c \neq c'$,

$$\sigma_{cc'} = 4\pi \lambda\!\!\!^{-2}_c g_c |\rho_{cc'}|^2 \tag{1.28}$$

$$\text{with } \rho_{cc'} = i \sum_\lambda \frac{P^{1/2}_{cc} \gamma_{\lambda c} P^{1/2}_{c'c'} \gamma_{\lambda c'}}{E - E'_\lambda + i\Gamma_\lambda/2}. \tag{1.29}$$

and particularly for $c = c'$,

$$\sigma_{cc} = 4\pi \lambda\!\!\!^{-2}_c g_c \left(\sin^2(\phi_c)(1 - 2\Re(\rho_{cc})) + \sin(2\phi_c)\Im(\rho_{cc}) + |\rho_{cc}|^2 \right) \tag{1.30}$$

$$\text{with } \rho_{cc} = \frac{i}{2} \sum_\lambda \frac{\Gamma_{\lambda c}}{E - E'_\lambda + i\Gamma_\lambda/2}. \tag{1.31}$$

The square modulus in formulae (1.28) and (1.30) account for interference between levels. The Multi-Level Breit-Wigner formalism does not account for interferences between channels. This is one of the improvements of the Reich-Moore formalism that I am about to present.

1.3.3 The Reich-Moore formalism

The approximations adopted in the Reich-Moore formalism are more subtle. We do not assume that A^{-1} is diagonal. Instead we start by separating the channels containing photons and those which do not,

$$\begin{aligned} A^{-1}_{\lambda\mu} &= (E_\lambda - E)\delta_{\lambda\mu} - \sum_c \gamma_{\lambda c}(L_{cc} - B_{cc})\gamma_{\mu c} \\ &= (E_\lambda - E)\delta_{\lambda\mu} - \sum_{c\in\gamma} \gamma_{\lambda c}(L_{cc} - B_{cc})\gamma_{\mu c} - \sum_{c\notin\gamma} \gamma_{\lambda c}(L_{cc} - B_{cc})\gamma_{\mu c}. \end{aligned} \tag{1.32}$$

Then we make the approximation that the only significant contribution of the photon channels are in the diagonal. The physical reasons for this choice are outside the scope of this summary. I refer to the article A.M. Lane and R.G. Thomas [7] and the subsequent article of C.W. Reich and M.S. Moore [13] for details.

$$\begin{aligned} A^{-1}_{\lambda\mu} &\approx \left((E_\lambda - E) - \sum_{c\in\gamma} \gamma^2_{\lambda c}(L_{cc} - B_{cc}) \right) \delta_{\lambda\mu} - \sum_{c\notin\gamma} \gamma_{\lambda c}(L_{cc} - B_{cc})\gamma_{\mu c} \\ &= \left((E_\lambda - E) - \sum_{c\in\gamma} \gamma^2_{\lambda c}(S_{cc} - B_{cc}) - i \sum_{c\in\gamma} \gamma^2_{\lambda c} P_{cc} \right) \delta_{\lambda\mu} - \sum_{c\notin\gamma} \gamma_{\lambda c}(L_{cc} - B_{cc})\gamma_{\mu c}. \end{aligned} \tag{1.33}$$

We define a shifted energy level,

$$E'_\lambda = E_\lambda - \sum_{c\in\gamma} \gamma^2_{\lambda c}(S_{cc} - B_{cc}). \tag{1.34}$$

We define a total photon width,

$$\Gamma_{\lambda\gamma} := \sum_{c\in\gamma} \Gamma_{\lambda c} \tag{1.35}$$

$$= \sum_{c\in\gamma} 2\gamma_{\lambda c}^2 P_{cc} \text{ by definition of } \Gamma_{\lambda c}. \tag{1.36}$$

Then with these new notations,

$$A^{-1}_{\lambda\mu} = (E'_\lambda - E - i\Gamma_{\lambda\gamma}/2)\,\delta_{\lambda\mu} - \sum_{c\notin\gamma} \gamma_{\lambda c}(L_{cc} - B_{cc})\gamma_{\mu c}. \tag{1.37}$$

We write,

$$Id = A^{-1}A, \tag{1.38}$$

and we substitute the expression of A^{-1},

$$\begin{aligned}\delta_{\lambda\mu} &= \sum_\alpha (E'_\lambda - E - i\Gamma_{\lambda\gamma}/2)\,\delta_{\lambda\alpha}A_{\alpha\mu} - \sum_\alpha \left(\sum_{c\notin\gamma} \gamma_{\lambda c}(L_{cc} - B_{cc})\gamma_{\alpha c}\right) A_{\alpha\mu} \\ &= (E'_\lambda - E - i\Gamma_{\lambda\gamma}/2)\,A_{\lambda\mu} - \sum_{c\notin\gamma} \left(\gamma_{\lambda c}(L_{cc} - B_{cc}) \sum_\alpha \gamma_{\alpha c}A_{\alpha\mu}\right),\end{aligned} \tag{1.39}$$

then,

$$\frac{\delta_{\lambda\mu}}{E'_\lambda - E - i\Gamma_{\lambda\gamma}/2} = A_{\lambda\mu} - \sum_{c\notin\gamma} \left(\frac{\gamma_{\lambda c}}{E'_\lambda - E - i\Gamma_{\lambda\gamma}/2}(L_{cc} - B_{cc}) \sum_\alpha \gamma_{\alpha c}A_{\alpha\mu}\right). \tag{1.40}$$

Let c' and c'' be two non-photon channels. We multiply the previous expression by $\gamma_{\lambda c'}\gamma_{\mu c''}$ and sum on λ and μ,

$$\begin{aligned}\sum_{\lambda\mu} \frac{\gamma_{\lambda c'}\delta_{\lambda\mu}\gamma_{\mu c''}}{E'_\lambda - E - i\Gamma_{\lambda\gamma}/2} &= \sum_{\lambda\mu} \gamma_{\lambda c'}A_{\lambda\mu}\gamma_{\mu c''} \\ &\quad - \sum_{\lambda\mu} \gamma_{\lambda c'} \sum_{c\notin\gamma} \left(\frac{\gamma_{\lambda c}}{E'_\lambda - E - i\Gamma_{\lambda\gamma}/2}(L_{cc} - B_{cc}) \sum_\alpha \gamma_{\alpha c}A_{\alpha\mu}\right) \gamma_{\mu c''} \\ \sum_{\lambda} \frac{\gamma_{\lambda c'}\gamma_{\lambda c''}}{E'_\lambda - E - i\Gamma_{\lambda\gamma}/2} &= \sum_{\lambda\mu} \gamma_{\lambda c'}A_{\lambda\mu}\gamma_{\mu c''} \\ &\quad - \sum_{c\notin\gamma} \left[\left(\sum_\lambda \frac{\gamma_{\lambda c'}\gamma_{\lambda c}}{E'_\lambda - E - i\Gamma_{\lambda\gamma}/2}\right)(L_{cc} - B_{cc}) \left(\sum_{\alpha\mu} \gamma_{\alpha c}A_{\alpha\mu}\gamma_{\mu c''}\right)\right].\end{aligned} \tag{1.41}$$

We define the reduced R-matrix by,

$$\boxed{\widehat{R}_{cc'} := \sum_\lambda \frac{\gamma_{\lambda c}\gamma_{\lambda c'}}{E'_\lambda - E - i\Gamma_{\gamma\lambda}/2}}, \tag{1.42}$$

and recall that,

$$\rho = -iP^{1/2}\gamma^T A\gamma P^{1/2},$$

so that the indexed relation (1.41) can be written with matrices as

$$\widehat{R} = iP^{-1/2}\rho P^{-1/2} - \widehat{R}(L-B)iP^{-1/2}\rho P^{-1/2}. \tag{1.43}$$

Multiplying by $P^{1/2}$ left and right yields

$$P^{1/2}\widehat{R}P^{1/2} = (Id - P^{1/2}\widehat{R}(L-B)P^{-1/2})i\rho. \tag{1.44}$$

A few algebraic manipulations give us the relation of the matrix ρ in terms of this newly defined reduced R-matrix :

$$\begin{aligned}\rho &= -i(Id - P^{1/2}\widehat{R}(L-B)P^{-1/2})^{-1}P^{1/2}\widehat{R}P^{1/2}\\ &= -i(P^{-1/2} - \widehat{R}(L-B)P^{-1/2})^{-1}\widehat{R}P^{1/2}\\ &= -iP^{1/2}(Id - \widehat{R}(L-B))^{-1}\widehat{R}P^{1/2}.\end{aligned} \tag{1.45}$$

Additionally, it is often assumed that $S_{cc} - B_{cc} = 0$. This means that $L - B = iP$, which simplifies the previous expression. The final relation between the matrix ρ and the reduced R-matrix is

$$\begin{aligned}\rho &= -iP^{1/2}(Id - i\widehat{R}P)^{-1}\widehat{R}P^{1/2}\\ &= P^{1/2}(Id - i\widehat{R}P)^{-1}(-i\widehat{R}P)P^{-1/2}\\ &= P^{1/2}(Id - i\widehat{R}P)^{-1}(Id - i\widehat{R}P - Id)P^{-1/2}\\ &= Id - P^{1/2}(Id - i\widehat{R}P)^{-1}P^{-1/2}\\ &= Id - (Id - iP^{1/2}\widehat{R}P^{1/2})^{-1}.\end{aligned} \tag{1.46}$$

The cross-sections are then defined again from the relations (1.17) and (1.18). The matrix inversion present here makes the Reich-Moore formalism significantly more costly from a computational standpoint than the Multi-Level Breit-Wigner formalism. However, it allows capturing the physics of interference between channels and particularly fission channels. This is particularly important for some heavy fissile nuclei, as Uranium 235 or Uranium 238.

1.4 Definition and properties of the penetration, level-shift and phase-shift factors

In this section, I will give a definition and some properties of the scattering factors defined in expressions (1.5) to (1.8). As I mentioned, the outgoing and incoming waves in each channel have well known expressions. Particularly, for non charged particles, they are the solutions to the projection of the Schrödinger equation on the spherical harmonics in the absence of potential : the special spherical Bessel functions. Their logarithmic derivative also have well known expressions that I will now describe.

They take an adimensioned argument just like trigonometric functions and they depend on the azimuthal number l of the spherical harmonic considered. For the channel c, their argument are built from the wave number k_c (the inverse of the De Broglie wavelength of the channel) and the radius a_c.

The expression of the **penetration factor** noted P_l, the **level-shift factor** noted S_l and the (hard-sphere) **phase-shift factor** noted ϕ_l for the first few values of l are,

l	$P_l(\rho)$	$S_l(\rho)$	$\phi_l(\rho)$
0	ρ	0	ρ
1	$\dfrac{\rho^3}{\rho^2+1}$	$\dfrac{-1}{\rho^2+1}$	$\rho - \arctan(\rho)$
2	$\dfrac{\rho^5}{\rho^4+3\rho^2+9}$	$\dfrac{-3\rho^2-18}{\rho^4+3\rho^2+9}$	$\rho - \arctan\left(\dfrac{3\rho}{3-\rho^2}\right)$

Table 1.1: Expressions of the penetration, level-shift and phase-shift factors for the first values of l

The following recursive formulae allow computing them at higher values of l :

$$\boxed{\begin{aligned} P_{l+1}(\rho) &= \frac{\rho^2 P_l(\rho)}{P_l^2(\rho) + \big(l+1-S_l(\rho)\big)^2}, \\ S_{l+1}(\rho) &= \frac{\rho^2\big(l+1-S_l(\rho)\big)}{P_l^2(\rho) + \big(l+1-S_l(\rho)\big)^2} - (l+1). \end{aligned}} \tag{1.47}$$

with the initial conditions $P_0(\rho) = \rho$ and $S_0(\rho) = 0$.

P_l and S_l are both rational functions of their argument ρ. Let me stress that this will be a very important point later in my work. As we can see in Table 1.1, they have a common denominator polynomial. Furthermore their numerator and denominator as they are presented here have no common roots. I give a proof of these properties during my study of the multipole representation of the Multi-Level Breit-Wigner formalism. If we write P_l and S_l as quotient of some polynomials,

$$P_l = \frac{p_l}{q_l}, \tag{1.48}$$

$$S_l = \frac{s_l}{q_l}. \tag{1.49}$$

I admit here the empirical properties on the degree of the numerator polynomials and (common) denominator polynomial,

$$\boxed{\begin{aligned} &\deg(p_l) = 2l+1, \\ &\deg(s_l) = \max(2l-2, 0), \\ &\deg(q_l) = 2l. \end{aligned}} \tag{1.50}$$

but I will demonstrate these properties later on.

The phase-shift factor ϕ_l has a slightly more complicated expression, specifically it is not a rational function of its argument. The contribution of ϕ_l in the cross-sections formulae is somewhat separated from that of the penetration and level shift factors. Particularly, it can be ignored during the study of the multipole representation. I will take interest in it when studying the Doppler broadening of the cross-sections with the multipole representation.

Chapter 2

Practical aspects of resonant cross-sections reconstruction in the ENDF format

As I explained in the introduction of this manuscript, resonant cross-sections are described by analytical formulae and a set of corresponding parameters. In the previous chapter, I have given an overview of the derivation of such formulae from physical models. In this chapter, I give the implementation details of the Multi-Level Breit-Wigner and Reich-Moore formalisms as well as a short description of the resonance data in the framework of the ENDF format.

An important change concerns the notation adopted for the energy of the system, and particularly in the cross-section formulae. In the presentation of the R-matrix theory, the energy E was expressed in the center of mass of the two particles. For experimental purposes, and later the fitting of the R-matrix parameters, it is more natural to work in terms of the energy of the incident neutron in the laboratory frame noted E^{lab}. The relation between these two definitions is

$$E^{lab} = \frac{M + m_n}{M} E \tag{2.1}$$

where the quantity m_n is the mass of the neutron and the quantity M is the mass of the target nucleus. As mentioned in [52], all formulae presented before can be kept identical just by multiplying reduced widths and energy levels by a constant :

$$E_\lambda^{lab} = \frac{M + m_n}{M} E_\lambda, \tag{2.2}$$

$$\gamma_{\lambda c}^{lab} = \sqrt{\frac{M + m_n}{M}} \gamma_{\lambda c}. \tag{2.3}$$

The parameters given in evaluations are those defined in the laboratory frame. Since we are concerned with these parameters, the lab superscript will not be noted explicitly in the formulae, and, from now on, the energy E will always designate the energy of the incident neutron in the laboratory frame where the target nucleus is motionless.

2.1 Implementation of the Multi-Level Breit-Wigner and Reich-Moore formalisms

2.1.1 Common simplifications and approximations

The formulae I have derived theoretically in the previous chapter, although resulting from some approximations, are still quite general. Practically, the Multi-Level Breit-Wigner and Reich-Moore formalisms are used to describe very specific interactions between a neutron and a target nucleus. The four corresponding cross-sections are the radiative capture, the elastic, the fission (when relevant) and the total cross-sections.

To obtain these cross-sections from the rather abstract channel cross-sections described before, one must sum the correct channel terms $\sigma_{cc'}$. In our case, the initial state of the system is that of a neutron and a nucleus. The final state of the system depends on the considered reaction. In the ENDF format, this sum on channel cross-sections is not done on the indices c and c'. Rather, the sum is explicit on the indices characterizing each channel : α, l, s and J^π (as explained before, the index m_J that completes the characterization of a channel is taken into account in cross-section formulae through the statistical spin factor g_c).

The indices characterizing each channel can be split into two parts. The first one, simply noted α, describes the pair of particles of the channels. It is replaced by n, for the entry composed of a neutron and a nucleus, and x for the considered reaction. The index x is either n for elastic scattering, f for fission, γ for capture and t for total. The second one is the quantum number triplet (l, s, J^π). In theory, only J^π (noted J in the rest of this manuscript) is conserved in nuclear reactions. This would imply a sum of terms of different (l, s) and (l', s') values. In practice, the ENDF evaluation format further imposes the conservation of l and s for the Multi-Level Breit-Wigner and Reich-Moore formalism implementations. As a result, the cross-section formulae in the ENDF format are a sum of terms noted $\sigma_{nx}^{(l,s,J)}$. To each quantum triplet (l, s, J) corresponds a specific set of resonances (with their individual energy and widths). Such a set will be called a pack of resonances throughout this manuscript.

The c indices in the quantities ϕ_c and g_c defined in (1.8) and (2.4) are replaced by the particular index of the channel they depend on. Consequently the phase-shift ϕ_c is noted ϕ_l as it depends only on the quantum number l. Similarly, the statistical spin factor g_c, defined in (1.2), is noted g_J as it only depends on the total angular momentum J :

$$g_J = \frac{2J+1}{2(2I+1)} \text{ for a neutron of spin } i = 1/2 \text{ and a target nucleus of spin } I \tag{2.4}$$

The wavelength $\lambda\!\!\!^{-}_c$ defined in (1.1) that appears in front of all cross-section terms $\sigma_{cc'}$ is replaced by the equivalent wave number $k = 1/\lambda\!\!\!^{-}_c$. Further, the index c can be dropped because the entry is always a neutron. The formula is

$$\frac{1}{k} = \lambda\!\!\!^{-} = \frac{A+1}{A}\frac{\hbar}{\sqrt{2m_n E}} \tag{2.5}$$

where the quantity A is the mass of the considered target nucleus expressed in neutron mass.

The energy E is the energy of the incident neutron in the laboratory frame as specified in the beginning of this subsection.

As hinted at before, there is a switch from the concept of levels to the concept of resonances in the cross-section formulae. The definition of levels in the R-matrix theory makes them mostly a mathematical concept. The exact link between levels and resonances, which are more a physical observation on the experimental cross-section profiles, is not trivial. Insights can be found in the article of P. Descouvemont [53] which proposes an overview of some aspects of the R-matrix theory. The level indices λ are replaced by resonance indices r. In combination with the change from channel indices c to reaction indices x, the reduced and non-reduced width are noted slightly differently :

$$\gamma_{\lambda c} \rightarrow \gamma_{xr} \text{ and } \Gamma_{\lambda c} \rightarrow \Gamma_{xr}.$$

For any practical applications the number of resonances taken into account in the formulae will always be finite.

In further contrast with the theory of the R-matrix, the channel-radii that appear in the computation of the penetration, level-shift and phase-shift factors are not necessarily the same. Three main possibilities are given :

- the use of a unique channel-radius computed as

$$a_c = 0.123\sqrt[3]{A^{(\text{in amu})}} + 0.08, \tag{2.6}$$

  where A is again the mass of the target nucleus, expressed in atomic mass unit,
- the use of a so-called **scattering radius** specified per nucleus. A l-dependent scattering radius is sometimes specified,
- in rare occasions, the use of an energy-dependent scattering radius. I hereby exclude the concerned nuclei from my study as no multipole representation can then be - mathematically - extracted as far as I know.

Based on the previous elements, I will now present the formulae given by ENDF for the cross-sections, for a neutron of incident energy E, at 0K (motionless target nucleus).

2.1.2 Multi-Level Breit-Wigner cross-section formulae

The formulae are :

$$\sigma_{nn}(E) = \frac{4\pi}{k^2} \sum_{(l,s,J)} g_J \left[\sin^2(\phi_l) + \Re\left(\rho_{nn}^{(l,s,J)} \exp(-2i\phi_l)\right) - \Re(\rho_{nn}^{(l,s,J)}) + \left|\rho_{nn}^{(l,s,J)}\right|^2 \right], \tag{2.7}$$

$$\sigma_{nf}(E) = \frac{\pi}{k^2} \sum_{(l,s,J)} g_J \sum_r \frac{\Gamma_{fr}\Gamma_{nr}}{(E - E_r')^2 + \Gamma_{tr}^2/4}, \tag{2.8}$$

$$\sigma_{n\gamma}(E) = \frac{\pi}{k^2} \sum_{(l,s,J)} g_J \sum_r \frac{\Gamma_{\gamma r}\Gamma_{nr}}{(E - E_r')^2 + \Gamma_{tr}^2/4}, \tag{2.9}$$

$$\rho_{nn}^{(l,s,J)}(E) = \frac{i}{2}\sum_r \frac{\Gamma_{nr}}{(E-E'_r)+i\Gamma_{tr}/2}, \tag{2.10}$$

$$\sigma_{nt}(E) = \sigma_{nn}(E) + \sigma_{n\gamma}(E) + \sigma_{nf}(E), \tag{2.11}$$

$$E'_r = E_r + \frac{\Gamma_{nr}}{2P_l(|E_r|)}\left[S_l(|E_r|) - S_l(E)\right]. \tag{2.12}$$

Although not explicitly noted, the resonance energies E_r and associated widths all pertain to a particular (l,s,J) index set. For clarity, these indices have been dropped from the notations.

The expression of the level-shifted energies varies slightly from its theoretical definition of expression (1.26). For channels concerned with the radiative capture and fission reaction, the boundary condition and the level-shift factor are entirely neglected. For channels concerned with the elastic reaction, the level-shift is not neglected but the boundary conditions are chosen level by level.

Finally, one has to note a major difference with the theoretical presentation and derivation of the Multi-Level Breit-Wigner formalism I talked about in the previous chapter. Namely, the radiative capture and fission cross-sections presented here do not account for interference between resonances.

2.1.3 Reich-Moore cross-section formulae

The formulae are :

$$\sigma_{nf}(E) = \frac{4\pi}{k^2}\sum_{(l,s,J)} g_J\left(|\rho_{na}|^2 + |\rho_{nb}|^2\right), \tag{2.13}$$

$$\sigma_{nn}(E) = \frac{4\pi}{k^2}\sum_{(l,s,J)} g_J\left(\sin^2(\phi_l) + \Re(\rho_{nn}^{(l,s,J)}\exp(-2i\phi_l)) - \Re(\rho_{nn}^{(l,s,J)}) + \left|\rho_{nn}^{(l,s,J)}\right|^2\right), \tag{2.14}$$

$$\sigma_{nt}(E) = \frac{4\pi}{k^2}\sum_{(l,s,J)} g_J\left(\sin^2(\phi_l) + \Re(\rho_{nn}^{(l,s,J)}\exp(-2i\phi_l))\right), \tag{2.15}$$

$$\sigma_{n\gamma}(E) = \frac{4\pi}{k^2}\sum_{(l,s,J)} g_J\left(\Re(\rho_{nn}^{(l,s,J)}) - \left|\rho_{nn}^{(l,s,J)}\right|^2\right) - \sigma_{nf}(E). \tag{2.16}$$

The matrix ρ appearing in these formulae, as well as the reduced R-matrix $\widehat{R}$ on which it is defined both have at most three entries here. These are the elastic entry noted n, the fission A entry noted a, and the fission B entry noted b. Here again I will drop the (l,s,J) index set for clarity, although it is important to keep in mind that there is a matrix ρ and a reduced matrix $\widehat{R}$ for each index set (l,s,J). We recall their respective expressions :

$$\rho = Id - \left(Id - iP^{1/2}\widehat{R}P^{1/2}\right)^{-1}, \tag{2.17}$$

$$\widehat{R}_{cd} = \sum_r \frac{\gamma_{cr}\gamma_{dr}}{E_r - E - i\Gamma_{\gamma r}/2}, \tag{2.18}$$

where c and d are generic indices that are either n, a or b.

Let us also note that there is no level-shift on the resonance energies. This results from the simplification described at the end of the theoretical derivation of the Reich-Moore formalism. Namely, the difference between boundary conditions B_c and level-shift factor S_c is taken to be zero.

2.1.4 Quick comparison of the cross-section formulae

We can already see similarities and differences between the formulae of the two formalisms. The elastic cross-sections written in terms of ρ are, not surprisingly, very close to each other. The differences lie in the definition of ρ which in the Multi-Level Breit-Wigner case is a single sum term, whereas it involves a matrix inversion for the Reich-Moore case.

The radiative capture and fission cross-sections are very different. On one hand, the practical Multi-Level Breit-Wigner formalism formulae for both these cross-sections are not even really "Multi-Level". Interference cross terms have been neglected from the definition of $\sigma_{cc'}$ of expression (1.28). On the other hand, for the Reich-Moore formalism formulae, the fission cross-section is obtained from a summation from two different channels. The multiplicity of these channels is a key component of this formalism and allows for a better description of the complexity of the fission phenomenon. The radiative capture cross-section is obtained by a perturbative treatment. It was initially separated during the approximations leading to the Reich-Moore formalism cross-section expressions.

Finally, in the Multi-Level Breit-Wigner formalism case, the total cross-section is obtained from a summation of the partial cross-sections. In the Reich-Moore formalism case, it is obtained with a formula involving some elements of the ρ matrix. It is worth mentioning that there exist other strictly equivalent formulations where an intermediary absorption cross-section is defined. I have chosen to only include here the formulae I will be working with later.

2.2 Specification of the nucleus and resonance data

The quantities of interest that occur in the cross-sections are provided in ENDF resonance data files. The general description of such files can be found in [14]. Notably, the format of the resonance data files may vary for different formalisms. Interestingly, the parameters used in Multi-Level Breit-Wigner and Reich-Moore formalisms are very similar. I provide here a short description of their important elements.

The mass of the target nucleus as well as the scattering radius are provided in the beginning of the resonance file. A set of flags indicates which radius to utilise in the penetration, level-shift and phase-shift factors.

The number of orbital quantum number l taken into account in the cross-section formulae is then specified. For each of these values of l, a list of resonances is provided. They all pertain

to a particular pack of resonances (identified by a triplet (l, s, J) as I mentioned before). They are individually characterized by their energy and a set of reaction widths. Intuitively, these specify the magnitude and importance of a reaction for that particular resonance. The usual ENDF notation for the parameters characterizing a resonance of index r are, E_r the **energy of the resonance** r, GX_r the **reaction width** X of the resonance r. X is a placeholder for one of the different reactions considered. Usually, we note GN_r the elastic width, GG_r the radiative capture width, GT_r the total width, and GF_r the fission width if relevant.

These parameters correspond to the evaluation of the widths noted Γ_{xr} at the energy of the resonance they belong to. Namely, if we recall that the widths hide an energy dependency :

$$\mathrm{GN}_r = \Gamma_{nr}(E_r) = 2\gamma_{nr}^2 P_l(E_r), \tag{2.19}$$
$$\mathrm{GF}_r = \Gamma_{fr}(E_r) = 2\gamma_{fr}^2, \tag{2.20}$$
$$\mathrm{GG}_r = \Gamma_{\gamma r}(E_r) = 2\gamma_{\gamma r}^2, \tag{2.21}$$
$$\mathrm{GT}_r = \Gamma_{nr}(E_r) + \Gamma_{fr}(E_r) + \Gamma_{\gamma r}(E_r) = 2\gamma_{nr}^2 P_l(E_r) + 2\gamma_{fr}^2 + 2\gamma_{\gamma r}^2. \tag{2.22}$$

We have written here the fact that the penetration for fission and radiative capture is always considered constant equal to 1. From these expressions, one can obtain the reduced widths γ_{xr}. These can in turn be used to compute the widths Γ_{xr} as needed.

2.3 Choice of notation for the scattering factors in this manuscript

As a final point, I would like to comment on a choice of notation. The penetration factors as they appear in (2.19) are noted in accordance with the definition of the ENDF formulae in [14]. A more correct notation, in my opinion, would be to first write

$$\begin{aligned} P_l(ka) &= P_l\left(\frac{M}{M+m_n}\frac{\sqrt{2m_nE}}{\hbar}a\right) \\ &= P_l\left(\frac{M}{M+m_n}\frac{\sqrt{2m_n}}{\hbar}a\sqrt{E}\right). \end{aligned}$$

In my work, when studying a pack and having fixed the value of a, I will note as often as possible :

$$P_l(\beta\sqrt{E}) \text{ with } \beta := \frac{M}{M+m_n}\frac{\sqrt{2m_n}}{\hbar}a. \tag{2.23}$$

Similarly, it is sometimes useful to replace k by its expression in terms of $\sqrt{E}$ in formulae. I will note

$$k = \alpha\sqrt{E} \text{ with } \alpha := \frac{M}{M+m_n}\frac{\sqrt{2m_n}}{\hbar}. \tag{2.24}$$

Chapter 3

Mathematical tools

This chapter is a standalone section that can be read almost separately from the rest of this manuscript. I will describe here the mathematical tools that I will repeatedly use during my work. They mainly concern rational functions and root-finding algorithms.

3.1 Summary of properties of rational functions

A vast portion of my work is devoted to the study of rational functions. A rational function is the quotient of two polynomial functions. I will list hereby some properties and simple results that will be useful in the following. Proofs of theorems and their corollaries can be found in [54].

3.1.1 Partial fraction decomposition

One of the most interesting properties of rational functions is the partial fraction decomposition theorem. I give here a simplified version in a set of cases of particular interest for my work.

Let f be a complex-valued polynomial (its coefficients are complex numbers) of degree m, and let g be a complex-valued polynomial of degree n. We assume that $m \leq n$, that the roots of g are all simple roots, and that none of these roots are roots of f. Then, there exists a set of n complex numbers (z_k) called poles (the roots of g) and n complex numbers (a_k) called residues, such that, for any complex number z,

$$\frac{f(z)}{g(z)} = c + \sum_k \frac{a_k}{z - z_k} \tag{3.1}$$

with c the remainder of the fraction, computed as the limit on the real axis of :

$$c = \lim_{x \to \pm\infty} \frac{f(x)}{g(x)}. \tag{3.2}$$

If $\deg(f) < \deg(g)$ then the remainder c is zero. In any case, the (a_k) are computed by

$$a_k = \frac{f(z_k)}{g'(z_k)}. \tag{3.3}$$

Note that if one of the root of g was also a root of f, the corresponding residue would be 0 and then the contribution to the sum in (3.1) would be 0.

3.1.2 Coprime polynomials

When working with the partial fraction decomposition theorem, it is important to ensure that the numerator and denominator polynomials have no common roots. If they share some roots, we have just seen that the partial fraction decomposition will have too many terms.

Just as with rational numbers, we ought to simplify the polynomial fractions we work with. Like integers, polynomial functions admit a unique prime factor decomposition (up to a multiplicative constant). Namely, any complex valued polynomial $f(z)$ of degree n admits a decomposition as a product of n prime factors of the form $(z - z_k)$, $z_k \in \mathbb{C}$, $1 \leq k \leq n$. The z_k are the roots of the polynomial.

We say that two polynomials are coprime when they admit no common prime factors. That is equivalent to saying that they have no common roots. Our work will focus on simplifying rational functions as much as possible before applying the partial fraction decomposition theorem.

3.1.3 Real valued polynomials with positive denominator

In our work, the rational functions that we will study often have additional properties. Firstly, the numerator is real-valued on the real axis. Secondly, the denominator is also real-valued and, additionally, positive on the real axis. With these hypotheses, we have additional results on the partial fraction decomposition theorem.

Let f and g be two non-zero polynomial functions. We assume that :

- f and g are real valued polynomials (their coefficients are real number),
- $\deg(f) < \deg(g)$,
- all the roots of g are simple roots,
- $g(x) > 0, \forall x \in \mathbb{R}$.

The positivity of g on the real axis implies that it is of even degree, which we will denote $2n$. Indeed if its degree was odd, it would necessarily change sign somewhere on the real axis. Furthermore, the fact that g is real-valued implies that the $2n$ complex roots of g are all conjugated by pair. We denote them $(z_1, \cdots, z_n, \overline{z_1}, \cdots, \overline{z_n})$.

We have the following partial fraction decomposition, for any complex number z :

$$\frac{f(z)}{g(z)} = \sum_k \frac{a_k}{z - z_k} + \sum_k \frac{b_k}{z - \overline{z_k}} \tag{3.4}$$

with

$$a_k = \frac{f(z_k)}{g'(z_k)}, \tag{3.5}$$

$$b_k = \frac{f(\overline{z_k})}{g'(\overline{z_k})}. \tag{3.6}$$

Under the hypothesis that f and g are real-valued we can further rewrite (3.6) as

$$b_k = \frac{f(\overline{z_k})}{g'(\overline{z_k})} = \frac{\overline{f(z_k)}}{\overline{g'(z_k)}} = \overline{a_k}. \tag{3.7}$$

The two important results are, for any complex number z :

$$\frac{f(z)}{g(z)} = \sum_k \frac{a_k}{z - z_k} + \sum_k \frac{\overline{a_k}}{z - \overline{z_k}}, \tag{3.8}$$

and in particular for any real number x,

$$\frac{f(x)}{g(x)} = \Re\left[\sum_k \frac{2a_k}{x - z_k}\right]. \tag{3.9}$$

3.1.4 Product of two partial fraction decompositions

The case will often arise that we have calculated separately the partial fraction decomposition of two rational functions and that we need to compute their product. The product of two rational functions is also a rational function. As such it also admits a partial fraction decomposition.

It is possible to give directly the partial fraction decomposition of the product from the partial fraction decomposition of each term of the product. I propose here some formulae for specific cases that will arise later on.

Let $(x_1, \cdots, x_m)$ be m complex poles and $(a_1, \cdots, a_m)$ be their residues for the first partial fraction decomposition. Let $(y_1, \cdots, y_n)$ be n complex poles and $(b_1, \cdots, b_n)$ be their residues for the second partial fraction decomposition.

We assume the restrictive condition that no x_k is equal to an y_l. This turns out to be true in all applications of interest in this work. In the most general case, poles with multiplicity could arise and make the situation somewhat more complicated.

We have the following relations, for any complex number z :

$$\begin{aligned}\left(\sum_{k=1}^{m} \frac{a_k}{z - x_k}\right)\left(\sum_{l=1}^{n} \frac{b_l}{z - y_l}\right) &= \sum_{k=1}^{m}\sum_{l=1}^{n}\left(\frac{a_k}{z - x_k}\frac{b_l}{z - y_l}\right) \\ &= \sum_{k=1}^{m}\sum_{l=1}^{n}\left(\frac{a_k b_l}{x_k - y_l}\left[\frac{1}{z - x_k} - \frac{1}{z - y_l}\right]\right)\end{aligned}$$

$$= \sum_{k=1}^{m} \sum_{l=1}^{n} \frac{\frac{a_k b_l}{x_k - y_l}}{z - x_k} + \sum_{k=1}^{m} \sum_{l=1}^{n} \frac{\frac{a_k b_l}{y_l - x_k}}{z - y_l}$$
$$= \sum_{k=1}^{m} \frac{a_k \sum_l \frac{b_l}{x_k - y_l}}{z - x_k} + \sum_{l=1}^{n} \frac{b_l \sum_k \frac{a_k}{y_l - x_k}}{z - y_l}. \tag{3.10}$$

A particular case is when $m = n$ and the (y_l) and (b_l) are exact complex conjugates of the (x_k) and (a_k). Then we have the following equality for any complex number z :

$$\left(\sum_{k=1}^{m} \frac{a_k}{z - x_k} \right) \left(\sum_{l=1}^{m} \frac{\overline{a_l}}{z - \overline{x_l}} \right) = \sum_{k=1}^{m} \frac{a_k \sum_l \frac{\overline{a_l}}{x_k - \overline{x_l}}}{z - x_k} + \sum_{l=1}^{m} \frac{\overline{a_l} \sum_k \frac{a_k}{\overline{x_l} - x_k}}{z - \overline{x_l}}. \tag{3.11}$$

In particular for any real number x,

$$\left(\sum_{k=1}^{m} \frac{a_k}{x - x_k} \right) \left(\sum_{l=1}^{m} \frac{\overline{a_l}}{x - \overline{x_l}} \right) = \Re \left[\sum_{k=1}^{m} \frac{2a_k \sum_l \frac{\overline{a_l}}{x_k - \overline{x_l}}}{x - x_k} \right]. \tag{3.12}$$

3.2 Root-finding algorithms

I have just described the principles of the partial fraction decomposition theorem of rational functions. One of the central issues to be able to give the partial fraction decomposition of these functions is to find the roots of their denominator polynomial.

The problem of finding the roots of a polynomial has been studied extensively in mathematics. In my work, I have investigated several methods to solve this problem. There exist multiple families of root-finding algorithms each adapted to tackle different issues. The ones that I have studied can be qualitatively split in three categories, namely :

- Companion matrix and eigenvalue problem formulation,
- Simultaneous root-finding algorithms,
- Newton type algorithms.

I will now provide a short description of the advantages and shortcomings of each family and explain my final choice of a Newton type algorithm.

3.2.1 Companion matrix and eigenvalue problem formulation

The matrix formulation consists in assembling a matrix whose eigenvalues will be the roots of the polynomial we are working with. Then, one can apply a power iteration approach to find the largest eigenvalue of the matrix and therefore a root of the polynomial. The Frobenius companion matrix is a constructive example of such matrix. It is readily built from the values of the coefficients of the polynomial we want to find the roots of. The size of the matrix will be that of the degree of the polynomial. This approach is somewhat interesting for small degree polynomials with well conditioned coefficients.

The root elimination is somewhat convoluted. A first idea is to compute (with good numerical accuracy) the eigenvector corresponding to the eliminated eigenvalue and work in some new restricted space. Numerical accuracy limits the application of this method past the first few eigenvalues. A second idea is to simplify the polynomial with the newly found roots and to form a new companion matrix. The numerical accuracy problems arise again and the computation of more than a few eigenvalues is very difficult. In general, finding the complete spectrum of a matrix is a complicated mathematical problem when the matrix is large. There exist less naive approaches which I will discuss briefly shortly thereafter [55].

3.2.2 Simultaneous root-finding algorithms

The simultaneous root-finding algorithms seems interesting in that they do not require some sort of successive root elimination. Indeed, successive elimination may lead to catastrophic error accumulation and propagation, so that only the first few roots can be computed with good accuracy.

There exist algorithms for finding all the eigenvalues of matrices (QR algorithm [56, 57]) at the same time but a closer look reveal that these still involve some form of sequential operations. This does not solve the problems of error accumulation. Moreover, as far as I know, these matrix algorithms require again to have computed the coefficients of the polynomial. I did not consider them for my work.

The Durand-Kerner method [58, 59] finds simultaneously the roots of polynomials without particularizing any of them. Interestingly for my work, the Durand-Kerner approach only requires to be able to compute the polynomial and its derivative (more precisely its logarithmic derivative). However, it appeared numerically unstable for the polynomials of high degree I studied so I did not investigate it further than for very simple cases.

3.2.3 Newton-Raphson algorithm

The family of algorithms I eventually settled with are the Newton type algorithms, and particularly the Newton-Raphson algorithm [60]. The general idea is to start from a guess of a root and to apply the iteration

$$x_{k+1} = x_k - \frac{P(x_k)}{P'(x_k)} \quad \text{with} \quad x_0 \quad \text{some guess about a root.} \tag{3.13}$$

There exist quite a few variations of this algorithm where the update term on the right-hand side differs but the general idea is always to have an update term that will be zero when we reach a root. Moreover, we wish the iteration to be stable in the vicinity of a root. Of all the variations that have been developed and studied through the years, the one presented above is one of the simplest. It requires a good knowledge of the logarithmic derivative of the polynomial we are working with, but no particular knowledge of the individual coefficients of that polynomial.

In the applications of my work, this was the key factor for choosing this family of algorithms. We have to keep in mind that there are a few issues with the Newton-Raphson algorithm.

First, the choice of the initial guess is very important for convergence. Indeed, there exist some initial points for which the algorithm will never converge. In my work I did not encounter this issue, provided the initial guesses were carefully chosen. As such, some insight on the particular polynomial we are working with goes a long way and the initial guesses are integral part of the work I will present.

Second, the root elimination is not necessarily trivial. If we do not have access to the coefficients of the polynomial, we cannot simplify it to eliminate the root. I consider for instance a polynomial of degree 3 with a trivial root x_0. In such a case, it is somewhat common knowledge that you can divide the polynomial by $X - x_0$ and obtain a polynomial of degree 2 with the two remaining roots to find. This procedure requires however the expression of the coefficients of the polynomial.

To solve this second concern, H.J. Maehly suggested an additional procedure to eliminate formally the roots by modifying slightly the Newton-Raphson algorithm [61, 62].

Let us assume that we have found the root z_0 of some polynomial P. The idea is to write the Newton-Raphson algorithm for the formal polynomial $P(X)/(X - z_0)$. The Newton-Raphson iteration becomes

$$\begin{aligned} x_{k+1} &= x_k - \frac{\dfrac{P(x_k)}{x_k - z_0}}{\dfrac{d}{dX}\left(\dfrac{P(X)}{X - z_0}\right)(x_k)} \\ &= x_k - \frac{\dfrac{P(x_k)}{x_k - z_0}}{\dfrac{P'(x_k)}{x_k - z_0} - \dfrac{P(x_k)}{(x_k - z_0)^2}} \\ &= x_k - \frac{1}{\dfrac{P'(x_k)}{P(x_k)} - \dfrac{1}{x_k - z_0}}. \end{aligned} \tag{3.14}$$

Interestingly, we find a form in which we still only need to be able to compute the logarithmic derivative of P. We add a second term which can be thought of as a repulsive term so as to avoid converging to an already found root. This idea is readily extended to multiple found roots by just adding to the denominator of (3.14) a repulsive term for each found root.

This is the algorithm I adopted in my work. The main motivation was my lack of access to the coefficients of the polynomials I had to find the roots of. Thankfully, it worked very well in all applications, provided good initial guesses are given. The challenges were to choose these guesses and, mainly, to find a way to evaluate the term P'/P in a numerically stable way.

3.2.4 A word on roots with multiplicity

It is well known by mathematicians that a major issue for most algorithms concerns roots with multiplicity. In this case all theoretical results on rates of convergence or stability of algorithms are much worse than for simple roots. I have not discussed this issue because I was always able to ensure in some way that the polynomials I worked with had only simple roots. As a side-note, the Newton-Raphson algorithm presented just above, in combination with Maehly's procedure, is still able to compute the roots with multiplicity but both the convergence rate and the numerical accuracy are greatly affected.

Part II

Theoretical study of the multipole representation

Chapter 1

Study of the multipole representation of the Multi-Level Breit-Wigner cross-sections

My goal in this chapter is to show that the elastic, radiative capture, fission - when relevant - and total cross-sections of the Multi-Level Breit-Wigner formalism can be written under the so-called multipole representation :

$$\sigma_{nx}(E) = \frac{4\pi}{k^2}\Re\left(\sum_p \frac{a_p + b_p \exp(-2i\phi_l)}{\sqrt{E} - z_p}\right) \tag{1.1}$$

where x is one of the aforementioned interaction and k is related to E by (2.24) from Part I.

The possibility of such representation has already been studied and proven in [19]. I will show that the number of so-called pole terms in the sum of (1.1) can be reduced compared to these previous results. Broadly, this chapter will involve the close study of the energy dependencies in the cross-sections formulae and the application of the partial fraction decomposition theorems provided in the mathematical tools chapter.

The formulae provided for the reconstruction of the cross-sections with the Multi-Level Breit-Wigner formalism can be found in [14]. As mentioned before, the contribution of each pack can be computed separately. The formulae for the contribution of a pack indexed (l, s, J) containing N resonances are :

$$\sigma_{nn}^{(l,s,J)}(E) = \frac{4\pi}{k^2}\sum_{(l,s,J)} g_J\left[\sin^2(\phi_l) + \Re\big(\rho_{nn}^{(l,s,J)}\exp(-2i\phi_l)\big) - \Re(\rho_{nn}^{(l,s,J)}) + \left|\rho_{nn}^{(l,s,J)}\right|^2\right], \tag{1.2}$$

$$\sigma_{nf}^{(l,s,J)}(E) = \frac{\pi}{k^2}\sum_{(l,s,J)} g_J \sum_r \frac{\Gamma_{fr}\Gamma_{nr}}{(E - E_r')^2 + \Gamma_{tr}^2/4}, \tag{1.3}$$

$$\sigma_{n\gamma}^{(l,s,J)}(E) = \frac{\pi}{k^2}\sum_{(l,s,J)} g_J \sum_r \frac{\Gamma_{\gamma r}\Gamma_{nr}}{(E - E_r')^2 + \Gamma_{tr}^2/4}, \tag{1.4}$$

$$\rho_{nn}^{(l,s,J)}(E) = \frac{i}{2}\sum_r \frac{\Gamma_{nr}}{(E - E'_r) + i\Gamma_{tr}/2}, \tag{1.5}$$

$$\sigma_{nt}^{(l,s,J)}(E) = \sigma_{nn}^{(l,s,J)}(E) + \sigma_{n\gamma}^{(l,s,J)}(E) + \sigma_{nf}^{(l,s,J)}(E). \tag{1.6}$$

The elastic and total widths hide some energy dependency. Given my choice of notation described in section 2.3 of Part I :

$$\Gamma_{nr} = P_l\big(\beta\sqrt{E}\big)\frac{\mathrm{GN}_r}{P_l\big(\beta\sqrt{|E_r|}\big)}, \tag{1.7}$$

$$\Gamma_{tr} = \mathrm{GT}_r - \left(\frac{P_l\big(\beta\sqrt{|E_r|}\big) - P_l\big(\beta\sqrt{E}\big)}{P_l\big(\beta\sqrt{|E_r|}\big)}\right)\mathrm{GN}_r. \tag{1.8}$$

On the contrary, the radiative capture and fission widths are independent of the energy :

$$\Gamma_{fr} = \mathrm{GF}_r, \tag{1.9}$$

$$\Gamma_{\gamma r} = \mathrm{GG}_r. \tag{1.10}$$

Furthermore, there is a shift on the resonance energies to use :

$$E'_r = E_r + \left(\frac{S_l\big(\beta\sqrt{|E_r|}\big) - S_l\big(\beta\sqrt{E}\big)}{2P_l\big(\beta\sqrt{|E_r|}\big)}\right)\mathrm{GN}_r. \tag{1.11}$$

These energy dependencies through the penetration and level-shift factors are the source of the complexity of the Multi-Level Breit-Wigner multipole representation.

I describe in this chapter the approach I followed to give the exact mathematical representation of the Multi-Level Breit-Wigner cross-sections. First I will focus on two simplified situations for which I will derive a multipole representation. Then, I will show the need to study the mathematical properties of the penetration and level-shift factors. I will give a summary and proof of the results I found during this study. Finally I will show that we can give an exact multipole representation (mathematical equivalency with the formulae) of the Multi-Level Breit-Wigner cross-sections with less poles than initially surmised.

We will omit the index (l, s, J) from now on as we will focus on a particular pack.

1.1 From a simplified setting to the full complexity of the MLBW formalism

1.1.1 Neglecting the energy dependency of the widths and the level-shift of the resonances

As a first step, I neglected all energy dependencies of the reaction widths. The elastic cross-section formula is more complicated than the radiative capture and fission cross-section

formulae. Indeed, we will see that the modulus square of the ρ_{nn} term in (1.2) imposes additional calculations.

For now we will focus on these two latter partial cross-section formulae. We will consider the index x to designate either of them as they are perfectly identical to the width involved. Neglecting the hidden energy dependencies of Γ_{nr}, Γ_{tr} and E'_r, we get

$$\sigma_{nx}(E) = \frac{\pi}{k^2} \sum_{r=1}^{N} \frac{\mathrm{GN}_r \mathrm{GX}_r}{(E - E_r)^2 + \mathrm{GT}_r^2/4}. \tag{1.12}$$

First, we see that the contribution of each resonance is linearly added to the contribution of the pack. This is not the case for elastic cross-section (and through it the total cross-section). This property is very useful for the multipole representation as it allows us to work separately on each resonance contribution.

Second, in our simplified setting, we can immediately give a partial fraction decomposition of each term as they are all simple rational functions. Indeed we have for any resonance r :

$$\frac{\mathrm{GN}_r\ \mathrm{GX}_r}{(E - E_r)^2 + \mathrm{GT}_r^2/4} = \frac{\mathrm{GN}_r \mathrm{GX}_r / i\mathrm{GT}_r}{(E - E_r) - i\mathrm{GT}_r/2} - \frac{\mathrm{GN}_r \mathrm{GX}_r / i\mathrm{GT}_r}{(E - E_r) + i\mathrm{GT}_r/2}. \tag{1.13}$$

This is one of the simplest case we will encounter. The rational function on the left hand side is the quotient of constant polynomial function with a polynomial function of degree 2. The roots of the denominator polynomial function are trivially computed. Given that they are not identical, we can give the partial fraction decomposition on the right hand side. This is already what we could call a multipole representation. However we have neglected energy dependencies, which unsurprisingly simplifies a lot the study.

Furthermore, for the Doppler broadening we are interested in, it is more convenient to work with $\sqrt{E}$. The idea to get an expression with $\sqrt{E}$ is to remark that the right-hand side is actually the real part of one term :

$$\frac{\mathrm{GN}_r \mathrm{GX}_r / i\mathrm{GT}_r}{(E - E_r) - i\mathrm{GT}_r/2} - \frac{\mathrm{GN}_r \mathrm{GX}_r / i\mathrm{GT}_r}{(E - E_r) + i\mathrm{GT}_r/2} = \Re\left[\frac{2\mathrm{GN}_r \mathrm{GX}_r / i\mathrm{GT}_r}{(E - E_r) - i\mathrm{GT}_r/2}\right]. \tag{1.14}$$

Then we look at the term inside the real part as a rational function of $\sqrt{E}$ and not simply E. It is again a rational function with a denominator polynomial of degree 2 in $\sqrt{E}$. Its roots are the complex roots of $E_r + i\mathrm{GT}_r/2$. We note u_r^+ the root with positive real value and u_r^- the root with negative real value. Therefore we have

$$\frac{\mathrm{GN}_r \mathrm{GX}_r}{(E - E_r)^2 + \mathrm{GT}_r^2/4} = \Re\left[\frac{2\mathrm{GN}_r \mathrm{GX}_r / i\mathrm{GT}_r}{(E - E_r) - i\mathrm{GT}_r/2}\right] \tag{1.15}$$

$$= \Re\left[\frac{(\mathrm{GN}_r \mathrm{GX}_r)/(i\mathrm{GT}_r u_r^+)}{\sqrt{E} - u_r^+} + \frac{(\mathrm{GN}_r \mathrm{GX}_r)/(i\mathrm{GT}_r u_r^-)}{\sqrt{E} - u_r^-}\right]. \tag{1.16}$$

We then gather these terms to form the contribution of the pack :

$$\sigma_{nx}(E) = \frac{\pi}{k^2} \sum_{r=1}^{N} \Re\left[\frac{(\mathrm{GN}_r \mathrm{GX}_r)/(i\mathrm{GT}_r u_r^+)}{\sqrt{E} - u_r^+} + \frac{(\mathrm{GN}_r \mathrm{GX}_r)/(i\mathrm{GT}_r u_r^-)}{\sqrt{E} - u_r^-}\right]. \tag{1.17}$$

This is the typical form we wish to achieve. We can see that each resonance can be represented with two pole terms. In the case we do not neglect energy dependency, more poles will be needed to exactly represent all resonances. However the two main points that we have shown here are true in the non-simplified situation. First, for the radiative capture and fission cross-section, each term can be computed separately. Second, the problem lies in computing the partial fraction decomposition of each of these terms. Here it was quite straightforward. This will not be the case later. Let us move to a slightly more complicated situation and see where the complexity arises from.

1.1.2 Preliminary study of the multipole representation of the radiative capture and fission cross-sections for a pack of quantum orbital number $l = 0$

The elastic width has a hidden energy dependency that cannot be neglected for a good representation of the cross-sections. This energy dependency is done through the penetration factor P_l, which is always a rational function of $\sqrt{E}$.

We have seen that the exact expression of the penetration factors involves the definition of a radius, either the so-called channel radius noted a_c or the scattering radius noted AP. Thankfully, in the case of a pack of quantum orbital number $l = 0$, the notations are lighter because much can be simplified in the expressions of the scattering factors from Table 1.1 of Part I. Namely,

$$\Gamma_{nr} = \mathrm{GN}_r \frac{\sqrt{E}}{\sqrt{|E_r|}}, \tag{1.18}$$

$$\Gamma_{tr} = \mathrm{GT}_r - \mathrm{GN}_r + \mathrm{GN}_r \frac{\sqrt{E}}{\sqrt{|E_r|}}, \tag{1.19}$$

$$E'_r = E_r. \tag{1.20}$$

There is no level-shift and the choice of the radius has no importance since it cancels between $P_l\big(\beta\sqrt{E}\big)$ and $P_l\big(\beta\sqrt{|E_r|}\big)$.

The contribution of a resonance for either the fission or radiative capture cross-section can be extended as

$$\frac{\Gamma_{xr}\Gamma_{nr}}{(E - E'_r)^2 + \Gamma_{tr}^2/4} = \frac{\mathrm{GX}_r\mathrm{GN}_r\sqrt{E}/\sqrt{|E_r|}}{(E - E_r)^2 + \left(\mathrm{GT}_r - \mathrm{GN}_r + \mathrm{GN}_r\sqrt{E}/\sqrt{|E_r|}\right)^2/4}.$$

The situation is already significantly more complicated than before. We cannot do separately a first partial fraction decomposition in term of E then a second one in term of $\sqrt{E}$ as we did previously when neglecting energy dependencies. The numerator polynomial is not a constant : it is a polynomial of degree 1 in $\sqrt{E}$. The denominator is neither a polynomial in E. It is a polynomial in $\sqrt{E}$ of degree 4.

We can however use the second property of rational function of subsection 3.1.3 of Part I. The numerator and denominator polynomials are

$$f(u) := \left(\mathrm{GX}_r\mathrm{GN}_r/\sqrt{|E_r|}\right) u, \tag{1.21}$$

$$g(u) := (u^2 - E_r)^2 + \left(\mathrm{GT}_r - \mathrm{GN}_r + \left(\mathrm{GN}_r/\sqrt{|E_r|}\right) u\right)^2 /4 \tag{1.22}$$

with $u = \sqrt{E}$.

Their coefficients are all real numbers. g is positive on the real axis provided that the two square terms do not cancel at the same time. The case can arise that this is not true but it is rather pathological and I exclude it from the study. The numerator and denominator are coprime polynomials because the only root of the numerator is 0 and it is not a root of the denominator.

The hypothesis of subsection 3.1.3 of Part I being verified, we note $u_r^{(1)}$, $u_r^{(2)}$ and their complex conjugates the 4 poles of g. We note $a_r^{(1)}$,$a_r^{(2)}$ and their complex conjugates the 4 corresponding residues. We can then write

$$\begin{aligned}\frac{\mathrm{GX}_r\mathrm{GN}_r\sqrt{E}/\sqrt{|E_r|}}{(E-E_r)^2 + \left(\mathrm{GT}_r - \mathrm{GN}_r + \mathrm{GN}_r\sqrt{E}/\sqrt{|E_r|}\right)^2/4} &= \frac{a_r^{(1)}}{\sqrt{E} - u_r^{(1)}} + \frac{a_r^{(2)}}{\sqrt{E} - u_r^{(2)}} \\ &\quad + \frac{\overline{a_r^{(1)}}}{\sqrt{E} - \overline{u_r^{(1)}}} + \frac{\overline{a_r^{(2)}}}{\sqrt{E} - \overline{u_r^{(2)}}} \\ &= \Re\left[\frac{2a_r^{(1)}}{\sqrt{E} - u_r^{(1)}} + \frac{2a_r^{(2)}}{\sqrt{E} - u_r^{(2)}}\right].\end{aligned}$$

We find back the very interesting result of the simplified case (1.17). The resonance contribution can be given a multipole representation in the form of the real part of only two pole terms. However, the poles are not as simple as before and one needs to perform a root-finding algorithm on a polynomial of degree 4. The Newton-Raphson algorithm I have proposed in subsection 3.2.3 performs very well on this kind of problem.

We have shown here that the multipole representation of the radiative capture and fission cross-section are relatively straightforward to compute for packs of quantum number $l = 0$. We need only two poles per resonance. We will now study the more general case and show that we need to add more poles per resonance to give an exact multipole representation of each resonance term.

1.1.3 Preliminary study of the multipole representation of the radiative capture and fission cross-sections for a pack of quantum orbital number $l > 0$

Rational function associated with each resonance term

R.N. Hwang was well aware of the energy dependencies hidden in the scattering factors. However, he remarked that since the penetration and level-shift factors were rational functions of $\sqrt{E}$, the resonance terms would still be rational functions. We have just seen that the $l = 0$ situation is not particularly difficult. The general energy dependency for higher $l > 0$ is much more complicated.

Let us unmask the hidden energy dependency to see the full problem we have to tackle. We start from a resonance term,

$$T_r(E) := \frac{\Gamma_{nr}\Gamma_{xr}}{(E - E'_r)^2 + \Gamma_{tr}^2/4} = \frac{\Gamma_{nr}\Gamma_{xr}}{|(E - E'_r) + i\Gamma_{tr}/2|^2}. \tag{1.23}$$

We note $u := \sqrt{E}$. Again we adopt the notations of subsection 3.1.3 of Part I for β and the scattering factors. The expanded expression of $T_r(E)$ becomes

$$\begin{aligned} T_r(E) &= \frac{\dfrac{\mathrm{GN}_r\mathrm{GX}_r}{P_l(\beta\sqrt{|E_r|})}P_l(\beta u)}{\left|u^2 - E_r + \mathrm{GN}_r\dfrac{S_l(\beta u) - S_l(\beta\sqrt{|E_r|})}{2P_l(\beta\sqrt{|E_r|})} + i(\mathrm{GT}_r - \mathrm{GN}_r)/2 + i\mathrm{GN}_r\dfrac{P_l(\beta u)}{2P_l(\beta\sqrt{|E_r|})}\right|^2} \\ &= \frac{\dfrac{\mathrm{GN}_r\mathrm{GX}_r}{P_l(\beta\sqrt{|E_r|})}P_l(\beta u)}{\left|u^2 - E_r + i\mathrm{GT}_r/2 - \mathrm{GN}_r\dfrac{S_l(\beta\sqrt{|E_r|}) + iP_l(\beta\sqrt{|E_r|})}{2P_l(\beta\sqrt{|E_r|})} + \mathrm{GN}_r\dfrac{S_l(\beta u) + iP_l(\beta u)}{2P_l(\beta\sqrt{|E_r|})}\right|^2}. \end{aligned}$$

We adopt two additional notations, first the reduced elastic width given by

$$\gamma_{nr} := \sqrt{\frac{\mathrm{GN}_r}{2P_l\left(\beta\sqrt{|E_r|}\right)}}, \tag{1.24}$$

then the perturbed (complex valued) energy,

$$\widetilde{E_r} := E_r - i\mathrm{GT}_r/2 + \mathrm{GN}_r\frac{S_l\big(\beta\sqrt{|E_r|}\big) + iP_l\big(\beta\sqrt{|E_r|}\big)}{2P_l\big(\beta\sqrt{|E_r|}\big)}. \tag{1.25}$$

We can then write the previous expression in a cleaner way :

$$T_r(u) = \frac{2\gamma_{nr}^2\mathrm{GX}_r P_l(\beta u)}{\left|u^2 - \widetilde{E_r} + \gamma_{nr}^2\big(S_l(\beta u) + iP_l(\beta u)\big)\right|^2}. \tag{1.26}$$

For $l = 0$ the numerator and denominator of this expression are polynomial functions and we can proceed to the partial fraction decomposition. This is exactly what we did just previously. For $l > 0$, S_l and P_l are rational functions and the numerator and denominator are no more directly polynomial functions.

My aim will be to give an expression of $T_r(u)$ as a quotient of two polynomial functions. Moreover, I want these polynomial functions to be coprime with each other. Namely, I need to find a form in which the numerator and denominator of $T_r(u)$ are polynomials with no common roots. I will then be able to do a partial fraction decomposition, and therefore obtain a multipole representation.

First approach to the problem

P_l and S_l have a common denominator polynomial as seen in Table 1.1 of Part I. We note $S_l = s_l/q_l$ and $P_l = p_l/q_l$. To do the partial fraction decomposition of (1.26), we need to rewrite the expression as a quotient of polynomial functions. Let us examine it with our new notations :

$$T_r(u) = \frac{2\gamma_{nr}^2 \mathrm{GX}_r \dfrac{p_l(\beta u)}{q_l(\beta u)}}{\left| u^2 - \widetilde{E_r} + \gamma_{nr}^2 \dfrac{s_l(\beta u) + i p_l(\beta u)}{q_l(\beta u)} \right|^2}. \tag{1.27}$$

The natural approach that had been used up until now [19] is to multiply the numerator and denominator by q_l^2. This yields

$$T_r(u) = \frac{2\gamma_{nr}^2 \mathrm{GX}_r p_l(\beta u) q_l(\beta u)}{\left| q_l(\beta u) \left(u^2 - \widetilde{E_r} \right) + \gamma_{nr}^2 \left(s_l(\beta u) + i p_l(\beta u) \right) \right|^2}. \tag{1.28}$$

The polynomial q_l enters the modulus square as it has real coefficients and u is a real number.

We have for numerator and denominator polynomials :

$$f(u) := 2\gamma_{nr}^2 \mathrm{GX}_r p_l(\beta u) q_l(\beta u), \tag{1.29}$$

$$g(u) := \left| q_l(\beta u) \left(u^2 - \widetilde{E_r} \right) + \gamma_{nr}^2 \left(s_l(\beta u) + i p_l(\beta u) \right) \right|^2. \tag{1.30}$$

The degrees of these polynomials are found from the degrees of p_l, s_l and q_l given in expression (1.50) of Part I. Namely,

$$\deg(f) = \deg(p_l) + \deg(q_l) = 4l + 1, \tag{1.31}$$

$$\deg(g) = 2 \max \left(\deg(q_l) + 2, \max(\deg(s_l), \deg(p_l)) \right) = 4l + 4. \tag{1.32}$$

We have not verified that f and g have no common roots but it is still possible to give a partial fraction decomposition. However, there will be no guarantee that the number of poles and residues is the minimal one.

In [19], C. Jammes and R.N. Hwang have done this exact development to give a multipole representation of the fission and radiative capture cross-sections. They surmise that one needs $2l+2$ poles to represent a resonance term. However, they also found the peculiar property that the residues of some poles were very small.

This is typical of the fact that the numerator and denominator in the fraction (1.28) may have a common root. We have seen that, in in this case, the expression of the residue corresponding to this pole from expression (3.3) of Part I will be zero. Numerically it is not surprising that we do not obtain exactly zero but some float number really close to it.

My approach was to further study the property of the P_l and S_l factors. Indeed it seems that for $l > 0$ there is always some common roots between f and g defined in (1.29) and (1.30). I show in the next part that q_l and $s_l + ip_l$ do have common roots for $l > 0$. From that I will show that the expression (1.28) can be simplified. This confirms and explains the existence of poles with null residues. It also provides a way to circumvent this over-determination of the number of poles.

1.2 Study of the mathematical properties of the penetration, level-shift and phase-shift factors

1.2.1 General properties and need for a closer study

The scattering factors have well known expressions for the first values of l. I have gathered them in Table 1.1 of Part I. For higher values of l, a recursive formula is provided, namely for the penetration and level-shift factors,

$$P_{l+1}(\rho) = \frac{\rho^2 P_l(\rho)}{P_l^2(\rho) + \big(l+1-S_l(\rho)\big)^2}, \tag{1.33}$$

$$S_{l+1}(\rho) = \frac{\rho^2 \big(l+1-S_l(\rho)\big)}{P_l^2(\rho) + \big(l+1-S_l(\rho)\big)^2} - (l+1), \tag{1.34}$$

with initial conditions $P_0(\rho) = \rho$ and $S_0(\rho) = 0$.

l	$P_l(\rho)$	$S_l(\rho)$
0	ρ	0
1	$\dfrac{\rho^3}{\rho^2+1}$	$\dfrac{-1}{\rho^2+1}$
2	$\dfrac{\rho^5}{\rho^4+3\rho^2+9}$	$\dfrac{-3\rho^2-18}{\rho^4+3\rho^2+9}$

In the context of our study, we wish to have separate formulae for the numerator and denominator of these rational functions for any l. Let us assume that we have the following

fractional representation at rank l,

$$P_l(\rho) = \frac{p_l(\rho)}{q_l(\rho)}, \tag{1.35}$$

$$S_l(\rho) = \frac{s_l(\rho)}{q_l(\rho)}. \tag{1.36}$$

Writing such a fractional representation, we have further assumed that the denominator polynomials are identical for the penetration and the level-shift factors. This is visibly true for the first values of l as seen in Table 1.1. We will later prove that this holds at any value of l.

Let us inject the expressions (1.35) and (1.36) in (1.33) and (1.34) :

$$P_{l+1}(\rho) = \frac{\rho^2 \dfrac{p_l(\rho)}{q_l(\rho)}}{\left(\dfrac{p_l(\rho)}{q_l(\rho)}\right)^2 + \left((l+1) - \dfrac{s_l(\rho)}{q_l(\rho)}\right)^2} \tag{1.37}$$

$$= \frac{\rho^2 p_l(\rho) q_l(\rho)}{p_l^2(\rho) + \big((l+1)q_l(\rho) - s_l(\rho)\big)^2}, \tag{1.38}$$

$$S_{l+1}(\rho) = \frac{\rho^2 \left((l+1) - \dfrac{s_l(\rho)}{q_l(\rho)}\right)}{\left(\dfrac{p_l(\rho)}{q_l(\rho)}\right)^2 + \left((l+1) - \dfrac{s_l(\rho)}{q_l(\rho)}\right)^2} - (l+1) \tag{1.39}$$

$$= \frac{\rho^2 \big((l+1)q_l(\rho) - s_l(\rho)\big) q_l(\rho)}{p_l^2(\rho) + \big((l+1)q_l(\rho) - s_l(\rho)\big)^2} - (l+1). \tag{1.40}$$

We would be very pleased to announce that,

$$p_{l+1}(\rho) = \rho^2 p_l(\rho) q_l(\rho), \tag{1.41}$$

$$q_{l+1}(\rho) = p_l^2(\rho) + \big((l+1)q_l(\rho) - s_l(\rho)\big)^2, \tag{1.42}$$

$$s_{l+1}(\rho) = \rho^2 \big((l+1)q_l(\rho) - s_l(\rho)\big) q_l(\rho) - (l+1) q_{l+1}^2(\rho). \tag{1.43}$$

Unfortunately, we have no guarantee that p_{l+1} and q_{l+1} have no common roots with these expressions. As a matter of fact we can already see that these formulae do not give back the expressions of the numerator and denominators for $l \geq 1$. The expressions that are given here are actually already simplified. The computation with the formulae (1.41) to (1.43) would yield polynomials whose degrees approximately double at each iteration. I will now detail the derivation of the correct formulae, namely formulae that give a fractional representation with coprime numerator and denominator polynomials.

1.2.2 Induction proof of the properties of the level-shift and penetration factors

The forms of (1.33) and (1.34) strongly suggest studying the recursive sequence of rational functions $(S_l - (l+1)) + iP_l$. The induction formula for these rational functions is given by

$$\big(S_{l+1}(\rho) - (l+2)\big) + iP_{l+1}(\rho) = \frac{\rho^2\big((l+1) - S_l(\rho) + iP_l(\rho)\big)}{P_l^2(\rho) + \big(l+1-S_l(\rho)\big)^2} - (2l+3) \tag{1.44}$$

$$= \frac{-\rho^2}{\big(S_l(\rho) - (l+1)\big) + iP_l(\rho)} - (2l+3). \tag{1.45}$$

For any $l \geq 0$, $(S_l - (l+1)) + iP_l$ is a rational function of ρ. We note g_l/h_l a possible fractional representation of this rational function, with g_l and h_l two coprime polynomials. We have a choice of a multiplicative constant to define g_l and h_l, we decide that h_l will have a leading coefficient equal to 1. We are going to prove the following properties of g_l and h_l, $l \geq 1$ by induction :

$$g_l(0) = -(i)^l \frac{(2l+1)!}{2^l l!}, \tag{1.46}$$

$$g_l(\rho) = i\rho^2 h_{l-1}(\rho) + i(2l+1)g_{l-1}(\rho), \tag{1.47}$$

$$h_l(\rho) = -ig_{l-1}(\rho), \tag{1.48}$$

$$\deg(g_l) = l+1 \text{ and its leading coefficient is 1}, \tag{1.49}$$

$$\deg(h_l) = l. \tag{1.50}$$

The initial values of the sequence are

$$(S_0(\rho) - 1) + iP_0(\rho) = -1 + i\rho = \frac{-1+i\rho}{1}, \tag{1.51}$$

$$(S_1(\rho) - 2) + iP_1(\rho) = \frac{-1}{\rho^2+1} - 2 + \frac{i\rho^3}{\rho^2+1} \tag{1.52}$$

$$= \frac{i\rho^3 - 2\rho^2 - 3}{\rho^2+1}. \tag{1.53}$$

We already see that $i\rho^3 - 2\rho^2 - 3$ and $\rho^2 + 1$ are not coprime polynomial since they both admit i as a root. We can thus divide numerator and denominator by $\rho - i$ yielding

$$(S_1(\rho) - 2) + iP_1(\rho) = \frac{i\rho^2 - 3\rho - 3i}{\rho + i}. \tag{1.54}$$

The numerator and the denominator are now coprime since the denominator has only one root, $-i$, and that the numerator is non zero at $-i$. Moreover, the denominator leading coefficient is 1 so we do not have to multiply by a constant to get the fractional representation we desire.

Finally we have the following expressions for the first values of g_l and h_l :

$$g_0(\rho) = i\rho - 1, \tag{1.55}$$

$$h_0(\rho) = 1, \tag{1.56}$$
$$g_1(\rho) = i\rho^2 - 3\rho - 3i, \tag{1.57}$$
$$h_1(\rho) = \rho + i. \tag{1.58}$$

The 5 induction properties are verified for both $l = 1$. Let us assume that they are true up to some $l \geq 1$. From expression (1.45), we have

$$\frac{g_{l+1}(\rho)}{h_{l+1}(\rho)} = \frac{-\rho^2 h_l(\rho)}{g_l(\rho)} - (2l+3) = \frac{-\rho^2 h_l(\rho) - (2l+3)g_l(\rho)}{g_l(\rho)}.$$

We have replaced $(S_{l+1} - (l+2)) + iP_{l+1}$ and $(S_l - (l+1)) + iP_l$ by their fractional representation.

First let us prove that the numerator and denominator of the right-hand side are coprime. Then we will just have to find the multiplicative coefficient to make the denominator polynomial leading coefficient be 1.

Let z be a root of g_l : if it were a root of the numerator then it would be a root of $\rho^2 h_l$. By the definition of the fractional representation g_l and h_l are coprime. Therefore z cannot be a root of h_l. We conclude that necessarily z is a root of ρ^2 i.e. $z = 0$. However, we know that $g_l(0) \neq 0$ by hypothesis of induction, which contradicts that $z = 0$ is a root of g_l. Therefore the numerator and denominator have no common root : they are coprime.

We now have to find the correct multiplicative coefficient so that the denominator has a leading coefficient of 1. By hypothesis of induction the leading coefficient of g_l is i so the correct multiplicative coefficient is $-i$. Finally we can write

$$\frac{g_{l+1}(\rho)}{h_{l+1}(\rho)} = \frac{i\rho^2 h_l(\rho) + i(2l+3)g_l(\rho)}{-ig_l(\rho)}. \tag{1.59}$$

By definition and unicity of the fractional representation we have chosen, we can identify numerator and denominator in the previous expression. This yields :

$$g_{l+1}(\rho) = i\rho^2 h_l(\rho) + i(2l+3)g_l(\rho), \tag{1.60}$$
$$h_{l+1}(\rho) = -ig_l(\rho). \tag{1.61}$$

We can compute the degrees :

$$\begin{aligned} \deg(g_{l+1}) &= \max(\deg(\rho^2 h_l), \deg(g_l)) \\ &= \max(2 + l, l + 1) \\ &= l + 2, \end{aligned} \tag{1.62}$$
$$\begin{aligned} \deg(h_{l+1}) &= \deg(g_l) \\ &= l + 1. \end{aligned} \tag{1.63}$$

Moreover the leading coefficient of g_{l+1} is i times the leading coefficient of h_l, namely i. Ultimately, from (1.60),

$$g_{l+1}(0) = i(2l+3)g_l(0) = -(i)^{l+1}\frac{(2l+1)!}{2^l l!}\frac{(2l+3)(2l+2)}{2l+2} = -(i)^{l+1}\frac{(2l+3)!}{2^{l+1}, (l+1)!}$$

. We have thus achieved the proof by induction. Therefore properties (1.46) to (1.50) are true for any $l \geq 1$.

An additional and striking result can be extracted from combining (1.47) and (1.48). We obtain a second order linear recursive relation for the sequence (g_l) (and simultaneously for the sequence (h_l)). Namely, for $l \geq 0$,

$$g_{l+2}(\rho) = \rho^2 g_l(\rho) + i(2l+5)g_{l+1}(\rho), \tag{1.64}$$
$$h_{l+2}(\rho) = \rho^2 h_l(\rho) + i(2l+3)h_{l+1}(\rho). \tag{1.65}$$

1.2.3 Using the underlying linear recurring sequence to give a formula of p_l, s_l and q_l

As it stands, we have a fractional representation for $(S_l(\rho) - (l+1)) + iP_l(\rho)$. We would like to give a fractional representation of $P_l(\rho)$ and $S_l(\rho)$ separately. In particular, we would like to have real valued polynomials for the numerator and denominator. For this purpose, we need to find an expression of the real part and imaginary part of the denominator so as to be able to multiply both numerator and denominator by the conjugate of the denominator in classical complex algebra approach.

The form of (1.65) does not allow to give an expression for the real and imaginary part of h_l separately. However, multiplying by $(-i)^{l+2}$ yields

$$\begin{aligned}(-i)^{l+2}h_{l+2}(\rho) &= (-i)^2(-i)^l\rho^2 h_l(\rho) + i(-i)(-i)^{l+1}(2l+3)h_{l+1}(\rho),\\ (-i)^{l+2}h_{l+2}(\rho) &= -(-i)^l\rho^2 h_l(\rho) + (-i)^{l+1}(2l+3)h_{l+1}(\rho).\end{aligned} \tag{1.66}$$

As such if we note $a_l = \Re((-i)^l h_l)$ and $b_l = -\Im((-i)^l h_l)$, these two newly defined sequences verify the recursive linear relations

$$a_{l+2}(\rho) = -\rho^2 a_l(\rho) + (2l+3)a_{l+1}(\rho), \tag{1.67}$$
$$b_{l+2}(\rho) = -\rho^2 b_l(\rho) + (2l+3)b_{l+1}(\rho). \tag{1.68}$$

Finally, we can write

$$\begin{aligned}(S_l(\rho) - (l+1)) + iP_l(\rho) &= \frac{g_l(\rho)}{h_l(\rho)}\\ &= \frac{ih_{l+1}(\rho)}{h_l(\rho)}\\ &= \frac{i(-i)^l h_{l+1}(\rho)}{(-i)^l h_l(\rho)}\\ &= -\frac{a_{l+1}(\rho) - ib_{l+1}(\rho)}{a_l(\rho) - ib_l(\rho)}\end{aligned} \tag{1.69}$$

and then, by taking real and imaginary parts,

$$P_l = \frac{a_l b_{l+1} - a_{l+1}b_l}{a_l^2 + b_l^2}, \tag{1.70}$$

$$S_l = \frac{(l+1)(a_l^2+b_l^2) - (a_{l+1}a_l + b_{l+1}b_l)}{a_l^2+b_l^2}. \tag{1.71}$$

This can be written for numerators and denominators separately :

$$p_l = a_l b_{l+1} - a_{l+1} b_l, \tag{1.72}$$
$$s_l = (l+1)(a_l^2+b_l^2) - (a_{l+1}a_l + b_{l+1}b_l), \tag{1.73}$$
$$q_l = a_l^2 + b_l^2. \tag{1.74}$$

The initial values are :

$$\begin{aligned} a_0(\rho) &= 1, \\ a_1(\rho) &= 1, \\ b_0(\rho) &= 0, \\ b_1(\rho) &= \rho. \end{aligned}$$

l	$a_l(\rho)$	$b_l(\rho)$	$q_l(\rho)$	$s_l(\rho) + ip_l(\rho)$
0	1	0	1	$i\rho$
1	1	ρ	ρ^2+1	$i\rho^3 - 1$
2	$3-\rho^2$	3ρ	$\rho^4+3\rho^2+9$	$i\rho^5 - 3\rho^2 - 18$
3	$15-6\rho^2$	$15\rho-\rho^3$	$\rho^6+6\rho^4+45\rho^2+225$	$i\rho^7 - 6\rho^4 - 90\rho^2 - 675$

Table 1.1: Expressions of a_l, b_l, q_l and $s_l + ip_l$ for the first values of l.

Table 1.1 gathers the expressions of these polynomials for the first few values of l.

1.2.4 Properties of p_l

We notice that for the first few values of l, we seem to consistently have $p_l = \rho^{2l+1}$. We are going to show this property by induction. Let $l \geq 0$, we have, from (1.72),

$$p_{l+1} = a_{l+1}b_{l+2} - a_{l+2}b_{l+1}. \tag{1.75}$$

We can replace a_{l+2} and b_{l+2} by their expression from the recursive formulae (1.67) and (1.68) :

$$\begin{aligned} p_{l+1}(\rho) &= a_{l+1}(\rho)\left(-\rho^2 b_l(\rho) + (2l+3)b_{l+1}(\rho)\right) - \left(-\rho^2 a_l(\rho) + (2l+3)a_{l+1}(\rho)\right) b_{l+1}(\rho) \\ &= -\rho^2 a_{l+1}(\rho)b_l(\rho) + \rho^2 a_l(\rho)b_{l+1}(\rho) \\ &= \rho^2 p_l(\rho). \end{aligned} \tag{1.76}$$

Furthermore $p_0(\rho) = \rho$, so for any $l \geq 0$, $p_l(\rho) = \rho^{2l+1}$.

1.2.5 Divisibility properties of p_l, s_l and q_l

We recall that our goal in this mathematical study is to find possible common roots between $s_l + ip_l$ and q_l. We note

$$r_l = a_l + ib_l. \tag{1.77}$$

From expressions (1.72), (1.73) and (1.74), we have

$$q_l = r_l\overline{r_l},$$
$$s_l + ip_l = (l+1)r_l\overline{r_l} - r_l\overline{r_{l+1}} = r_l\big((l+1)\overline{r_l} - \overline{r_{l+1}}\big).$$

This shows that $s_l + ip_l$ do indeed have common roots, at least all those of r_l. We know that $\deg(r_l) = \deg((-i)^l\overline{h_l}) = \deg(h_l) = l$. In the case of $l = 0$ previously studied, r_l is equal to 1 and there are no roots in common to be found.

Formally speaking we have not proven that these are all the roots in common between $s_l + ip_l$. We need to show that the other terms have no common roots. Namely that $\overline{r_l}$ and $(l+1)\overline{r_l} - \overline{r_{l+1}}$ are coprime polyomials. This is equivalent to showing that $\overline{r_l}$ and $\overline{r_{l+1}}$ are coprime polynomials, which is itself equivalent to showing that r_l and r_{l+1} are coprime polynomials. Given the definition of r_l and the recursive formulae (1.67) and (1.68) :

$$r_{l+2}(\rho) = (2l+3)r_{l+1}(\rho) - \rho^2 r_l(\rho). \tag{1.78}$$

From this formula we can show that the only common roots of q_l and $s_l + ip_l$ are exactly those of r_l. Let us assume that for some rank $l \geq 0$, r_{l+1} and r_l are coprime. Let us assume then that r_{l+2} and r_{l+1} have a common root z. From the recursive formula we would have $z^2 r_l(z)$. We know that $z \neq 0$ because $r_k(0) \neq 0$ for all $k \geq 0$. Therefore we would have $r_l(z) = 0$. We would have found a common root of r_l and r_{l+1}, which is absurd by our initial hypothesis : r_{l+1} and r_{l+2} have no common roots. To complete this proof by induction we only need to show that r_0 and r_1 are coprime, which is true since $r_0 = 1$, and as such has no roots.

The final divisiblity result we were looking for is

$$\frac{s_l + ip_l}{q_l} = \frac{(l+1)\overline{r_l} - \overline{r_{l+1}}}{\overline{r_l}} \tag{1.79}$$

where the numerator and the denominator on the right hand side are coprime polynomials.

1.3 Theoretical results for a multipole representation of the Multi-Level Breit-Wigner cross-sections with less poles

1.3.1 Multipole representation of the radiative capture and fission cross-sections

We wanted to find the partial fraction decomposition of resonance terms in the radiative capture and fission cross-sections. Let us recall the expression of a resonance term from (1.26),

$$T_r(u) = \frac{2\gamma_{nr}^2 \mathrm{GX}_r P_l(\beta u)}{\Big|u^2 - \widetilde{E_r} + \gamma_{nr}^2\big(S_l(\beta u) + iP_l(\beta u)\big)\Big|^2}. \tag{1.80}$$

Instead of multiplying numerator and denominator by q_l^2 as in (1.28), we are going to just multiply by q_l. This yields,

$$T_r(u) = \frac{2\gamma_{nr}^2 \mathrm{GX}_r p_l(\beta u)}{q_l(\beta u)\left|u^2 - \widetilde{E_r} + \gamma_{nr}^2 \left(\frac{(l+1)\overline{r_l}(\beta u) - \overline{r_{l+1}}(\beta u)}{\overline{r_l}(\beta u)}\right)\right|^2}. \tag{1.81}$$

Since $q_l = r_l \overline{r_l}$, we can further write

$$T_r(u) = \frac{2\gamma_{nr}^2 \mathrm{GX}_r p_l(\beta u)}{\left|\overline{r_l}(\beta u)(u^2 - \widetilde{E_r}) + \gamma_{nr}^2\big((l+1)\overline{r_l}(\beta u) - \overline{r_{l+1}}(\beta u)\big)\right|^2}. \tag{1.82}$$

To give a partial fraction decomposition we need to find the roots of the denominator. We note

$$D_r(u) := \overline{r_l}(\beta u)(u^2 - \widetilde{E_r}) + \gamma_{nr}^2\big((l+1)\overline{r_l}(\beta u) - \overline{r_{l+1}}(\beta u)\big), \tag{1.83}$$

$$f_r(u) := 2\gamma_{nr}^2 \mathrm{GX}_r p_l(\beta u), \tag{1.84}$$

$$g_r(u) := |D_r(u)|^2. \tag{1.85}$$

We are in the situation of a positive denominator polynomial (3.9). D_r admits $l+2$ roots that we note $(z_r^{(k)})$. We note the corresponding residues of the rational function $(a_r^{(k)})$ and we have the following equality for all complex number z :

$$\begin{aligned} T_r(u) &= \frac{f_r(u)}{g_r(u)} \\ &= \frac{2\gamma_{nr}^2 \mathrm{GX}_r p_l(\beta z)}{|D_r|^2(z)} \\ &= \sum_{k=1}^{l+2} \frac{a_r^{(k)}}{z - z_r^{(k)}} + \sum_{k=1}^{l+2} \frac{\overline{a_r^{(k)}}}{z - \overline{z_r^{(k)}}}. \end{aligned} \tag{1.86}$$

Particularly, for u a real number,

$$T_r(u) = \Re\left[\sum_{k=1}^{l+2} \frac{2a_r^{(k)}}{u - z_r^{(k)}}\right]. \tag{1.87}$$

We now need to actually find the roots of D_r. We adopt the approach I have described in section 3.2. Without discussing here the details of the algorithm, we need to choose some initial guesses to find the roots. Looking at (1.83), we see that if γ_{nr}^2 is small compared to $\widetilde{E_r}$, it is a good choice to take as initial guesses the l roots of $\overline{r_l}(\beta u)$ and the two complex square roots of $\widetilde{E_r}$.

This choice of initial guess appeared to be quite reasonable in most practical numerical applications I have performed. Then, we need to compute the residues corresponding to

these roots of the denominator. Given $z_r^{(k)}$ $(1 \leq k \leq l+2)$ a root of D_r, the residue $a_r^{(k)}$ is computed by,

$$\begin{aligned} a_r^{(k)} &= \frac{2\gamma_{nr}^2 \mathrm{GX}_r p_l(\beta z_r^{(k)})}{D_r(z_r^{(k)})\overline{D'_r}(z_r^{(k)}) + D'_r(z_r^{(k)})\overline{D_r}(z_r^{(k)})} \\ &= \frac{2\gamma_{nr}^2 \mathrm{GX}_r p_l(\beta z_r^{(k)})}{D'_r(z_r^{(k)})\overline{D_r}(z_r^{(k)})} \\ &= \frac{2\gamma_{nr}^2 \mathrm{GX}_r p_l(\beta z_r^{(k)})}{D'_r(z_r^{(k)})\overline{D_r\left(\overline{z_r^{(k)}}\right)}}. \end{aligned} \tag{1.88}$$

Finally, we have given a multipole representation of each resonance term and we can substitute them in (1.12) to give the multipole representation of the radiative capture and fission cross-section for a pack :

$$\sigma_{nx}^{(l,s,J)}(E) = \frac{\pi}{k^2} \sum_{r=1}^{N} \sum_{j=1}^{l+2} \Re \left[\frac{2a_r^{(j)}}{\sqrt{E} - z_r^{(j)}} \right]. \tag{1.89}$$

Interestingly, the poles for the radiative capture of fission reaction are the same. However, the corresponding widths do appear in the residue calculation.

The number of poles we have found is lower than previously thought. Namely $l+2$ per resonance instead of $2l+2$. This does not affect the resonance of pack of orbital quantum number $l = 0$ but yields a lower number of poles for packs of higher orbital quantum number value.

1.3.2 Multipole representation of the elastic and total cross-sections

We have chosen to focus on the radiative capture and fission cross-sections at first because it allowed us to study the resonance terms separately. In the case of the elastic cross-section there is a square modulus of a sum of contributions of each resonance. We will proceed in two steps. First we will give a partial fraction decomposition of ρ_{nn} from (1.5). Then we will take the square modulus of this partial fraction decomposition and show that it can be simplified to take again a suitable form for multipole representation.

We recall that

$$\rho_{nn}(E) = \frac{i}{2} \sum_{r=1}^{N} \frac{\Gamma_{nr}}{(E - E'_r) + i\Gamma_{tr}/2}, \tag{1.90}$$

and, with the notation adopted before,

$$\rho_{nn}(E) = \sum_{r=1}^{N} \frac{i\gamma_{nr}^2 p_l(\beta u)/q_l(\beta u)}{D_r(u)/\overline{r_l}(\beta u)}$$

$$= \frac{1}{r_l(\beta u)} \sum_{r=1}^{N} \frac{i\gamma_{nr}^2 p_l(\beta u)}{D_r(u)}. \tag{1.91}$$

Let us recall that $p_l(\beta u) = (\beta u)^{2l+1}$, as I have proven in subsection 1.2.4. If we separate it into two parts we obtain

$$\rho_{nn}(E) = \frac{(\beta u)^l}{r_l(\beta u)} \sum_{r=1}^{N} \frac{i\gamma_{nr}^2 (\beta u)^{l+1}}{D_r(u)}. \tag{1.92}$$

The interest of this form is that both terms of the products are rational functions with denominator of degree non smaller than the degree of their respective numerator. Indeed $\deg(r_l) = l$ and $\deg(D_r) = l + 2$ for any resonance r.

We have already computed the roots of D_r, so it is straightforward to give the partial fraction decomposition of the terms inside the sum. We note the corresponding residues $b_r^{(k)}$. They are computed as

$$b_r^{(k)} = \frac{i\gamma_{nr}^2 \left(\beta z_r^{(k)}\right)^{l+1}}{D_r'(z_r^{(k)})}. \tag{1.93}$$

Separately we compute the partial fraction decomposition of the left term in (1.92). This can be done quite easily by storing the l roots of r_l for the first values of $l \geq 0$. We note them v_j, $1 \leq j \leq l$. Then the roots of $u \mapsto r_l(\beta u)$ are (v_j/β). We have the following partial fraction decomposition :

$$\frac{(\beta u)^l}{r_l(\beta u)} = c + \sum_{j=1}^{l} \frac{(v_j)^l/(\beta r_l'(v_j))}{u - v_j/\beta}. \tag{1.94}$$

It is a slightly different partial fraction decomposition that we have not seen before. There is a constant noted c in front of the sum because numerator and denominator have the same degree. Fortunately it can be easily computed as the limit of the rational function when u goes to infinity. This yields $c = 1/i^l$.

Gathering (1.93) and (1.94) yields

$$\rho_{nn}(E) = \left(c + \sum_{j=1}^{l} \frac{c_j}{u - v_j/\beta} \right) \left(\sum_{r=1}^{N} \sum_{k=1}^{l+2} \frac{b_r^{(k)}}{u - z_r^{(k)}} \right). \tag{1.95}$$

We are basically in the situation of the product of two partial fraction decompositions. Let us clean a bit the notations. We note N the number of resonances in the pack we are working on. We write (w_p) the $(l+2)N$ poles of the right term and (d_p) the corresponding residues,

$$\rho_{nn}(E) = \left(c + \sum_{j=1}^{l} \frac{c_j}{u - v_j/\beta} \right) \left(\sum_{p=1}^{(l+2)N} \frac{d_p}{u - w_p} \right). \tag{1.96}$$

We can thus give a partial fraction decomposition of $\rho_{nn}(E)$ in terms of $u = \sqrt{E}$ with exactly $l + (l+2)N$ poles and residues. We refer to expression (3.10) of Part I for the computations of the residues. A final gathering of notations with the set of poles noted z_p and the residues a_p, $1 \leq p \leq l + (l+2)N$,

$$\rho_{nn}(E) = \sum_{p=1}^{l+(l+2)N} \frac{a_p}{u - z_p}. \tag{1.97}$$

We revert to the formulae for the elastic cross section (1.2) :

$$\sigma_{nn}^{(l,s,J)}(E) = \frac{4\pi}{k^2} \left[\sin^2(\phi_l) + \Re\left(\rho_{nn} \exp(-2i\phi_l)\right) - \Re(\rho_{nn}) + |\rho_{nn}|^2 \right].$$

The point (3.12) of Part I allows us to compute the partial fraction decomposition of the $|\rho_{nn}|^2$ from the partial fraction decomposition of ρ_{nn},

$$|\rho_{nn}|^2 = \Re\left[\sum_{p=1}^{l+(l+2)N} \frac{b_p}{u - z_p} \right] \tag{1.98}$$

$$\text{with } b_p := 2a_p \sum_{q=1}^{l+(l+2)N} \frac{\overline{a_q}}{z_p - \overline{z_q}}. \tag{1.99}$$

Then we have,

$$\sigma_{nn}^{(l,s,J)}(E) = \frac{4\pi}{k^2} \left[\sin^2(\phi_l) + \Re\left(\sum_{p=1}^{l+(l+2)N} \frac{a_p(\exp(-2i\phi_l) - 1) + b_p}{\sqrt{E} - z_p} \right) \right]. \tag{1.100}$$

which is almost the multipole representation that we set out to find at the beginning of the chapter. Namely, there are some additional $\sin^2(\phi_l)$ terms in front of the pole terms. These are usually considered part of the multipole representation. They are inherent to the elastic cross-sections and will also appear in the multipole representation of the Reich-Moore formalism cross-sections.

Speaking of ϕ_l, we have ignored the energy dependency of the phase shift factor until now. This dependency is precisely the reason why the multipole representation is not strictly speaking just a partial fraction decomposition. Let us keep in mind that one of our goals is to perform on-the-fly Doppler broadening. In that context, we will see that this remaining energy dependency is not a major issue. The total cross-section is computed as a sum of the three partial cross-sections. A tabulated background must be added in some cases. The formulae I have given for the total cross-section could be more aptly named resonant total cross-section. Through the elastic cross-section, this resonant total cross-section has two types of pole terms as in (1.100). The corresponding residues are computed as the sum of the residues of the three partial cross-sections.

We have found that we needed $l + 2$ poles per resonance for the radiative capture and fission cross-sections. Then we have shown that we need the same $l + 2$ poles per resonance

for the elastic cross-section. We also need an additional l poles for the whole pack. Being only related to the aforementioned polynomial r_l, they are actually common to all packs of same quantum orbital number l. However, I choose to not factorize them from the packs, since the development I have proposed until now is clearer if we work with packs of resonances strictly separated.

Our results improve those of the article of C. Jammes [19] by reducing the number of poles. It also provides an adequate explanation for the poles with residues very close to zero. Let us summarize the method to obtain our new multipole representation of the Multi-Level Breit-Wigner cross-sections.

1.4 Algorithmic summary

Inside each pack, resonances are treated separately. We recall that they are characterized by a resonance energy and up to 4 widths. We form the polynomial D_r from expression (1.83) :

$$D_r(u) = \overline{r_l}(\beta u)(u^2 - \widetilde{E_r}) + \gamma_{nr}^2\big((l+1)\overline{r_l}(\beta u) - \overline{r_{l+1}}(\beta u)\big). \tag{1.101}$$

The reduced elastic widths are defined by (1.24). The perturbed resonance energies $\widetilde{E_r}$ are defined by (1.25). Finally, the polynomials r_l are defined by (1.77). Each resonance belongs to a pack of resonance defined by a set of quantum number (l, s, J). This determines the value of l in $\overline{r_l}$ and $\overline{r_{l+1}}$.

We then need to find the roots of each polynomial D_r. This polynomial is of degree $l+2$. One can use the Newton-Raphson algorithm I described in subsection 3.2.3 of Part I. This algorithm performs better with some guesses. On one hand, we chose the 2 complex square roots of $\widetilde{E_r}$. On the other hand, we chose the l roots of $z \mapsto r_l(\beta z)$. I will discuss these choices in the qualitative study of the poles. The quantity β is computed according to expression (2.23) of Part I and is fixed for each pack. The roots of this polynomial are, up to a division by β, those of $\overline{r_l}$. They can be computed once and for all for each value of l. The roots obtained are exactly the poles of the multipole decomposition.

For the elastic and total cross-sections, l poles have to be added per pack of resonances. For $l = 0$, there are no such additional poles. For higher value of l, the poles are directly the roots of $z \mapsto r_l(\beta z)$. These are exactly the complex conjugate of the roots of $z \mapsto \overline{r_l}(\beta z)$.

Once the poles have been computed, we look for the corresponding residues. There is one residue per pole for the radiative capture and fission cross-sections. They are computed with expression (1.88). There are two residues per pole for the elastic and total cross-sections (terms with or without a phase-shift). They are computed with expression (1.99).

Chapter 2

Study of the multipole representation of the Reich-Moore cross-sections

Our goal in this chapter is very similar to that of the previous one, although the means to achieve it will be rather different. Again, we want to show that the elastic, radiative capture, fission and total cross-sections can be written under the so-called multipole representation

$$\sigma_{nx}(E) = \frac{4\pi}{k^2}\Re\left(\sum_p \frac{a_p + b_p \exp(-2i\phi_l))}{\sqrt{E} - z_p}\right) \tag{2.1}$$

where k is related to E by expression (2.24) of Part I.

We have seen in the previous chapter that it is possible to give a multipole representation for the Multi-Level Breit-Wigner cross-sections. One of the key points we used was that the representation of each resonance could be computed completely separately for partial cross-sections with no interference between resonances (i.e. fission and radiative capture cross-sections). For the elastic cross-section (and through it, the total cross-section), this result was not directly applicable, since the Multi-Level Breit-Wigner does take into account interferences between resonances for this reaction. However, the derivation process was still quite similar and allowed for a somewhat separated treatment of each resonance.

This is not the case for the Reich-Moore formalism. The Reich-Moore formalism takes into account interferences between resonances - and additionally channels - for all partial cross-sections that are to be reconstructed : the radiative capture, fission, elastic and total cross-sections. The resonance parameters that are provided are used through formulae that involve matrix inversions. The different entries of those matrices correspond to different channels and different partial cross-sections. The inversion insures that there will always be some interferences between all resonances within a pack. Again, it is possible to give a multipole representation for each pack separately, since their contribution to the cross-sections are added linearly.

A reduced R-matrix is defined for each pack of resonances. It has up to 3 entries that correspond to the different channel considered in the model, namely the elastic, fission A

and fission B. The existence of two fission channels (and so two entries) is a choice of the formalism that allows representing more physical subtleties of the fission phenomenon (there will still be only one fission cross-section in the end). The radiative capture channel is not a proper entry, as this physical phenomenon is treated as a perturbation of the resonance energy (it does not mean it is neglected, but rather that the corresponding width of this reaction compared to others makes it more suited to a perturbative treatment).

The three entries of the reduced R-matrix are noted n,a and b. They correspond respectively to the elastic, fission a and fission b reactions. It is defined by

$$\widehat{R}_{cd} = \sum_{r=1}^{N} \frac{\gamma_{cr}\gamma_{dr}}{E_r - E - i\Gamma_{\gamma r}/2} \tag{2.2}$$

where c and d are either n, a or b. The reduced widths are related to the ENDF resonance parameters by

$$\gamma_{nr} = \sqrt{\mathrm{GN}_r/2P_l(|E_r|)}, \tag{2.3}$$
$$\gamma_{ar} = \sqrt{\mathrm{GFA}_r/2}, \tag{2.4}$$
$$\gamma_{br} = \sqrt{\mathrm{GFB}_r/2}, \tag{2.5}$$
$$\Gamma_{\gamma r} = \mathrm{GG}_r. \tag{2.6}$$

The penetration factor is equal to 1 for the fission entries. In accordance to my choice of notation concerning the energy dependency of the penetration factors described in (2.23) of Part I, the penetration matrix is defined by

$$\mathcal{P}(E) = \begin{pmatrix} P_l(\beta\sqrt{E}) & 0 & 0 \\ 0 & 1 & 0 \\ 0 & 0 & 1 \end{pmatrix}. \tag{2.7}$$

Then the ρ matrix is defined by

$$\rho = Id - \left(Id - i\mathcal{P}^{1/2}\widehat{R}\mathcal{P}^{1/2}\right)^{-1} \tag{2.8}$$

where Id is the 3×3 identity matrix. I had previously noted P the matrix containing the penetration factors when deriving the Reich-Moore formalism. I have chosen to note it $\mathcal{P}$ here so as to differentiate it from the notation of its elements P_l

ρ is also a 3×3 matrix whose computation involves a matrix inversion. From the coefficients of this ρ matrix, we have the following formulae for the contribution of a pack to the different cross-sections :

$$\sigma_{nf}(E) = \frac{4\pi}{k^2}\left(|\rho_{na}|^2 + |\rho_{nb}|^2\right), \tag{2.9}$$
$$\sigma_{nn}(E) = \frac{4\pi}{k^2}\left(\sin^2(\phi_l) + \Re(\rho_{nn}\exp(-2i\phi_l)) - \Re(\rho_{nn}) + |\rho_{nn}|^2\right), \tag{2.10}$$
$$\sigma_{nt}(E) = \frac{4\pi}{k^2}\left(\sin^2(\phi_l) + \Re(\rho_{nn}\exp(-2i\phi_l))\right), \tag{2.11}$$

$$\sigma_{n\gamma}(E) = \frac{4\pi}{k^2}\left(\Re(\rho_{nn}) - |\rho_{nn}|^2\right) - \sigma_{nf}(E). \tag{2.12}$$

The radiative capture and fission cross-sections have a more complicated formula than before. We see that they both involve a square modulus and the coefficient of the newly defined ρ matrix. As such we do not expect their study to be particularly easier than that of the elastic and total cross-sections. This is in contrast to the approach we adopted for the Multi-Level Breit-Wigner multipole representation.

Given the formulae for the R and ρ matrix, we will begin by considering non-fissile nuclei treated under the Reich-Moore formalism. For such nuclei, the R and ρ matrix will be significantly easier to study. I will show that the problem of the multipole representation is akin to solving a polynomial of potentially high degree. I will propose an adapted Newton-Raphson algorithm to find the roots of these polynomials. I will then show that the more general problem of fissile nuclei - and its more complicated reduced R matrix - can be solved as the non fissile nuclei with some additional calculations.

2.1 Study of the multipole representation of non-fissile Reich-Moore nuclei

In the case of non-fissile nuclei, the parameters GFA and GFB are set to zero for all resonances. As such the reduced R-matrix of (2.11) takes a somewhat simplified form :

$$\widehat{R} = \begin{pmatrix} \sum_{r=1}^{N} \dfrac{\gamma_{nr}^2}{E_r - E - i\Gamma_{\gamma r}/2} & 0 & 0 \\ 0 & 0 & 0 \\ 0 & 0 & 0 \end{pmatrix}. \tag{2.13}$$

Then

$$\mathcal{P}^{1/2}\widehat{R}\mathcal{P}^{1/2} = \begin{pmatrix} \sum_{r=1}^{N} \dfrac{\gamma_{nr}^2 P_l(\beta\sqrt{E})}{E_r - E - i\Gamma_{\gamma r}/2} & 0 & 0 \\ 0 & 0 & 0 \\ 0 & 0 & 0 \end{pmatrix}. \tag{2.14}$$

Hence, the ρ matrix of (2.8) takes the form

$$\rho = \begin{pmatrix} 1 - \dfrac{1}{1 + i\sum_{r=1}^{N} \frac{\gamma_{nr}^2 P_l(\beta\sqrt{E})}{E - E_r + i\Gamma_{\gamma r}/2}} & 0 & 0 \\ 0 & 0 & 0 \\ 0 & 0 & 0 \end{pmatrix}. \tag{2.15}$$

As we could expect it for non-fissile nuclei, the only non zero element of the ρ matrix will be the upper left one coefficient, noted ρ_{nn} in the formulae (2.12) to (2.11). Namely,

$$\rho_{nn} = 1 - \frac{1}{1 + i\sum_{r=1}^{N} \frac{\gamma_{nr}^2 P_l(\beta\sqrt{E})}{E - E_r + i\Gamma_{\gamma r}/2}}. \tag{2.16}$$

The resonance energies E_r are assumed to have no shift, in contrast with the Multi-Level Breit-Wigner formalism. The radiative capture widths $\Gamma_{\gamma r}$ are independent of the energy so that

$$\rho_{nn} = 1 - \frac{1}{1 + \sum_{r=1}^{N} \frac{i\gamma_{nr}^2 P_l(\beta\sqrt{E})}{E - E_r + i\mathrm{GG}_r/2}}. \tag{2.17}$$

The denominator is a rational function of $\sqrt{E}$. As such, the quantity ρ_{nn} is also rational function of $\sqrt{E}$. However, the situation is quite different from the Multi-Level Breit-Wigner formalism. The sum on the resonance terms is at the denominator. Our goal is to find its partial fraction decomposition. We first need to write it as a quotient of polynomial functions.

First let us adopt some more convenient notations :

$$u = \sqrt{E}, \tag{2.18}$$

$$\widetilde{E_r} = E_r - i\mathrm{GG}_r/2, \tag{2.19}$$

$$a_r = i\gamma_{nr}^2. \tag{2.20}$$

With these new notations, expression (2.17) becomes

$$\rho_{nn} = 1 - \frac{1}{1 + \sum_{r=1}^{N} \frac{a_r P_l(\beta u)}{u^2 - \widetilde{E_r}}}. \tag{2.21}$$

We recall that P_l can be written p_l/q_l with p_l and q_l two polynomial functions whose properties are given in section 1.4 and section 1.2. We adopt the aditionnal notations :

$$Q(u) = \prod_{r=1}^{N} (u^2 - \widetilde{E_r}), \tag{2.22}$$

$$Q_r(u) = \prod_{s \neq r} (u^2 - \widetilde{E_s}). \tag{2.23}$$

We multiply the numerator and denominator of (2.17) by $Q(u)q_l(\beta u)$, yielding

$$\rho_{nn} = 1 - \frac{Q(u)q_l(\beta u)}{Q(u)q_l(\beta u) + \sum_{r=1}^{N} a_r Q_r(u) p_l(\beta u)} \tag{2.24}$$

$$= \frac{-\sum_{r=1}^{N} a_r Q_r(u) p_l(\beta u)}{Q(u)q_l(\beta u) + \sum_{r=1}^{N} a_r Q_r(u) p_l(\beta u)}. \tag{2.25}$$

We note the numerator and denominator polynomials

$$f(u) := -\sum_{r=1}^{N} a_r Q_r(u) p_l(\beta u), \tag{2.26}$$

$$g(u) := Q(u)q_l(\beta u) + \sum_{r=1}^{N} a_r Q_r(u) p_l(\beta u). \tag{2.27}$$

The degree of these polynomials are,

$$\begin{aligned}
\deg(f) &= \max_{r=1}^{N}(\deg(Q_r p_l)) \\
&= \max_{r=1}^{N}(\deg(Q_r) + \deg(p_l)) \\
&= 2N - 2 + (2l+1) = 2N + 2l - 1, \qquad (2.28)\\
\deg(g) &= \max_{r=1}^{N}(\deg(Qq_l), \deg(f)) \\
&= \max_{r=1}^{N}(2N + 2l, 2N + 2l - 1) = 2N + 2l. \qquad (2.29)
\end{aligned}$$

We now have to find the roots of g so as to give the partial fraction decomposition of f/g.

2.1.1 Finding the roots of the denominator

As explained in subsection 3.2.3 of Part I, we need to find a way to compute the logarithmic derivative of the polynomial g, and doing so without computing its coefficients. Under the form

$$g(u) = Q(u)q_l(\beta u) + \sum_{r=1}^{N} a_r Q_r(u) p_l(\beta u), \tag{2.30}$$

a straightforward differentiation of g seems rather complicated. The idea here is to go a few steps back and factorize $Q(u)q_l(\beta u)$. We get

$$g(u) = Q(u)q_l(\beta u)\left(1 + \frac{p_l(\beta u)}{q_l(\beta u)} \sum_{r=1}^{N} \frac{a_r}{u^2 - \widetilde{E_r}}\right). \tag{2.31}$$

We would like to get an even simpler expression before differentiation. Let us consider in particular the term

$$\frac{p_l(\beta u)}{q_l(\beta u)} \sum_{r=1}^{N} \frac{a_r}{u^2 - \widetilde{E_r}}. \tag{2.32}$$

This is a rational function of u and as such we can give it a partial fraction decomposition. We have the asymptotic properties

$$p_l(\beta u)/q_l(\beta u) = \mathcal{O}(u), \tag{2.33}$$

$$\sum_{r=1}^{N} \frac{a_r}{u^2 - \widetilde{E_r}} = \mathcal{O}(1/u^2). \tag{2.34}$$

Therefore their product tends to zero. Its poles are readily seen to be the roots of $z \mapsto q_l(\beta z)$ and the complex square roots of the $\widetilde{E_r}$.

We note v_j, $1 \leq j \leq 2l$, the roots of q_l. Thus, the roots of $z \mapsto q_l(\beta z)$ are the v_j/β, $1 \leq j \leq 2l$. We admit that we can compute them very accurately. The corresponding residues are computed as

$$b_j := \frac{p_l(v_j)}{\beta q_l'(v_j)} \sum_{r=1}^{N} \frac{a_r}{(v_j/\beta)^2 - \widetilde{E_r}}. \tag{2.35}$$

We note u_r^+ (resp. u_r^-), $1 \leq r \leq N$, the complex square root of the $\widetilde{E_r}$ with positive (resp. negative) real part. The corresponding residues are computed as

$$c_r^+ := \frac{p_l(\beta u_r^+)}{q_l(\beta u_r^+)} \frac{a_r}{2u_r^+}. \tag{2.36}$$

We have a total of $2l+2N$ roots and we note them under a common notation (w_k), and their corresponding residues (b_k) with $1 \leq k \leq 2N+2l$.

We now have

$$\frac{p_l(\beta u)}{q_l(\beta u)} \sum_{r=1}^{N} \frac{a_r}{u^2 - \widetilde{E_r}} = \sum_{k=1}^{2N+2l} \frac{b_k}{u - w_k}. \tag{2.37}$$

Furthermore, under these notations,

$$\begin{aligned} Q(u)q_l(\beta u) &= \prod_{r=1}^{N}(u^2 - \widetilde{E_r}) \prod_{j=1}^{2l}(\beta u - v_j) \\ &= \beta^{2l} \prod_{r=1}^{N}(u - u_r^+) \prod_{r=1}^{N}(u - u_r^-) \prod_{j=1}^{2l}(u - \frac{v_j}{\beta}) \\ &= \beta^{2l} \prod_{k=1}^{2N+2l} (u - w_k). \end{aligned} \tag{2.38}$$

Let us revert to (2.31), we can now write

$$g(u) = Q(u)q_l(\beta u) \left(1 + \frac{p_l(\beta u)}{q_l(\beta u)} \sum_{r=1}^{N} \frac{a_r}{u^2 - \widetilde{E_r}}\right) \tag{2.39}$$

$$= \beta^{2l} \prod_{k=1}^{2N+2l} (u - w_k) \left(1 + \sum_{k=1}^{2N+2l} \frac{b_k}{u - w_k}\right). \tag{2.40}$$

The logarithmic derivative of g now has an expression that does not involve computing the coefficients of a potentially huge polynomial :

$$\frac{g'(u)}{g(u)} = \sum_{k=1}^{2N+2l} \frac{1}{u - w_k} - \frac{\displaystyle\sum_{k=1}^{2N+2l} \frac{b_k}{(u - w_k)^2}}{\displaystyle 1 + \sum_{k=1}^{2N+2l} \frac{b_k}{u - w_k}}. \tag{2.41}$$

The w_k are easily computed, they are either a root of $q_l(\beta u)$ (the v_j/β where the v_j can be computed once for each value of l) or the complex square root of a $\widetilde{E_r}$. From the w_k, the b_k are readily computed in an accurate fashion.

The expression (2.41) to compute the logarithmic derivative of g is rather stable. There are three potentially large sums to compute, each one can be done with good accuracy if care is applied (Kahan summation for instance [63]). The final step is the addition of the left sum and the right fraction. This one can be trickier, as for values of u close to w_k they are both very large and yet almost exactly compensate each other. In all practical cases I have never noticed that it was a particular problem if the two terms to add had been previously computed with good accuracy.

We admit that with the Newton-Raphson algorithm decribed in subsection 3.2.3 it is possible to compute the $2N+2l$ roots of g. I will later give some numerical insight concerning the difficulties arising when this number of roots to compute is large. We note the roots of g, z_k, $1 \leq k \leq 2N+2l$. We now need to compute the residues corresponding to these poles for the rational function f/g.

2.1.2 Giving a partial fraction decomposition of ρ_{nn}

We go back to expression (2.25),

$$\rho_{nn} = \frac{-\sum_{r=1}^{N} a_r Q_r(u) p_l(\beta u)}{Q(u) q_l(\beta u) + \sum_{r=1}^{N} a_r Q_r(u) p_l(\beta u)}. \tag{2.42}$$

Given the roots z_k of g computed with the expression of the logarithmic derivative of g we have derived before, we want to compute the residues to give a partial fraction decomposition of ρ_{nn}. To that end, we need to evaluate f/g' at these roots. We have an expression of g'/g, the idea is to use a convenient expression of f/g. We use expressions (2.21) and (2.37) :

$$\rho_{nn} = 1 - \frac{1}{1 + \sum_{k=1}^{2N+2l} \frac{b_k}{u - w_k}}. \tag{2.43}$$

Then, we write

$$\frac{f(u)}{g'(u)} = \frac{f(u)/g(u)}{g'(u)/g(u)} = \frac{1 - \dfrac{1}{1 + \displaystyle\sum_{k=1}^{2N+2l} \dfrac{b_k}{u - w_k}}}{\displaystyle\sum_{k=1}^{2N+2l} \frac{1}{u - w_k} - \frac{\displaystyle\sum_{k=1}^{2N+2l} \dfrac{b_k}{(u - w_k)^2}}{1 + \displaystyle\sum_{k=1}^{2N+2l} \dfrac{b_k}{u - w_k}}} \tag{2.44}$$

$$= \frac{\displaystyle\sum_{k=1}^{2N+2l} \frac{b_k}{u - w_k}}{\left(1 + \displaystyle\sum_{k=1}^{2N+2l} \frac{b_k}{u - w_k}\right) \displaystyle\sum_{k=1}^{2N+2l} \frac{1}{u - w_k} - \displaystyle\sum_{k=1}^{2N+2l} \frac{b_k}{(u - w_k)^2}}. \tag{2.45}$$

Finally we evaluate this expression at one z_j to get its corresponding residue

$$\alpha_j := \frac{f(z_j)}{g'(z_j)} = \frac{\displaystyle\sum_{k=1}^{2N+2l} \frac{b_k}{z_j - w_k}}{\left(\displaystyle\sum_{k=1}^{2N+2l} \frac{1}{z_j - w_k}\right)\left(1 + \displaystyle\sum_{k=1}^{2N+2l} \frac{b_k}{z_j - w_k}\right) - \displaystyle\sum_{k=1}^{2N+2l} \frac{b_k}{(z_j - w_k)^2}}. \tag{2.46}$$

Gathering all previous results and notations we finally have the partial fraction decomposition of ρ_{nn}. Namely,

$$\rho_{nn}(u) = \sum_{j=1}^{2N+2l} \frac{\alpha_j}{u - z_j}. \tag{2.47}$$

2.1.3 Multipole representation of non-fissile Reich-Moore nuclei

In the case of non fissile materials, we have formulae for the radiative capture, elastic and total cross-sections. Let us recall that the contribution of a pack of resonances is :

$$\sigma_{n\gamma}(E) = \frac{4\pi}{k^2} \left(\Re(\rho_{nn}) - |\rho_{nn}|^2\right), \tag{2.48}$$

$$\sigma_{nn}(E) = \frac{4\pi}{k^2} \left(\sin^2(\phi_l) + \Re(\rho_{nn} \exp(-2i\phi_l)) - \Re(\rho_{nn}) + |\rho_{nn}|^2\right), \tag{2.49}$$

$$\sigma_{nt}(E) = \frac{4\pi}{k^2} \left(\sin^2(\phi_l) + \Re(\rho_{nn} \exp(-2i\phi_l))\right). \tag{2.50}$$

We now also have the partial fraction decomposition of ρ_{nn}, so we are very close to the multipole representation we are looking for.

We use the previously proven result about the partial fraction decomposition of $|\rho_{nn}|^2$, namely for any real number u,

$$|\rho_{nn}|^2 = \left| \sum_{k=1}^{2N+2l} \frac{\alpha_k}{u - z_k} \right|^2 \tag{2.51}$$

$$= 2\Re \left(\sum_{k=1}^{2N+2l} \frac{\alpha_k \sum_{j=1}^{2N+2l} \frac{\overline{\alpha_l}}{z_k - \overline{z_j}}}{u - z_k} \right). \tag{2.52}$$

We note the new residues

$$\delta_k := 2\alpha_k \sum_{j=1}^{2N+2l} \frac{\overline{\alpha_j}}{z_k - \overline{z_j}}. \tag{2.53}$$

We substitute these partial fraction decompositions in the cross-sections formulae and give the final multipole representation of the radiative capture, elastic and total cross-sections for non-fissile Reich-Moore nuclei :

$$\sigma_{n\gamma}(E) = \frac{4\pi}{k^2} \Re \left(\sum_{p=1}^{2N+2l} \frac{\alpha_p - \delta_p}{\sqrt{E} - z_p} \right), \tag{2.54}$$

$$\sigma_{nn}(E) = \frac{4\pi}{k^2} \sin^2(\phi_l) + \frac{4\pi}{k^2} \Re \left(\sum_{p=1}^{2N+2l} \frac{\alpha_p \left(e^{-2i\phi_l} - 1 \right) + \delta_p}{\sqrt{E} - z_p} \right), \tag{2.55}$$

$$\sigma_{nt}(E) = \frac{4\pi}{k^2} \sin^2(\phi_l) + \frac{4\pi}{k^2} \Re \left(\sum_{p=1}^{2N+2l} \frac{\alpha_p e^{-2i\phi_l}}{\sqrt{E} - z_p} \right). \tag{2.56}$$

The (α_p), (δ_p) and (z_p) are all independent of the energy E. However, ϕ_l has an energy dependency. Its variations are sufficiently small in the broadening zone so that we do not look for a further decomposition of the cross-sections.

We have proven that we need exactly $2N+2l$ poles and 2 times that amount of residues, to be able to give the multipole representation of a pack of resonance of quantum number l. As far as I know, no result has been given separately for the non-fissile and fissile Reich-Moore nucleus. This first step was very successful in understanding the requirement of the root finding algorithm. We will see in the next section that this approach can even be extended to fissile nuclei after some work. This will yield a more effective algorithm to give the multipole representation of nuclei with a large amount of resonances and multiple reaction channels.

2.2 Study of the multipole representation of fissile Reich-Moore nuclei

We now go back to the more general (and complicated) case of fissile Reich-Moore nuclei. As outlined in the introduction of this chapter, not only the elements to compute involve the inversion of a 3×3 matrix (with rational function coefficients of very high degree) but

the number of resonances in each pack is usually way larger than for non-fissile nuclei. This is due to the fact that fissile nuclei are often heavier nuclei, and heavier nuclei tend to have more resonances in their cross-section profiles on the energy range of interest.

We wish to show here that we can get back to the mathematical situation of the non-fissile nuclei multipole representation.

2.2.1 Understanding the complexity of the R-matrix partial fraction decomposition problem

For the sake of clarity, we assume that the penetration factor is 1 for all channels. This does not change much the mathematical situation and allows for a better understanding of the problem to solve. As such, the ρ matrix is given by

$$\rho = Id - (Id - i\widehat{R})^{-1} \tag{2.57}$$

$$= Id - \left(Id + \begin{pmatrix} \sum_{r=1}^{N} \frac{i\gamma_{nr}\gamma_{nr}}{E - \widetilde{E_r}} & \sum_{r=1}^{N} \frac{i\gamma_{nr}\gamma_{ar}}{E - \widetilde{E_r}} & \sum_{r=1}^{N} \frac{i\gamma_{nr}\gamma_{br}}{E - \widetilde{E_r}} \\ \sum_{r=1}^{N} \frac{i\gamma_{ar}\gamma_{nr}}{E - \widetilde{E_r}} & \sum_{r=1}^{N} \frac{i\gamma_{ar}\gamma_{ar}}{E - \widetilde{E_r}} & \sum_{r=1}^{N} \frac{i\gamma_{ar}\gamma_{br}}{E - \widetilde{E_r}} \\ \sum_{r=1}^{N} \frac{i\gamma_{br}\gamma_{nr}}{E - \widetilde{E_r}} & \sum_{r=1}^{N} \frac{i\gamma_{br}\gamma_{ar}}{E - \widetilde{E_r}} & \sum_{r=1}^{N} \frac{i\gamma_{br}\gamma_{br}}{E - \widetilde{E_r}} \end{pmatrix} \right)^{-1}. \tag{2.58}$$

Therefore, for instance, the expression of the element ρ_{nn} (first row, first column), which was previously (2.25), is now (with the cofactor formula),

$$\rho_{nn} = 1 - \frac{\begin{vmatrix} 1 + \sum_{r=1}^{N} \frac{i\gamma_{ar}\gamma_{ar}}{E - \widetilde{E_r}} & \sum_{r=1}^{N} \frac{i\gamma_{ar}\gamma_{br}}{E - \widetilde{E_r}} \\ \sum_{r=1}^{N} \frac{i\gamma_{br}\gamma_{ar}}{E - \widetilde{E_r}} & 1 + \sum_{r=1}^{N} \frac{i\gamma_{br}\gamma_{br}}{E - \widetilde{E_r}} \end{vmatrix}}{\begin{vmatrix} 1 + \sum_{r=1}^{N} \frac{i\gamma_{nr}\gamma_{nr}}{E - \widetilde{E_r}} & \sum_{r=1}^{N} \frac{i\gamma_{nr}\gamma_{ar}}{E - \widetilde{E_r}} & \sum_{r=1}^{N} \frac{i\gamma_{nr}\gamma_{br}}{E - \widetilde{E_r}} \\ \sum_{r=1}^{N} \frac{i\gamma_{ar}\gamma_{nr}}{E - \widetilde{E_r}} & 1 + \sum_{r=1}^{N} \frac{i\gamma_{ar}\gamma_{ar}}{E - \widetilde{E_r}} & \sum_{r=1}^{N} \frac{i\gamma_{ar}\gamma_{br}}{E - \widetilde{E_r}} \\ \sum_{r=1}^{N} \frac{i\gamma_{br}\gamma_{nr}}{E - \widetilde{E_r}} & \sum_{r=1}^{N} \frac{i\gamma_{br}\gamma_{ar}}{E - \widetilde{E_r}} & 1 + \sum_{r=1}^{N} \frac{i\gamma_{br}\gamma_{br}}{E - \widetilde{E_r}} \end{vmatrix}}. \tag{2.59}$$

The coefficients in each determinant are rational functions. As such, the determinant themselves are guaranteed to also be rational functions. Finally, ρ_{nn} is itself a rational function as a quotient of two rational functions. However, it is not clear how to proceed to find its partial decomposition.

First we need to get ρ_{nn} an expression as a quotient of two polynomials, at least formally. In (2.59) we see that the coefficients in the determinants diverge when $E \to \widetilde{E_r}$, for any $1 \leq r \leq N$. As such, my first approach was to multiply numerator and denominator by

$$\big(Q(E)\big)^3 = \left(\prod_{r=1}^{n}(E - \widetilde{E_r})\right)^3 . \tag{2.60}$$

The polynomial enters in the determinants and we have

$$\rho_{nn} = 1 - \frac{Q\begin{vmatrix} Q + \sum_{r=1}^{N} i\gamma_{ar}\gamma_{ar}Q_r & \sum_{r=1}^{N} i\gamma_{ar}\gamma_{br}Q_r \\ \sum_{r=1}^{N} i\gamma_{br}\gamma_{ar}Q_r & Q + \sum_{r=1}^{N} i\gamma_{br}\gamma_{br}Q_r \end{vmatrix}}{\begin{vmatrix} Q + \sum_{r=1}^{N} i\gamma_{nr}\gamma_{nr}Q_r & \sum_{r=1}^{N} i\gamma_{nr}\gamma_{ar}Q_r & \sum_{r=1}^{N} i\gamma_{nr}\gamma_{br}Q_r \\ \sum_{r=1}^{N} i\gamma_{ar}\gamma_{nr}Q_r & Q + \sum_{r=1}^{N} i\gamma_{ar}\gamma_{ar}Q_r & \sum_{r=1}^{N} i\gamma_{ar}\gamma_{br}Q_r \\ \sum_{r=1}^{N} i\gamma_{br}\gamma_{nr}Q_r & \sum_{r=1}^{N} i\gamma_{br}\gamma_{ar}Q_r & Q + \sum_{r=1}^{N} i\gamma_{br}\gamma_{br}Q_r \end{vmatrix}} \tag{2.61}$$

with, again,

$$Q(u) = \prod_{r=1}^{N}(u^2 - \widetilde{E_r}), \tag{2.62}$$

$$Q_r(u) = \prod_{s \neq r}(u^2 - \widetilde{E_s}). \tag{2.63}$$

Under this new form, the determinants both have polynomial coefficients. As such, they are both polynomial functions themselves. However, we do not know whether these numerator and denominator polynomials have common roots or not.

Let us assume for the moment that they have no common roots. For the pack of N resonances we are studying, we would have to find some $3N$ roots. Furthermore, we have neglected the energy dependency of the penetration factor and as such we should be working in terms of $\sqrt{E}$. Then, we would have to find twice as many roots, namely $6N$. For a pack of some 1000 resonances, not uncommon for some heavy nuclei, it would imply finding about 6000 roots. This is definetely not an easy task, even more so considering that we do not have a very simple expression of the denominator polynomial in (2.61).

R.N. Hwang surmised in [17], and correctly so, that there are only $2N$ poles to be found (in the case of quantum level $l = 0$). In other words, there are some common roots between the numerator and denominator in the form of ρ_{nn} in (2.61). I give in the next section a mathematical proof of this result based on a mathematical study of the polynomial denominator.

Let us keep neglecting the energy dependency of the penetration factor and work with E as a variable. We would like to find the $3N$ roots of the denominator in (2.61), or at least find some of them. We note this denominator polynomial

$$D(E) := \begin{vmatrix} Q + \sum_{r=1}^{N} i\gamma_{nr}\gamma_{nr}Q_r & \sum_{r=1}^{N} i\gamma_{nr}\gamma_{ar}Q_r & \sum_{r=1}^{N} i\gamma_{nr}\gamma_{br}Q_r \\ \sum_{r=1}^{N} i\gamma_{ar}\gamma_{nr}Q_r & Q + \sum_{r=1}^{N} i\gamma_{ar}\gamma_{ar}Q_r & \sum_{r=1}^{N} i\gamma_{ar}\gamma_{br}Q_r \\ \sum_{r=1}^{N} i\gamma_{br}\gamma_{nr}Q_r & \sum_{r=1}^{N} i\gamma_{br}\gamma_{ar}Q_r & Q + \sum_{r=1}^{N} i\gamma_{br}\gamma_{br}Q_r \end{vmatrix}. \tag{2.64}$$

The first idea is to look at the value of D at one of the resonance energy E_r, $1 \leq r \leq N$. From the definition of the Q_s in (2.63), we see that for $s \neq r$, $Q_s(E_r) = 0$. Therefore,

$$D(E_r) = \begin{vmatrix} i\gamma_{nr}\gamma_{nr}Q_r(E_r) & i\gamma_{nr}\gamma_{ar}Q_r(E_r) & i\gamma_{nr}\gamma_{br}Q_r(E_r) \\ i\gamma_{ar}\gamma_{nr}Q_r(E_r) & i\gamma_{ar}\gamma_{ar}Q_r(E_r) & i\gamma_{ar}\gamma_{br}Q_r(E_r) \\ i\gamma_{br}\gamma_{nr}Q_r(E_r) & i\gamma_{br}\gamma_{ar}Q_r(E_r) & i\gamma_{br}\gamma_{br}Q_r(E_r) \end{vmatrix} \tag{2.65}$$

$$= \big(iQ_r(E_r)\big)^3 \begin{vmatrix} \gamma_{nr}\gamma_{nr} & \gamma_{nr}\gamma_{ar} & \gamma_{nr}\gamma_{br} \\ \gamma_{ar}\gamma_{nr} & \gamma_{ar}\gamma_{ar} & \gamma_{ar}\gamma_{br} \\ \gamma_{br}\gamma_{nr} & \gamma_{br}\gamma_{ar} & \gamma_{br}\gamma_{br} \end{vmatrix} \tag{2.66}$$

$$= \big(iQ_r(E_r)\big)^3 \gamma_{nr}^2\gamma_{ar}^2\gamma_{br}^2 \begin{vmatrix} 1 & 1 & 1 \\ 1 & 1 & 1 \\ 1 & 1 & 1 \end{vmatrix}. \tag{2.67}$$

A very striking result is that the determinant is equal to 0, since the matrix is of rank 1. Namely, for any resonance $1 \leq r \leq N$, $D(E_r) = 0$. We have immediately found N roots out of the $3N$ we are looking for.

It is actually possible to show that the E_r, $1 \leq r \leq N$, are not only roots of D but also roots of the derivative of D. This is not a completely obvious result and I do not show here the mathematical proof as this is more a pedagogical example than the solution I finally adopted. Admitting that they are roots of multiplicity 2, we actually have found $2N$ roots out of the $3N$ we are looking for.

With a similar approach, we could show that the E_r, $1 \leq r \leq N$ are also roots of the numerator with multiplicity 2. The numerator is a product of Q and a 2×2 determinant. Q has the E_r, $1 \leq r \leq N$, as roots. The 2×2 determinant also has the E_r, $1 \leq r \leq N$, as roots by the same proof that for D.

We can conclude that multiplication by Q^3 of the numerator and denominator in (2.59) was a bit excessive. Indeed it resulted in numerator and denominator polynomials sharing some $2N$ roots.

In theory we could have just multiplied numerator and denominator of (2.59) by Q. However, even if we know that the numerator and denominator are polynomials, it does

not seem easy to compute the logarithmic derivative of the denominator, which is needed to compute the partial fraction decomposition. To tackle this issue, I tried to write some matrix algebra giving a form of the denominator polynomial easier to work with. I am going to show that we can actually go back to the non-fissile case and study of ρ_{nn} that I have presented previously.

2.2.2 Study of the determinant and cofactors of the reduced R-matrix

We now take into account the energy dependency of the elastic width. We will see that this merely adds a few poles to compute. We recall that the ρ matrix is defined by

$$\rho = Id - \left(Id - i\mathcal{P}^{1/2}\widehat{R}\mathcal{P}^{1/2}\right)^{-1}. \tag{2.68}$$

The main obstacle is the matrix inversion so we wish to extract the $\mathcal{P}^{1/2}$ terms from it. From (2.68), we can write

$$\begin{aligned}\rho &= Id - \left(Id - i\mathcal{P}^{1/2}\widehat{R}\mathcal{P}^{1/2}\right)^{-1} \\ &= Id - \mathcal{P}^{-1/2}\left(\mathcal{P}^{-1/2} - i\mathcal{P}^{1/2}\widehat{R}\right)^{-1} \\ &= Id - \mathcal{P}^{-1/2}\left(Id - i\mathcal{P}\widehat{R}\right)^{-1}\mathcal{P}^{1/2}.\end{aligned} \tag{2.69}$$

We will first focus on the matrix inversion and worry about the surrounding $\mathcal{P}^{-1/2}$ and $\mathcal{P}^{1/2}$ terms later. We note $u = \sqrt{E}$ and

$$\begin{aligned}M(u) &:= Id - i\mathcal{P}R \\ &= \begin{pmatrix} 1 + P_l(\beta u)\sum_{r=1}^{N}\frac{i\gamma_{nr}\gamma_{nr}}{u^2 - \widetilde{E_r}} & P_l(\beta u)\sum_{r=1}^{N}\frac{i\gamma_{nr}\gamma_{ar}}{u^2 - \widetilde{E_r}} & P_l(\beta u)\sum_{r=1}^{N}\frac{i\gamma_{nr}\gamma_{br}}{u^2 - \widetilde{E_r}} \\ \sum_{r=1}^{N}\frac{i\gamma_{ar}\gamma_{nr}}{u^2 - \widetilde{E_r}} & 1 + \sum_{r=1}^{N}\frac{i\gamma_{ar}\gamma_{ar}}{u^2 - \widetilde{E_r}} & \sum_{r=1}^{N}\frac{i\gamma_{ar}\gamma_{br}}{u^2 - \widetilde{E_r}} \\ \sum_{r=1}^{N}\frac{i\gamma_{br}\gamma_{nr}}{u^2 - \widetilde{E_r}} & \sum_{r=1}^{N}\frac{i\gamma_{br}\gamma_{ar}}{u^2 - \widetilde{E_r}} & 1 + \sum_{r=1}^{N}\frac{i\gamma_{br}\gamma_{br}}{u^2 - \widetilde{E_r}} \end{pmatrix}.\end{aligned} \tag{2.70}$$

Among the coefficients of the matrix inverse of M, only some are relevant for the cross-sections formulae. We will focus on these terms, although the other terms can be treated likewise.

The coefficients of the inverse of M can be computed by the cofactor formula. We note $N := M^{-1}$. Then we have the following relations :

$$N_{nn} := (M^{-1})_{nn} = +\frac{\det_{nn}(M)}{\det(M)}, \tag{2.71}$$

$$N_{na} := (M^{-1})_{na} = -\frac{\det_{an}(M)}{\det(M)}, \tag{2.72}$$

$$N_{nb} := (M^{-1})_{nb} = +\frac{\det_{bn}(M)}{\det(M)}. \tag{2.73}$$

with $\det_{cd}$ the determinant of the matrix M where we have extracted the row indexed c and the column index d. The signs will have limited importance later on but I put them here so as to respect the exact definitions of the cofactor formula.

The coefficients of M are rational functions. As such, the determinant and the extracted determinants will also be rational functions. We would like to give a partial fraction decomposition of N_{nn}, N_{na} and N_{nb}.

We are going to proceed in a few steps,

- The rational function $\det(M)$ appears in the denominator of the three terms that we are studying. We are going to show that it admits a partial fraction decomposition with at most $2N + 2l$ simple poles.
- The numerator are extracted determinants. They are also rational functions. We are going to show that the three of them admit a partial fraction decomposition with at most the same $2N + 2l$ simple poles of $\det(M)$.
- Given these numerators and the denominator partial fraction decompositions, we are going to work on the partial fraction decomposition of the quotients.

2.2.3 Partial fraction decomposition of the determinant

We want to give a partial fraction decomposition of the determinant. The usual approach for this problem is to write the rational function that we are studying as a quotient of polynomials. Then we look at the roots of the denominator polynomials, which are exactly the poles.

For $\det(M)$, this is not possible since we definitely do not have any simple expression as a quotient of polynomials. We do know however that a rational function diverges when evaluated at its poles.

If we examine the coefficients of the matrix M, we see that for most values of u all of them are finite. Then for these values the determinant of the matrix will necessarily be finite. This immediately narrows down our search to a restricted set of values of u.

Namely, the coefficients can only diverge at one of the $2N$ $u_r^{\pm}$ complex square roots of the $\widetilde{E_r}$ or at a pole of $z \mapsto P_l(\beta z)$ (one of the $2l$ roots of $z \mapsto q_l(\beta z)$). This limits the possible poles, but does not guarantee that they are exactly the poles. It is possible that the coefficients diverge in such a way that the determinant will still be finite. In that case the divergent value is not a pole. Conversely, it is possible that the pole has larger multiplicity than 1. To answer these two questions, we are going to look at the value of the corresponding residue with a limit formula.

Residue corresponding to a resonance pole

We know that $\det(M(u))$ can diverge when u goes to some $u_r^{\pm}$. Our goal is to find an expression of the limit of $(u-u_r^{\pm})\det(M(u))$. There are three possible cases that will help us decide if $u_r^{\pm}$ is a pole, not a pole, or a pole with high multiplicity :

- the limit is zero, in which case $u_r^{\pm}$ was actually not a pole even if some coefficients of the matrix M were divergent at that value.
- the limit is finite and not zero, in which case $u_r^{\pm}$ is a simple pole and the limit is the residue corresponding to this pole. This is what we aim at proving.
- the expression diverges, in which case $u_r^{\pm}$ is a pole with multiplicity larger than 1.

It took me quite a long time during my work to find a suitable expression of $(u-u_r^{\pm})\det(M(u))$. The following development is the shortest derivation I eventually settled with, although not necessarilly the most intuitive.

Let r be the index of a resonance, $1 \leq r \leq N$. We note

$$\gamma_r = \begin{pmatrix} \gamma_{nr} \\ \gamma_{ar} \\ \gamma_{br} \end{pmatrix}. \tag{2.74}$$

This allows writing M in a more compact way :

$$M(u) = Id + i\mathcal{P}(\beta u)\sum_{r=1}^{N} \frac{\gamma_r \gamma_r^T}{u^2 - u_r^2} \tag{2.75}$$

where γ_r^T is the transpose of the vector γ_r, and $\gamma_r\gamma_r^T$ is a 3×3 matrix.

We consider the following 4×4 matrix defined by blocks, where we have somewhat separated a resonance indexed s. The upper-left block is a scalar. The upper-right block is a horizontal vector. The lower-left block is a vector. The lower-right block is a 3×3 matrix.

$$H_s(u) := \begin{pmatrix} 1 & -\gamma_s^T \\ i\dfrac{\mathcal{P}(\beta u)\gamma_s}{u^2-u_s^2} & Id + i\mathcal{P}(\beta u)\displaystyle\sum_{r\neq s} \frac{\gamma_r\gamma_r^T}{u^2-u_r^2} \end{pmatrix}. \tag{2.76}$$

We have the following block matrices multiplication equality :

$$H_s(u) \times \begin{pmatrix} 1 & \gamma_s^T \\ 0 & Id \end{pmatrix} = \begin{pmatrix} 1 & 0 \\ i\dfrac{\mathcal{P}(\beta u)\gamma_s}{u^2-u_s^2} & M(u) \end{pmatrix}. \tag{2.77}$$

Then, by taking the determinant of (2.77), where the block triangular matrices determinant are trivially evaluated, we have

$$\det(H_s(u)) = \det(M(u)). \tag{2.78}$$

In particular, by multiplying the first column of $H_s(u)$ by $u-u_s^{\pm}$, from (2.76) and (2.78) we have

$$\begin{aligned}(u-u_s^{\pm})\det(M(u)) &= (u-u_s^{\pm})\det\left(H_s(u)\right)\\ &= (u-u_s^{\pm})\begin{vmatrix} 1 & -\gamma_s^T \\ i\dfrac{\mathcal{P}(\beta u)\gamma_s}{u^2-u_s^2} & Id+i\mathcal{P}(\beta u)\displaystyle\sum_{r\neq s}\frac{\gamma_r\gamma_r^T}{u^2-u_r^2}\end{vmatrix}\\ &= \begin{vmatrix} (u-u_s^{\pm}) & -\gamma_s^T \\ i\dfrac{\mathcal{P}(\beta u)\gamma_s}{u-u_s^{\mp}} & Id+i\mathcal{P}(\beta u)\displaystyle\sum_{r\neq s}\frac{\gamma_r\gamma_r^T}{u^2-u_r^2}\end{vmatrix}. \end{aligned} \tag{2.79}$$

Finally, taking limits yields

$$(u-u_s^{\pm})\det\big(M(u)\big) \xrightarrow[u\to u_s^{\pm}]{} \begin{vmatrix} 0 & -\gamma_s^T \\ i\dfrac{\mathcal{P}(\beta u_s^{\pm})\gamma_s}{2u_s^{\pm}} & Id+i\mathcal{P}(\beta u_s^{\pm})\displaystyle\sum_{r\neq s}\frac{\gamma_r\gamma_r^T}{u_s^2-u_r^2}\end{vmatrix}. \tag{2.80}$$

Let us discuss the value of the limit determinant in (2.80). First, let us remark that the resonances all have different energies. As such, the $u_s^2-u_r^2$ will never cancel in the lower right block. The only possible divergence of the coefficients would come from $P_l(\beta u_s^{\pm})$. The poles of $z\mapsto P_l(\beta z)$ are the roots of $z\mapsto q_l(\beta z)$. For $l=0$ there are no such roots so there is no divergence. For $l=1$ these roots are pure imaginary numbers. The $u_r^{\pm}$ are the complex square roots of the perturbed resonances and are never pure imaginary so, again, there is no divergence. For $l>1$ the situation is more complicated. As it stands, I have not found a simple condition to guarantee that $\beta u_s^{\pm}$ cannot be a root of q_l. However, it seems highly unlikely and has never happened in any numerical applications.

As it stands we are almost guaranteed that the determinant will be finite. If it is zero, then the $u_r^{\pm}$ of interest is not a pole. I have not found a simple condition to guarantee a non zero value. However, it is of limited practical importance. Indeed, most of the following developments will not rely on the $u_r^{\pm}$ being or not a pole but rather on the number of possible poles being limited and identified.

From now on we admit that this limit is always numerically finite and not zero. Under this assumption, we have found $2N$ simple poles of $\det(M)$. Their residues are computed by (2.80).

Residue corresponding to an orbital pole

Let v_k/β, $1\leq k\leq 2l$, be one of the $2l$ poles of $z\mapsto P_l(\beta z)$. As we have seen section 1.2, we can write the rational function P_l as a quotient of two polynomials p_l and q_l. We multiply the first line of (2.75) by $(u-v_k/\beta)$:

$$\begin{pmatrix} u-v_k/\beta & 0 & 0\\ 0 & 1 & 0\\ 0 & 0 & 1\end{pmatrix}\times M(u) = \begin{pmatrix} u-v_k/\beta & 0 & 0\\ 0 & 1 & 0\\ 0 & 0 & 1\end{pmatrix}$$

$$+ i \begin{pmatrix} (u - v_k/\beta)\, P_l(\beta u) & 0 & 0 \\ 0 & 1 & 0 \\ 0 & 0 & 1 \end{pmatrix} \sum_{r=1}^{N} \frac{\gamma_r \gamma_r^T}{u^2 - u_r^2}. \tag{2.81}$$

By taking the determinant of (2.81), and then the limit when u goes to v_k/β, we obtain

$$\left(u - \frac{v_k}{\beta}\right) \det\left(M(u)\right) \xrightarrow[u \to \frac{v_k}{\beta}]{} \left| \begin{pmatrix} 0 & 0 & 0 \\ 0 & 1 & 0 \\ 0 & 0 & 1 \end{pmatrix} + \begin{pmatrix} \frac{i p_l(v_k)}{\beta q_l'(v_k)} & 0 & 0 \\ 0 & 1 & 0 \\ 0 & 0 & 1 \end{pmatrix} \left(\sum_{r=1}^{N} \frac{\gamma_r \gamma_r^T}{(v_k/\beta)^2 - u_r^2} \right) \right|. \tag{2.82}$$

We need to ask the same question as just before. Provided we have assumed that the $u_r^{\pm}$ are never roots of q_l, the $(v_k/\beta)^2 - u_r^2$ are never zero. Then, no coefficient in the right hand determinant of (2.82) can diverge. Under the assumption of separation of orbital poles and resonance poles, the limit is finite.

Again, there is no simple guarantee that the limit is non zero. For the same reason as for the resonance poles, we proceed as if it were.

Again, we admit that this limit is finite and numerically always not zero. Under this assumption, the v_k/β, $1 \leq k \leq 2l$, are simple poles of $z \mapsto \det(M(z))$ with the corresponding residues given by the limit in (2.82).

Partial fraction decomposition formula

We have found all the poles of $\det(M)$ and their residues. Let us look at the limit of this rational function when u goes to ∞. From (2.70) that M converges to the 3×3 identity matrix. Indeed, $P_l(\beta u)$ behaves like $\mathcal{O}(u)$ while the sums on resonance terms all behave as $\mathcal{O}(1/u^2)$. It then follows that their product goes to zero and only the 1 in the diagonal remain. By continuity of the determinant

$$\det\big(M(z)\big) \xrightarrow[z \to \infty]{} 1. \tag{2.83}$$

Finally ,we have the partial fraction decomposition of $\det(M)$:

$$\boxed{\det\big(M(u)\big) = 1 + \sum_{r=1}^{N} \frac{a_r^+}{u - u_r^+} + \sum_{r=1}^{N} \frac{a_r^-}{u - u_r^-} + \sum_{k=1}^{2l} \frac{b_k}{u - v_k/\beta}} \tag{2.84}$$

with

$$a_r^+ = \left| \begin{matrix} 0 & -\gamma_r^T \\ i\dfrac{\mathcal{P}(\beta u_r^+)\gamma_r}{2u_r^+} & Id + i\mathcal{P}(\beta u_r^+) \displaystyle\sum_{s \neq r} \frac{\gamma_s \gamma_s^T}{\widetilde{E_r} - \widetilde{E_s}} \end{matrix} \right|, \tag{2.85}$$

$$a_r^- = \begin{vmatrix} 0 & -\gamma_r^T \\ i\dfrac{\mathcal{P}(\beta u_r^-)\gamma_r}{2u_r^-} & Id + i\mathcal{P}(\beta u_r^-)\displaystyle\sum_{s\neq r}\frac{\gamma_s\gamma_s^T}{\widetilde{E_r}-\widetilde{E_s}} \end{vmatrix}, \tag{2.86}$$

$$b_k = \left| \begin{pmatrix} 0 & 0 & 0 \\ 0 & 1 & 0 \\ 0 & 0 & 1 \end{pmatrix} + \begin{pmatrix} \dfrac{ip_l(v_k)}{\beta q_l'(v_k)} & 0 & 0 \\ 0 & 1 & 0 \\ 0 & 0 & 1 \end{pmatrix} \left(\sum_{r=1}^{N} \frac{\gamma_r\gamma_r^T}{(v_k/\beta)^2 - u_r^2} \right) \right|. \tag{2.87}$$

We have found a partial fraction decomposition of $\det(M)$ (with possibly some zero residues). We are going to show that most of the arguments we have used can also be applied to the extracted determinants.

2.2.4 Partial fraction decomposition of the extracted determinants

Let us write the extracted determinants formulae :

$$\det_{nn}(M(u)) = \begin{vmatrix} 1 + \displaystyle\sum_{r=1}^{N} \frac{i\gamma_{ar}\gamma_{ar}}{u^2 - \widetilde{E_r}} & \displaystyle\sum_{r=1}^{N} \frac{i\gamma_{ar}\gamma_{br}}{u^2 - \widetilde{E_r}} \\ \displaystyle\sum_{r=1}^{N} \frac{i\gamma_{br}\gamma_{ar}}{u^2 - \widetilde{E_r}} & 1 + \displaystyle\sum_{r=1}^{N} \frac{i\gamma_{br}\gamma_{br}}{u^2 - \widetilde{E_r}} \end{vmatrix}, \tag{2.88}$$

$$\begin{aligned} \det_{an}(M(u)) &= \begin{vmatrix} P_l(\beta u)\displaystyle\sum_{r=1}^{N} \frac{i\gamma_{nr}\gamma_{ar}}{u^2 - \widetilde{E_r}} & P_l(\beta u)\displaystyle\sum_{r=1}^{N} \frac{i\gamma_{nr}\gamma_{br}}{u^2 - \widetilde{E_r}} \\ \displaystyle\sum_{r=1}^{N} \frac{i\gamma_{br}\gamma_{ar}}{u^2 - \widetilde{E_r}} & 1 + \displaystyle\sum_{r=1}^{N} \frac{i\gamma_{br}\gamma_{br}}{u^2 - \widetilde{E_r}} \end{vmatrix} \\ &= P_l(\beta u) \begin{vmatrix} \displaystyle\sum_{r=1}^{N} \frac{i\gamma_{nr}\gamma_{ar}}{u^2 - \widetilde{E_r}} & \displaystyle\sum_{r=1}^{N} \frac{i\gamma_{nr}\gamma_{br}}{u^2 - \widetilde{E_r}} \\ \displaystyle\sum_{r=1}^{N} \frac{i\gamma_{br}\gamma_{ar}}{u^2 - \widetilde{E_r}} & 1 + \displaystyle\sum_{r=1}^{N} \frac{i\gamma_{br}\gamma_{br}}{u^2 - \widetilde{E_r}} \end{vmatrix}. \end{aligned} \tag{2.89}$$

Examining these determinants and the argument I have developed previously to identify the possible poles of $\det(M)$, I surmised that I could apply the same approach to them. I do not detail the whole derivation here but it possible to show that we have the following partial fraction decompositions :

$$\det_{nn}(M(u)) = 1 + \sum_{r=1}^{N} \frac{\omega_{nr}^+}{u - u_r^+} + \sum_{r=1}^{N} \frac{\omega_{nr}^-}{u - u_r^-}, \tag{2.90}$$

$$\det_{an}(M(u)) = P_l(\beta u) \left(\sum_{r=1}^{N} \frac{\omega_{ar}^+}{u - u_r^+} + \sum_{r=1}^{N} \frac{\omega_{ar}^-}{u - u_r^-} \right), \tag{2.91}$$

$$\det_{bn}(M(u)) = P_l(\beta u)\left(\sum_{r=1}^{N}\frac{\omega_{br}^{+}}{u-u_r^{+}}+\sum_{r=1}^{N}\frac{\omega_{br}^{-}}{u-u_r^{-}}\right). \tag{2.92}$$

Moreover, the residues $\omega_{nr}^{\pm}$, $\omega_{ar}^{\pm}$ and $\omega_{br}^{\pm}$ are computed from the formulae (2.85) and (2.86). One needs to extract the line and column corresponding to the extracted determinant being studied (the determinant becomes 3×3).

2.2.5 Partial fraction decomposition of the coefficients of ρ

We have shown that

$$\det(M(u)) = 1+\sum_{r=1}^{N}\frac{a_r^{+}}{u-u_r^{+}}+\sum_{r=1}^{N}\frac{a_r^{-}}{u-u_r^{-}}+\sum_{k=1}^{2l}\frac{b_k}{u-v_k/\beta}. \tag{2.93}$$

The formula (2.69) and the cofactor formulae (2.71), (2.72) and (2.73) yields

$$\rho_{nn}(u) = 1-\frac{\det_{nn}(M(u))}{\det(M(u))}, \tag{2.94}$$

$$\rho_{na}(u) = \frac{-1}{P_l^{1/2}(\beta u)}\frac{\det_{an}(M(u))}{\det(M(u))}, \tag{2.95}$$

$$\rho_{nb}(u) = \frac{+1}{P_l^{1/2}(\beta u)}\frac{\det_{bn}(M(u))}{\det(M(u))}. \tag{2.96}$$

Partial fraction decomposition of $\boldsymbol{\rho_{nn}}$

We have

$$\rho_{nn}(u) = 1-\frac{1+\sum_{r=1}^{N}\frac{\omega_{nr}^{+}}{u-u_r^{+}}+\sum_{r=1}^{N}\frac{\omega_{nr}^{-}}{u-u_r^{-}}}{1+\sum_{r=1}^{N}\frac{a_r^{+}}{u-u_r^{+}}+\sum_{r=1}^{N}\frac{a_r^{-}}{u-u_r^{-}}+\sum_{k=1}^{2l}\frac{b_k}{u-v_k/\beta}}. \tag{2.97}$$

At the cost of an additional step to compute the coefficients ω_{nr}^{+}, ω_{nr}^{-}, a_r^{+}, a_r^{-} and b_k, we have found a very similar formula to that of the non-fissile case for ρ_{nn}. The difference lies in the numerator, which is not constant and equal to 1 anymore. However, we are going to give the partial fraction decomposition of ρ_{nn} by using the same ideas that we used previously.

The problem is, as in the non-fissile case, that we do not have a polynomial numerator and denominator. However, the numerator and denominator partial fraction decompositions have the same poles. We multiply by $Q(u)q_l(\beta u)$ as we did in the non-fissile case. Then, we define

$$f(u) = Q(u)q_l(\beta u)\left(1+\sum_{r=1}^{N}\frac{\omega_{nr}^{+}}{u-u_r^{+}}+\sum_{r=1}^{N}\frac{\omega_{nr}^{-}}{u-u_r^{-}}\right), \tag{2.98}$$

$$g(u) = Q(u)q_l(\beta u)\left(1 + \sum_{r=1}^{N}\frac{a_r^+}{u-u_r^+} + \sum_{r=1}^{N}\frac{a_r^-}{u-u_r^-} + \sum_{k=1}^{2l}\frac{b_k}{u-v_k/\beta}\right). \tag{2.99}$$

We do not develop the product with the expression between parentheses. f and g are both polynomials and we have

$$\rho_{nn}(u) = 1 - \frac{f(u)}{g(u)}. \tag{2.100}$$

To find the roots of g, we can apply the exact same idea as the one I used in the non-fissile case in (2.41). Namely, the logarithmic derivative of g admits the following expression :

$$\begin{aligned}\frac{g'(u)}{g(u)} =& \frac{Q'(u)}{Q(u)} + \frac{\beta q_l'(\beta u)}{q_l(\beta u)} - \frac{\displaystyle\sum_{r=1}^{N}\frac{a_r^+}{(u-u_r^+)^2} + \sum_{r=1}^{N}\frac{a_r^-}{(u-u_r^-)^2} + \sum_{k=1}^{2l}\frac{b_k}{(u-v_k/\beta)^2}}{\displaystyle 1 + \sum_{r=1}^{N}\frac{a_r^+}{u-u_r^+} + \sum_{r=1}^{N}\frac{a_r^-}{u-u_r^-} + \sum_{k=1}^{2l}\frac{b_k}{u-v_k/\beta}} \\ =& \sum_{r=1}^{N}\frac{1}{u-u_r^+} + \sum_{r=1}^{N}\frac{1}{u-u_r^-} + \sum_{k=1}^{2l}\frac{1}{u-v_k/\beta} \\ & - \frac{\displaystyle\sum_{r=1}^{N}\frac{a_r^+}{(u-u_r^+)^2} + \sum_{r=1}^{N}\frac{a_r^-}{(u-u_r^-)^2} + \sum_{k=1}^{2l}\frac{b_k}{(u-v_k/\beta)^2}}{\displaystyle 1 + \sum_{r=1}^{N}\frac{a_r^+}{u-u_r^+} + \sum_{r=1}^{N}\frac{a_r^-}{u-u_r^-} + \sum_{k=1}^{2l}\frac{b_k}{u-v_k/\beta}}.\end{aligned} \tag{2.101}$$

This might seem complicated, and it is in some sense, but compared to computing a polynomial of degree $2N+2l$ and its derivative, this expression is quite satisfactory. It involves only sums and very few multiplications. Applying the algorithm described in subsection 3.2.3, we can then compute the roots of g that we note z_p, $1 \leq p \leq 2N + 2l$. We compute the residues using the same idea as in the non-fissile case. Specifically, we use a convenient expression of f/g,

$$\frac{f(u)}{g(u)} = \frac{\displaystyle 1 + \sum_{r=1}^{N}\frac{\omega_{nr}^+}{u-u_r^+} + \sum_{r=1}^{N}\frac{\omega_{nr}^-}{u-u_r^-}}{\displaystyle 1 + \sum_{r=1}^{N}\frac{a_r^+}{u-u_r^+} + \sum_{r=1}^{N}\frac{a_r^-}{u-u_r^-} + \sum_{k=1}^{2l}\frac{b_k}{u-v_k/\beta}}, \tag{2.102}$$

so that

$$\frac{f(u)}{g'(u)} = \frac{f(u)/g(u)}{g'(u)/g(u)}. \tag{2.103}$$

The full expanded expression is very long and is composed of the following four terms :

$$A(u) := 1 + \sum_{r=1}^{N}\frac{\omega_{nr}^+}{u-u_r^+} + \sum_{r=1}^{N}\frac{\omega_{nr}^-}{u-u_r^-}, \tag{2.104}$$

$$B(u) := 1 + \sum_{r=1}^{N} \frac{a_r^+}{u - u_r^+} + \sum_{r=1}^{N} \frac{a_r^-}{u - u_r^-} + \sum_{k=1}^{2l} \frac{b_k}{u - v_k/\beta}, \tag{2.105}$$

$$C(u) := \sum_{r=1}^{N} \frac{1}{u - u_r^+} + \sum_{r=1}^{N} \frac{1}{u - u_r^-} + \sum_{k=1}^{2l} \frac{1}{u - v_k/\beta}, \tag{2.106}$$

$$D(u) := \sum_{r=1}^{N} \frac{a_r^+}{(u - u_r^+)^2} + \sum_{r=1}^{N} \frac{a_r^-}{(u - u_r^-)^2} + \sum_{k=1}^{2l} \frac{b_k}{(u - v_k/\beta)^2}. \tag{2.107}$$

Then

$$\frac{f(u)}{g'(u)} = \frac{A(u)}{B(u)C(u) - D(u)}. \tag{2.108}$$

The residues corresponding to the roots of g are finally computed as

$$\eta_{np} := \frac{f(z_p)}{g'(z_p)} = \frac{A(z_p)}{B(z_p)C(z_p) - D(z_p)}. \tag{2.109}$$

Finally, the partial fraction decomposition of ρ_{nn} is

$$\zeta_{np} := \frac{1 + \sum_{r=1}^{N} \frac{\omega_{nr}^+}{z_p - u_r^+} + \sum_{r=1}^{N} \frac{\omega_{nr}^-}{z_p - u_r^-}}{\sum_{r=1}^{N} \frac{a_r^+}{(z_p - u_r^+)^2} + \sum_{r=1}^{N} \frac{a_r^-}{(z_p - u_r^-)^2} + \sum_{k=1}^{2l} \frac{b_k}{(z_p - v_k/\beta)^2}}. \tag{2.110}$$

By taking the limit of f/g when u goes to infinity, the remainder is 1. Finally we have the partial fraction decomposition of f/g :

$$\frac{f(u)}{g(u)} = 1 + \sum_{p=1}^{2N+2l} \frac{\zeta_{np}}{u - z_p}; \tag{2.111}$$

this immediately yields the partial fraction decomposition of ρ_{nn} :

$$\rho_{nn}(u) = 1 - (1 + \sum_{p=1}^{2N+2l} \frac{\zeta_{np}}{u - z_p}) \tag{2.112}$$

$$:= \sum_{p=1}^{2N+2l} \frac{\eta_{np}}{u - z_p}. \tag{2.113}$$

Partial fraction decomposition of $|\rho_{na}|^2$ and $|\rho_{nb}|^2$

The situation for ρ_{na} and ρ_{nb} is a bit different, since there is a term of the form $P_l^{1/2}(\beta u)$. I will focus on ρ_{na}, since the study is exactly the same for ρ_{nb}. We have the following expression

for ρ_{na} :

$$\rho_{na}(u) = P_l^{1/2}(\beta u)\frac{\displaystyle\sum_{r=1}^{N}\frac{\omega_{ar}^{+}}{u-u_r^{+}} + \sum_{r=1}^{N}\frac{\omega_{ar}^{-}}{u-u_r^{-}}}{1+\displaystyle\sum_{r=1}^{N}\frac{a_r^{+}}{u-u_r^{+}} + \sum_{r=1}^{N}\frac{a_r^{-}}{u-u_r^{-}} + \sum_{k=1}^{2l}\frac{b_k}{u-v_k/\beta}}. \tag{2.114}$$

Conveniently, the terms appearing in the cross-sections formulae are the modulus square of ρ_{na} and ρ_{nb}. Therefore, the terms we want to study are rational functions and admit a partial fraction decomposition :

$$|\rho_{na}(u)|^2 = P_l(\beta u)\left|\frac{\displaystyle\sum_{r=1}^{N}\frac{\omega_{ar}^{+}}{u-u_r^{+}} + \sum_{r=1}^{N}\frac{\omega_{ar}^{-}}{u-u_r^{-}}}{1+\displaystyle\sum_{r=1}^{N}\frac{a_r^{+}}{u-u_r^{+}} + \sum_{r=1}^{N}\frac{a_r^{-}}{u-u_r^{-}} + \sum_{k=1}^{2l}\frac{b_k}{u-v_k/\beta}}\right|^2. \tag{2.115}$$

Similarly to ρ_{nn}, we can write a partial fraction decomposition for the term inside the modulus square. The partial fraction decomposition in the denominator is exactly the same and so are the resulting poles of the quotient. We do not detail the exact expressions of the residues as they are very similar to that of ρ_{nn} previously made explicit. We then have the following relation :

$$\frac{\displaystyle\sum_{r=1}^{N}\frac{\omega_{ar}^{+}}{u-u_r^{+}} + \sum_{r=1}^{N}\frac{\omega_{ar}^{-}}{u-u_r^{-}}}{1+\displaystyle\sum_{r=1}^{N}\frac{a_r^{+}}{u-u_r^{+}} + \sum_{r=1}^{N}\frac{a_r^{-}}{u-u_r^{-}} + \sum_{k=1}^{2l}\frac{b_k}{u-v_k/\beta}} = \sum_{p=1}^{2N+2l}\frac{\eta_{ap}}{u-z_p}. \tag{2.116}$$

The relation (2.116) will come in handy shortly thereafter.

Then,

$$|\rho_{na}(u)|^2 = P_l(\beta u)\left(\sum_{p=1}^{2N+2l}\frac{\eta_{ap}}{u-z_p}\right)\left(\sum_{p=1}^{2N+2l}\frac{\overline{\eta_{ap}}}{u-\overline{z_p}}\right). \tag{2.117}$$

This is a rational function of u. We have, for u going to ∞,

$$\begin{aligned} P_l(\beta u) &= \mathcal{O}(u), \\ \sum_{p=1}^{2N+2l}\frac{\eta_{ap}}{u-z_p} &= \mathcal{O}(1/u), \\ \sum_{p=1}^{2N+2l}\frac{\overline{\eta_{ap}}}{u-\overline{z_p}} &= \mathcal{O}(1/u). \end{aligned}$$

We conclude that their product goes to 0 when u goes to ∞. Its poles are all simple and are the poles of $z \mapsto P_l(\beta z)$, the z_p and the $\overline{z_p}$. Therefore, it admits a partial fraction decomposition of the form

$$|\rho_{na}(u)|^2 = \sum_{k=1}^{2l} \frac{g_k}{u - v_k/\beta} + \sum_{p=1}^{2N+2l} \frac{h_{ap}}{u - z_p} + \sum_{p=1}^{2N+2l} \frac{\overline{h_{ap}}}{u - \overline{z_p}}. \tag{2.118}$$

The residues are computed by

$$g_k = \frac{p_l(v_k)}{\beta q_l'(v_k)} \left(\sum_{p=1}^{2N+2l} \frac{\eta_{ap}}{v_k/\beta - z_p} \right) \left(\sum_{p=1}^{2N+2l} \frac{\overline{\eta_{ap}}}{v_k/\beta - \overline{z_p}} \right), \tag{2.119}$$

$$h_{ap} = P_l(\beta z_p)\eta_{ap} \sum_{q=1}^{2N+2l} \frac{\overline{\eta_{aq}}}{z_p - \overline{z_q}}. \tag{2.120}$$

Using relation (2.116), we can show that the g_k are all mathematically null. Indeed, evaluating it at some v_k/β yields

$$0 = \sum_{p=1}^{2N+2l} \frac{\eta_{ap}}{v_k/\beta - z_p}. \tag{2.121}$$

Using this expression in (2.119) yields that the corresponding g_k is zero. The key factor here is that the partial fraction decomposition in the numerator of (2.116) has no term corresponding to the v_k/β. Consequently, the numerator is finite whereas the denominator diverges when evaluated.

Finally, the partial fraction decomposition of $|\rho_{na}|^2$ is

$$|\rho_{na}(u)|^2 = \sum_{p=1}^{2N+2l} \frac{h_{ap}}{u - z_p} + \sum_{p=1}^{2N+2l} \frac{\overline{h_{ap}}}{u - \overline{z_p}} \tag{2.122}$$

$$= 2\Re \left(\sum_{p=1}^{2N+2l} \frac{h_{ap}}{u - z_p} \right). \tag{2.123}$$

Partial fraction decomposition of $|\rho_{nn}|^2$

We need to write the partial fraction decomposition of one last term, namely $|\rho_{nn}|^2$. We have given a partial fraction decomposition of ρ_{nn}. From (3.12), we can write for some real u,

$$|\rho_{nn}(u)|^2 = \Re \left(\sum_{p=1}^{2N+2l} \frac{\delta_p}{u - z_p} \right) \tag{2.124}$$

with

$$\delta_p := 2\eta_{np} \sum_{q=1}^{2N+2l} \frac{\overline{\eta_{nq}}}{z_p - \overline{z_q}}. \tag{2.125}$$

We have been able to give a partial fraction decomposition of all the terms of interest of the cross-sections formulae with $2N + 2l$ poles. Let us give a multipole representation of these cross-sections.

2.2.6 Multipole representation of the fission, radiative capture, elastic and total cross-sections

After substitution of the different partial fraction decompositions (2.123), (2.113) and (2.124) into the cross-sections formulae (2.9) to (2.11) :

$$\sigma_{nf}(E) = \frac{4\pi}{k^2}\Re\left(\sum_{p=1}^{2N+2l}\frac{2h_{ap}+2h_{bp}}{\sqrt{E}-z_p}\right), \tag{2.126}$$

$$\sigma_{n\gamma}(E) = \frac{4\pi}{k^2}\Re\left(\sum_{p=1}^{2N+2l}\frac{\eta_{np}-\delta_p-2h_{ap}-2h_{bp}}{\sqrt{E}-z_p}\right), \tag{2.127}$$

$$\sigma_{nn}(E) = \frac{4\pi}{k^2}\sin^2(\phi_l) + \frac{4\pi}{k^2}\Re\left(\sum_{p=1}^{2N+2l}\frac{\eta_{np}(\exp(-2i\phi_l)-1)+\delta_p}{\sqrt{E}-z_p}\right), \tag{2.128}$$

$$\sigma_{nt}(E) = \frac{4\pi}{k^2}\sin^2(\phi_l) + \frac{4\pi}{k^2}\Re\left(\sum_{p=1}^{2N+2l}\frac{\eta_{np}\exp(-2i\phi_l)}{\sqrt{E}-z_p}\right). \tag{2.129}$$

We have shown that for a pack of quantum number l containing N resonances, we need exactly $2N+2l$ poles to give the multipole representation. The previous result was $2N(l+1)$ poles [17, 18].

I surmise that this previous result was not a problem for the practical use of the multipole representation. The authors of [17, 18] have noticed that some of these poles are very close to each other. Indeed we have proven by a mathematical study that only $2l$ are needed for a whole pack and not $2l$ per resonance as before. A pseudo-pole approach, which aims at reducing numerically the number of poles, should then be very effective at gathering these pole contributions into a few approximated poles.

However, the main advantage of the present result is sensible for the pole/root finding algorithm. Finding the roots of a polynomial is not at all linear with respect to the degree of the polynomial. The difference in terms of speed and numerical accuracy between finding the roots of a polynomial of degree $2N + 2l$ and $2N + 2lN$ is tremendous.

2.3 Algorithmic summary

The resonances of a pack have to be treated together. We recall that they are characterized by an energy E_r and a set of widths. The first step is to form the perturbed resonance energies $\widetilde{E_r}$ from formula (2.19).

In the case of non-fissile nuclei, one must compute the formal inversion of a partial fraction decomposition whose poles are the complex roots of the perturbed resonance energies $\widetilde{E_r}$ and the roots of $z \mapsto q_l(\beta z)$. The corresponding residues are computed according to formulae (2.36) and (2.35). The result of this formal inversion will be a partial fraction decomposition of ρ_{nn}, which then allows giving the multipole representation of the cross-section according to formulae (2.54) to (2.56). The formal inversion requires finding the roots of a polynomial (defined by expression (2.30)), which is done by a modified Newton-Raphson algorithm described in subsection 3.2.3 of Part I. This approach requires computing the logarithmic derivative of the polynomial of interest. This is done by formula (2.41).

In the case of fissile nuclei, an additional step is needed to get back to a situation very similar to the non-fissile case. This additional step consists in computing the partial fraction decomposition of the determinant, and extracted determinants, of a 3×3 matrix defined by expression (2.70). The poles of these partial fraction decompositions are again the perturbed resonance energies and the roots of $z \mapsto q_l(\beta z)$. Finding the corresponding residues constitutes the main added computational step. This is done according to subsection 2.2.3 and subsection 2.2.4. Once this is done, a formal inversion is required to obtain the partial fraction decomposition of ρ_{nn}, ρ_{na} and ρ_{nb}. The formal inversion is common to these three elements and uses the exact same Newton-Raphson algorithm as in the non-fissile case. The computation of the corresponding residues is slightly more complicated and is described in subsection 2.2.5. This yields the multipole representation of the cross-sections of formulae (2.126) to (2.129).

Chapter 3

Qualitative aspects of the multipole representation

In the previous two chapters, we have been interested in finding a multipole representation for the cross-sections described under the Multi-Level Breit-Wigner and Reich-Moore formalisms. This new representation of the 0K cross-sections allows manipulating them from a new perspective a priori agnostic of the original formalism they were reconstructed with. The challenges to obtain these poles are rather different for the two formalisms I worked with. However, I will show that they can be classified in a rather similar way for both cases. I will describe some of their qualitative properties and discuss the contribution of individual pole terms to the cross-sections profiles.

3.1 Classification of the poles

3.1.1 Multi-Level Breit-Wigner multipole representation

We have shown in the corresponding theoretical chapters that the cross-sections reconstructed with the Multi-Level Breit-Wigner formalism admit a multipole representation. This was already proven by R.N. Hwang and C. Jammes in [19]. The contribution of my work is that we need only $l+2$ poles per resonances instead of $2(l+1)$ at the cost of l poles for a whole pack of resonances.

We began by working with the radiative capture and fission cross-sections. For these, the multipole representation is obtained by studying the contribution to the cross-sections of each resonance separately. For one such resonance contribution, we gave its partial fraction decomposition. This involved finding the roots of the denominator polynomials

$$D_r(u) := \overline{r_l}(\beta u)(u^2 - \widetilde{E_r}) + \gamma_{nr}^2\big((l+1)\overline{r_l}(\beta u) - \overline{r_{l+1}}(\beta u)\big). \tag{3.1}$$

The exact definition of each element appearing in this polynomial can be found in chapter 1. As explained, this polynomial is of degree $l+2$. The roots are obtained by a Newton-Raphson

algorithm, which uses some guesses as starting point. In all practical situations the roots to which the algorithm converged were always close to the guesses.

I give here no theoretical proof of this observation. The intuitive reasoning is as follows. The polynomial D_r is a sum of two polynomials. One of these is considered small because it is multiplied by the reduced elastic width of the resonance. In numerical applications, this width is always small. The generic mathematical study would be that of a polynomial of the form

$$P(u) + \epsilon Q(u); \tag{3.2}$$

If ϵ is sufficiently small, it is not unreasonable to expect that the roots of this polynomial will be close to that of P. A mathematically correct approach would necessitate a more careful study of Q and its roots in relation to those of P. We admit that the intuitive rationale is valid in my applications provided that γ_{nr}^2 in (3.1) are small compared to $\widetilde{E_r}$ (defined in (1.25)).

The roots of $z \mapsto \overline{r_l}(\beta z)(z^2 - \widetilde{E_r})$, which I chose as my guesses, are well known. Two of them are the complex square roots of $\widetilde{E_r}$.

On one hand, this perturbed resonance energy is a complex number, although it usually has a small imaginary part compared to its real part. As such, we expect its complex square roots to be close to the real axis. One will lie on the negative part of that axis, the other on the positive part. If we admit that the roots are close to the guesses, the roots corresponding to these two guesses will also lie in the aforementioned locations. This is the first result that I wish to underline. For each resonance, two poles are inherited from the resonance energies and will lie close to the real axis.

On the other hand, l guesses are the roots of $z \mapsto r_l(\beta z)$. Let us discuss briefly the cases for the first few values of l. For $l = 0$ resonances, the polynomial r_l is constant and there are no such additional guess and root to find. For $l = 1$, r_1 has one root, the unit complex number i. Hence the guess is i/β which lies on the imaginary axis. It is again expected by the perturbative argument, that the roots found with this guess will also be very close to the imaginary axis. For higher values of l, there is no simple location for the root of r_l. However, these roots can be computed once and for all, as the definition of r_l is not only independent of the resonance but also of the studied nuclei themselves. Such a preliminary study shows that they are always away from the real axis. As a result, the roots obtained with such guesses are expected to also lie away from the real axis.

For the elastic and total cross-sections we saw that we need l additional poles for the multipole representation of each pack of quantum number l. These are not obtained from guesses and a Newton-Raphson algorithm as before. Rather, they are directly the l roots of r_l. They lie on the opposite side of the real axis from the roots of $\overline{r_l}$. As I have just mentioned for the roots of the latter - that we used as guesses - they are far away from the real axis.

We see that three types of poles naturally emerge. Some are obtained from the perturbed resonance energies $\widetilde{E_r}$. They have either negative or positive real part and are close to the real axis. Others are obtained from roots of r_l or are directly roots of r_l.

3.1.2 Reich-Moore multipole representation

I have shown that the cross-sections reconstructed with the Reich-Moore formalism also admit a multipole representation. Again, this was already proven by R.N. Hwang in [17, 18]. I have obtained a representation with less poles and provided a new algorithm to compute it.

The different cross-sections are treated together through a reduced R-matrix. The existence of the multipole representation had already been proven. The first step was to find and prove the exact number of poles needed. This was done in subsection 2.2.1 of the theoretical chapter about the Reich-Moore formalism

The multipole representation has to be computed pack of resonances by pack of resonances and cannot be computed for each resonance separately as for the Multi-Level Breit-Wigner formalism. However, the root-finding algorithm still uses some guesses.

We have proven in Chapter 2 that we need $2N + 2l$ poles for a pack of quantum number l containing N resonances. We previously chose the guesses with a perturbative argument. The polynomials to solve in the Reich-Moore case do not lend themselves easily to such an intuitive approach. However, the location of the poles in the results of R.N. Hwang for the Reich-Moore case are not significantly different than for the Multi-Level Breit-Wigner case. This is despite the significant difference in the number of poles needed for the multipole representation. I surmise that we still expect some poles to be inherited from the resonances and others from the penetration factors.

On one hand, we chose the complex square roots of the perturbed resonance energy $\widetilde{E_r}$. These do not have the same expression as in the Multi-Level Breit-Wigner case, but have the similar property of having a small imaginary part. Consequently, their square roots lie close to the real axis with one having a negative real part and the other one a positive real part.

On the other hand, there are $2l$ guesses which correspond to the poles of the penetration factor. These are the roots of $z \mapsto q_l(\beta z)$. These are exactly the l roots of r_l and the l roots of $\overline{r_l}$ defined in subsection 1.2.5 of the theoretical chapter about the Multi-Level Breit-Wigner formalism.

This choice proved to be very good, provided again that the resonance widths were small compared to the resonance energies. This may suggest that a perturbative argument still apply, although I must admit it eluded me.

3.1.3 Types of poles

As explained, although the number of poles required for the multipole representation of the Reich-Moore and Multi-Level Breit-Wigner formalisms is different, a common natural classification of them emerges. Namely, they fall under three categories :

- Poles with positive real part and small imaginary part. These are obtained from the positive real part complex square root of the perturbed energies. I denote them **posi-**

tive resonance poles.

- Conjointly, poles with negative real part and small imaginary part. These are obtained from the negative real part complex square root of the perturbed energies. I denote them **negative resonance poles**.
- Poles that lie away from the real axis, or (said differently), have a larger imaginary part than real part. These are obtained from the roots of r_l or $\overline{r_l}$. A closer look at their location depends on the value of l considered. I admit that the property of being far away from the real axis is always true. I denote them **orbital poles**.

There are two pathological cases I wish to discuss before looking at the qualitative contribution of these three types of poles.

First, some resonances described in the ENDF files, both for the Multi-Level Breit-Wigner and Reich-Moore formalism, have negative resonance energies. Those can serve as background correction for the cross-section. I did not pay attention to these in my theoretical study as they have no impact on the results that I have presented. However, the resonance poles corresponding to these resonance are significantly different from the first two categories I have presented above. Their resonance energies being negative, the corresponding $\widetilde{E_r}$ has a negative real part. As such, its complex square roots lie cloes to the imaginary axis. Conveniently, from a practical standpoint, I have noticed that they are very similar to orbital poles with $l = 1$. I will not discuss them further.

Second, it can happen for some nuclei that a resonance has an energy and a corresponding width similar in order of magnitude. This is the case, for instance, for the first resonance of Plutonium 239 around 0.3 eV. For such a resonance, the perturbed energy $\widetilde{E_r}$ does not lie particularly close to the real axis. As a direct consequence, its complex square roots do not either. From a qualitative standpoint, I still treat the poles obtained with these guesses as positive and negative resonance pole, even though they do not have the property of being close to the real axis.

3.2 Qualitative description of the contribution of the different types of poles

3.2.1 Types of pole terms

The types of poles differ notably by their locations in the complex plan. I am now going to briefly show the qualitative difference of the contribution of each pole terms given their type.

A pole term contribution is either of the form,

$$A_p(E) := \frac{4\pi}{k^2} \Re \left(\frac{a_p}{\sqrt{E} - z_p} \right) \tag{3.3}$$

or,

$$B_p(E) := \frac{4\pi}{k^2}\Re\left(\frac{b_p \exp(-2i\phi_l(\beta\sqrt{E}))}{\sqrt{E}-z_p}\right). \tag{3.4}$$

I will not study the latter type of terms as the variations of the ϕ_l term, while not negligible for $l = 0$ or $l = 1$, do not affect the qualitative study I will now present.

We focus on the terms noted A_p. A more convenient form would be :

$$A_p(E) \propto \frac{1}{E}\Re\left(\frac{a_p(\sqrt{E}-\overline{z_p})}{(\sqrt{E}-\Re(z_p))^2+\Im(z_p)^2}\right) \tag{3.5}$$

$$\propto \frac{1}{E}\left(\frac{\Re(a_p)\sqrt{E}}{(\sqrt{E}-\Re(z_p))^2+\Im(z_p)^2} - \frac{\Re(a_p\overline{z_p})}{(\sqrt{E}-\Re(z_p))^2+\Im(z_p)^2}\right). \tag{3.6}$$

We write $a_p = a + ib$ and $z_p := x + iy$,

$$A_p(E) \propto \frac{1}{E}\left(\frac{a\sqrt{E}}{(\sqrt{E}-x)^2+y^2} - \frac{ax+by}{(\sqrt{E}-x)^2+y^2}\right) \tag{3.7}$$

$$\propto \frac{1}{E}\left(\frac{a(\sqrt{E}-x)}{(\sqrt{E}-x)^2+y^2} - \frac{by}{(\sqrt{E}-x)^2+y^2}\right). \tag{3.8}$$

We see that A_p is a linear combination of two sub-terms,

$$\frac{1}{E}\frac{\sqrt{E}-x}{(\sqrt{E}-x)^2+y^2}, \tag{3.9}$$

$$\frac{1}{E}\frac{y}{(\sqrt{E}-x)^2+y^2}. \tag{3.10}$$

I have not studied the exact features of the mix depending on the values of the residues. The main idea is to show their variation and their asymptotic behavior. I will show both the shape of (3.9) and (3.10) for the different types of poles. I will do so by choosing representative values of x and y for each of these types. These choices are not completely arbitrary and are motivated by numerical applications of the multipole representation that I will discuss later. In Figure 3.1 to Figure 3.3, the red line corresponds to the first type of terms and the blue line to the second type.

3.2.2 Negative resonance poles

First let us consider a pole $z = -10 + 0.03i$. This is typical of a negative resonance pole whose resonance energy is around 100 eV and total width 0.001 eV.

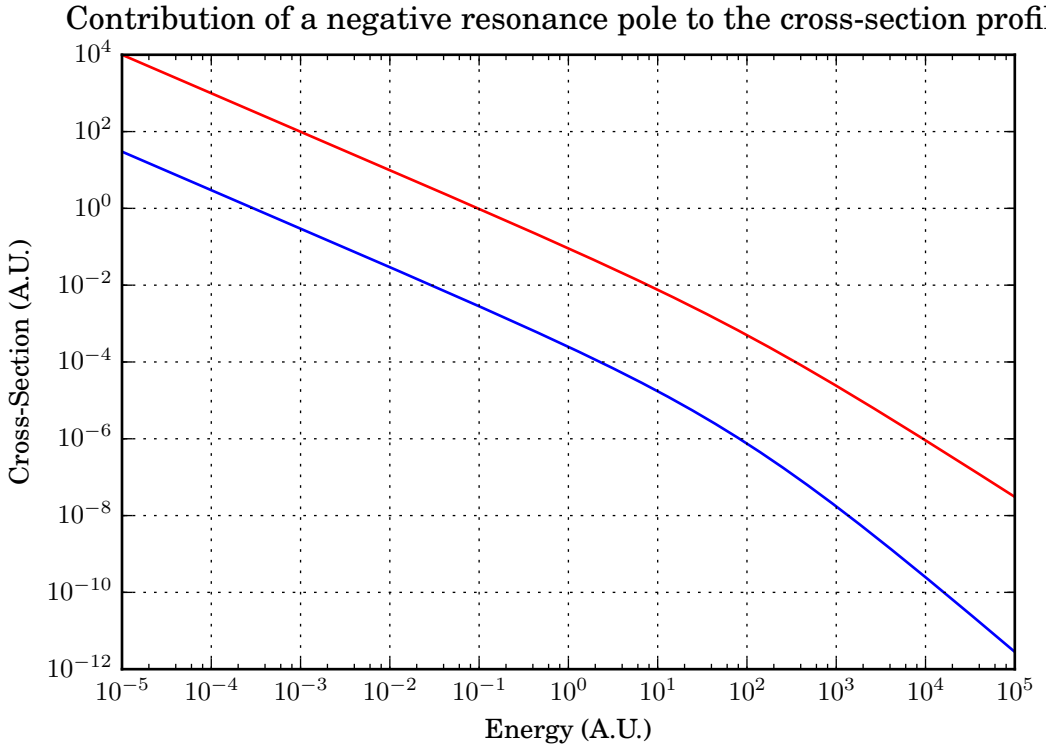

Figure 3.1: Qualitative contribution of a negative resonance pole to a cross-section profile

An immediate asymptotic study of the terms (3.9) and (3.10) would show the observed behavior on the left and right parts of the range on Figure 3.1. There is a slow variation on the energy range presented. This type of poles are called non-fluctuating by R.N. Hwang in his study of [18, 19].

The vertical spacing between the red and blue line has no particular significance. The choice of the normalization of each type of sub-terms is arbitrary. This translates into this separation in the logarithmic scale.

3.2.3 Orbital poles

Let us now consider a pole $z = 1000i$. This is typical of an orbital pole for a quantum number $l = 1$.

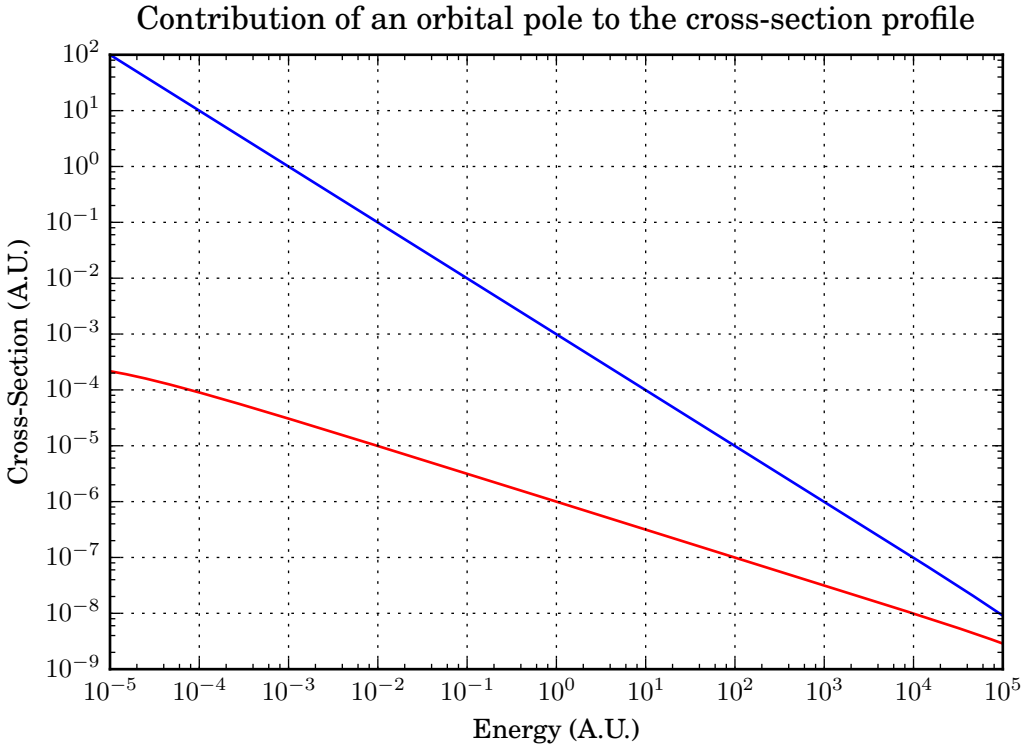

Figure 3.2: Qualitative contribution of an orbital pole to a cross-section profile

We observe on Figure 3.2 a very similar behavior to that of a negative resonance pole of Figure 3.1. Namely, there is no major variation on the energy range and we also consider them non-fluctuating poles.

3.2.4 Positive resonance poles

The last type of pole is the most interesting as far as resonant cross-sections are concerned. I have chosen a pole $z = 10 + 0.03i$, which would typically correspond to the same resonance as the negative resonance pole I have chosen before.

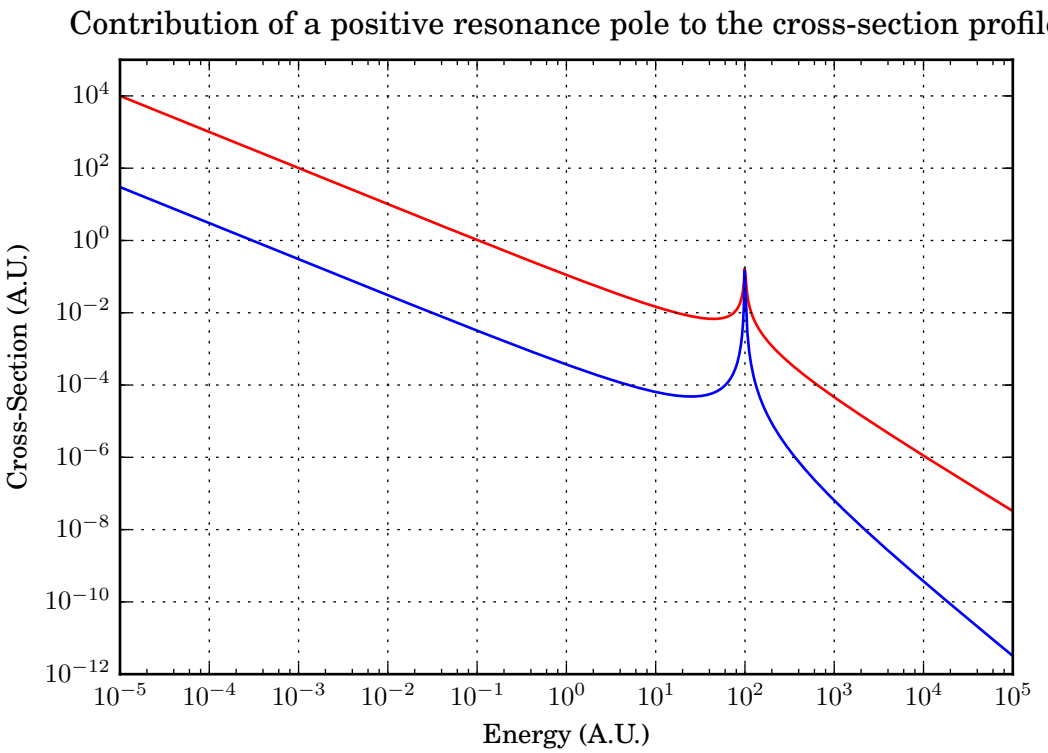

Figure 3.3: Qualitative contribution of a positive resonance pole to a cross-section profile

As it can be seen on Figure 3.3, the contribution is sharply peaked around the square of the real part for both sub-terms (3.9) and (3.10).

The absolute value of sub-term (3.9) is presented here because the logarithmic scale does not allow for negative values. Practically these negative values are not a problem for the reconstruction of cross-section profiles. Indeed, the other types of poles are able to provide a positive background such that the sum of all pole terms is always positive.

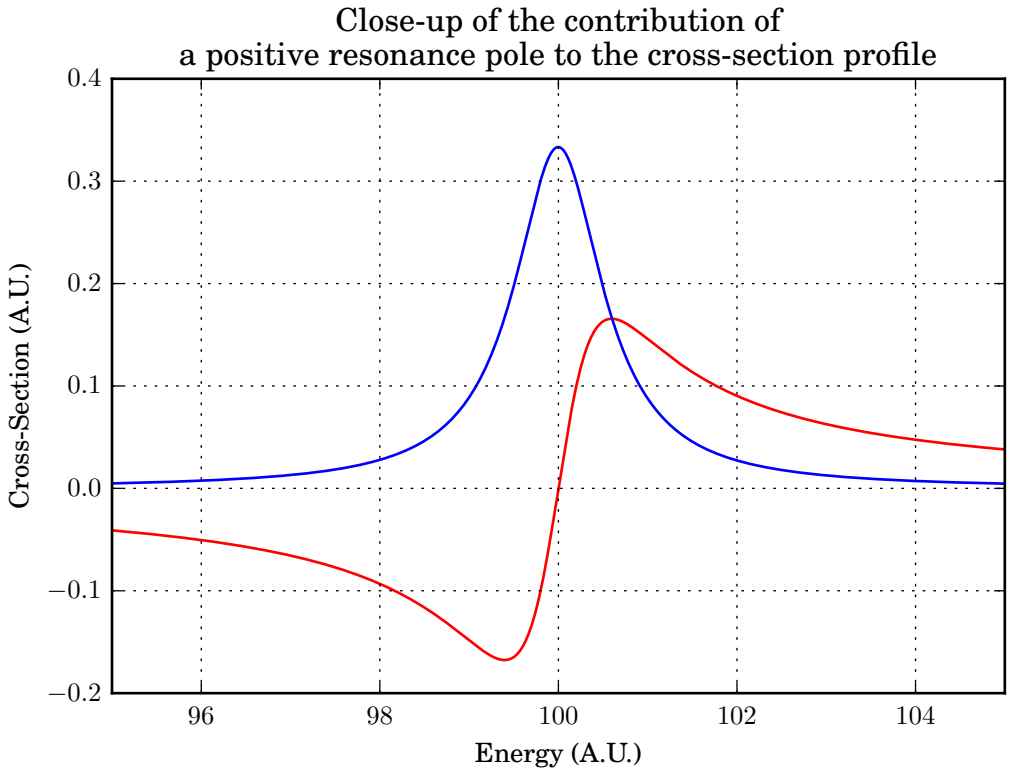

Figure 3.4: Close-up of the qualitative contribution of a positive resonance pole to a cross-section profile around its resonant part

Figure 3.4 offers a close-up look around the resonant part in a linear scale. We see that the two types of sub-terms can be interpreted as symmetric and anti-symmetric contribution to the cross-section profile, which was not the case for the two previous types of poles.

The next part of this manuscript is devoted to applications of the multipole representation. We will see how these pole types are mirrored in the cross-section profiles reconstructed from multipole parameters.

Part III

Some applications of the multipole representation

Chapter 1

Reconstruction of the 0K cross-sections with the multipole representation

The previous chapters have been devoted to the theoretical aspects of the multipole representation. In this chapter, I wish to discuss the reconstruction of the 0K cross-sections with the multipole representation.

I wrote a code performing the conversion from standard resonance parameters to multipole parameters for the Multi-Level Breit-Wigner and Reich-Moore formalisms. This is a direct implementation of the theoretical results that I have presented. The aim was then to verify the correctness of the obtained parameters. One way to do this is to compare the reconstruction of the cross-sections with multipole parameters to a classic reconstruction with resonance data and the analytical formulae derived from the R-matrix theory. As I mentioned in the introduction of this manuscript, these are done by codes such as PREPRO, NJOY or GALILÉE-1. I chose to compare my results to NJOY considering that these three codes agree to a very good accuracy for the reconstruction of the 0K cross-sections.

My goal was to achieve a uniformly lower than 10^{-6} relative error for the four reconstructed cross-sections : elastic, fission (when relevant), radiative capture and total. The relative error is defined by

$$\epsilon_{\text{relative}} = \frac{|\sigma_{\text{multipole}} - \sigma_{\text{NJOY}}|}{|\sigma_{\text{NJOY}}|}. \tag{1.1}$$

This choice of maximum relative error corresponds to the limit on the precision of resonance parameters in the ENDF format. This is also a good enough precision for most uses of cross-sections, particularly considering the errors introduced when broadening them. This goal proved to be realistic and attainable for numerous nuclei.

In this chapter, I will show the successful reconstruction of 0K cross-sections with multipole parameters for such nuclei. I will try and explain that they are representative of the different challenges of the conversion to multipole parameters. In relation to the previous chapter about the qualitative types of poles, I will describe the contribution of individual

pole terms to the cross-section profile on a particular example. Finally, I will comment on the scope and challenges of a conversion of an entire ENDF library to this new representation.

1.1 Reconstruction of 0K cross-sections

The theoretical studies leading to the multipole representation of the different formalisms involved rather different challenges for each case. As such, I will present separate results for Multi-Level Breit-Wigner, non-fissile Reich-Moore and fissile Reich-Moore nuclei. For each of these three categories, I will discuss the expected issues and present successful reconstruction with the newly computed multipole parameters.

For each nucleus, I will show a graph of elastic, radiative capture, fission (when relevant) and total cross-sections on the resolved resonance range reconstructed with multipole parameters. Together with these cross-section profiles, I will also display the relative error to NJOY reconstructed cross-sections. A table will give the maximum relative error for each cross-section. Additionally, a table will summarize some properties of the packs of resonances of the considered nucleus. This will include the number of resonances of each pack, the previous number of poles required to represent them (established by R.N. Hwang and C. Jammes in [18, 19]), as well as the new number of poles I have established. The reconstructions presented on the aforementioned graphs are done with this new reduced number of poles.

1.1.1 Multi-Level Breit-Wigner nuclei

Let us first focus on the Multi-Level Breit-Wigner case. The main issues I have identified while working on the multipole representation of the cross-sections are the energy dependencies of the penetration and level-shift factors. The form of this dependency depends on the quantum number l of the considered pack of resonances. For a pack of quantum number l, a careful mathematical study allowed reducing the multipole representation from $2l+2$ poles per resonance to only $l+2$ per resonance at the cost of l poles for the whole pack. I will present two reconstruction results that confirm that this theoretical result does not impact the numerical accuracy of the multipole representation. First, Silver 107 which possesses only packs of resonances of quantum number $l=0$. I have shown that, in this case, the multipole representation is rather easy to obtain. Second, Zirconium 91 which contains packs with quantum number $l=1$ where there is an effective reduction of the number of poles required.

Another concern could be that of the number of resonances in each pack. This aspect is largely irrelevant as the multipole representation is mostly obtained resonance by resonance (except for one additional step for the elastic cross-section). Obviously, if a nucleus has a large number of resonances, small numerical inacuracies on the multipole representation of each of them might accumulate in a more problematic way than for a small number of resonances. The opposite argument could also be made, namely, errors on individual resonance multipole representation might be hidden in the sheer number of resonances. Practically, I did not encounter particular problems when studying Multi-Level Breit-Wigner nuclei with

higher number of resonances. In the development stage of my conversion code, errors on the multipole representation of specific resonances always appeared clearly around them and made the debugging process rather easy.

l	J	Number of resonances	Previous number of poles	New number of poles
0	0	14	28	28
	1	43	86	86
total		57	114	114

Table 1.1: Number of resonances and poles for Silver 107

Silver 107 is a nucleus with two packs of resonances, both with quantum number $l = 0$. The resolved resonance range extends from 10^{-5} eV to 1057.9 eV. Table 1.1 displays the relevant pack and pole properties. The packs are only characterized by (l, J) and not with a triplet of quantum numbers (l, s, J) as they were before. This is but a mere peculiarity of the implementation of the Multi-Level Breit-Wigner formalism that I chose not to specify as it has absolutely no impact on the multipole representation. Otherwise, as expected, there is no gain in the number of poles for the representation of packs of quantum number $l = 0$.

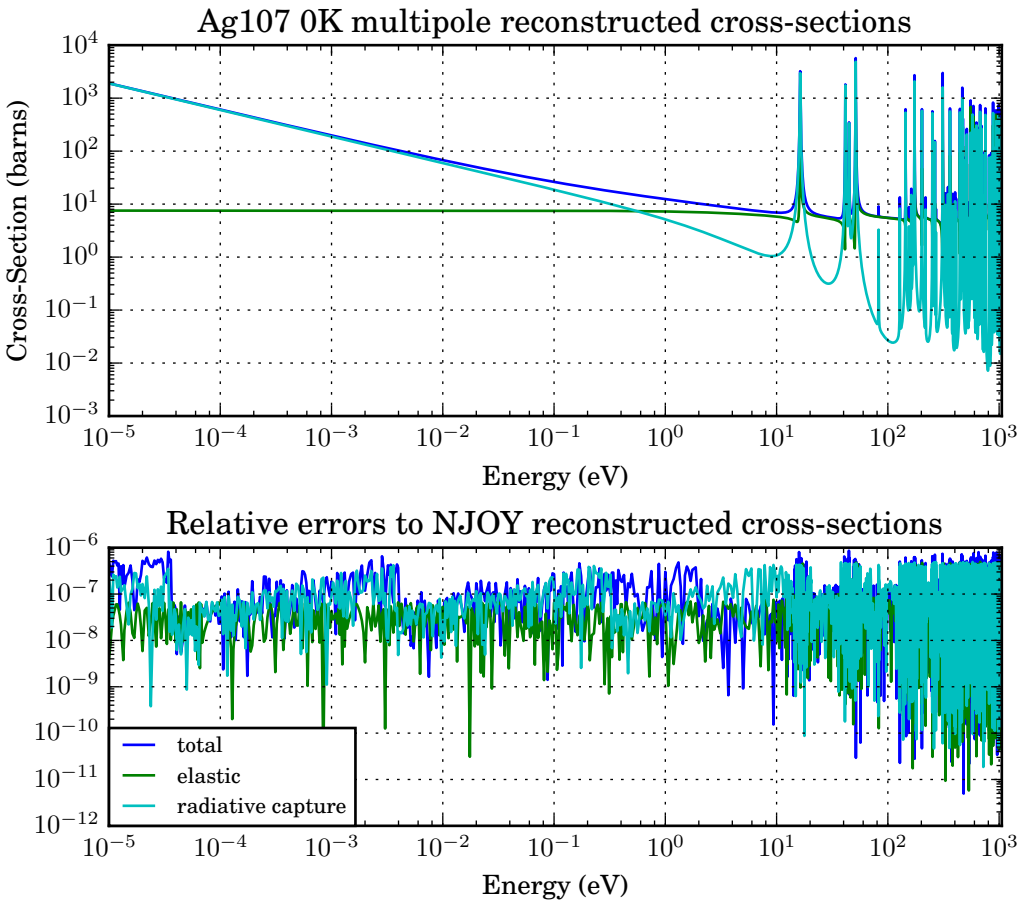

Maximum relative errors

total	elastic	fission	radiative capture
8.61E-07	4.97E-07	-	4.93E-07

Figure 1.1: Reconstruction with multipole parameters of the 0K cross-sections of the Multi-Level Breit-Wigner nucleus Silver 107

Figure 1.1 shows the reconstructed radiative capture, elastic and total cross-sections with the newly computed multipole parameters. The relative error is consistently under $5 \cdot 10^{-7}$ for the partial cross-sections and below 10^{-6} for the total cross-section. This demonstrates that the conversion to multipole parameters is correct. This is a good result but not an unexpected one given the simplicity of the resonance data of this nucleus.

The second case I chose to present is that of Zirconium 91, which has packs of resonances of quantum number $l = 1$. For such nuclei, I have improved the previous theoretical results concerning the number of poles. Table 1.2 displays the relevant pack and pole properties. We do lower the total number of poles from 502 to 396 (approximately 20% reduction). The resolved resonance range extends from 10^{-5} eV to 30160 eV.

l	J	Number of resonances	Previous number of poles	New number of poles
0	2	16	32	32
	3	15	30	30
1	1	6	24	19
	2	32	128	97
	3	39	156	118
	4	33	132	100
total		141	502	396

Table 1.2: Number of resonances and poles for Zirconium 91

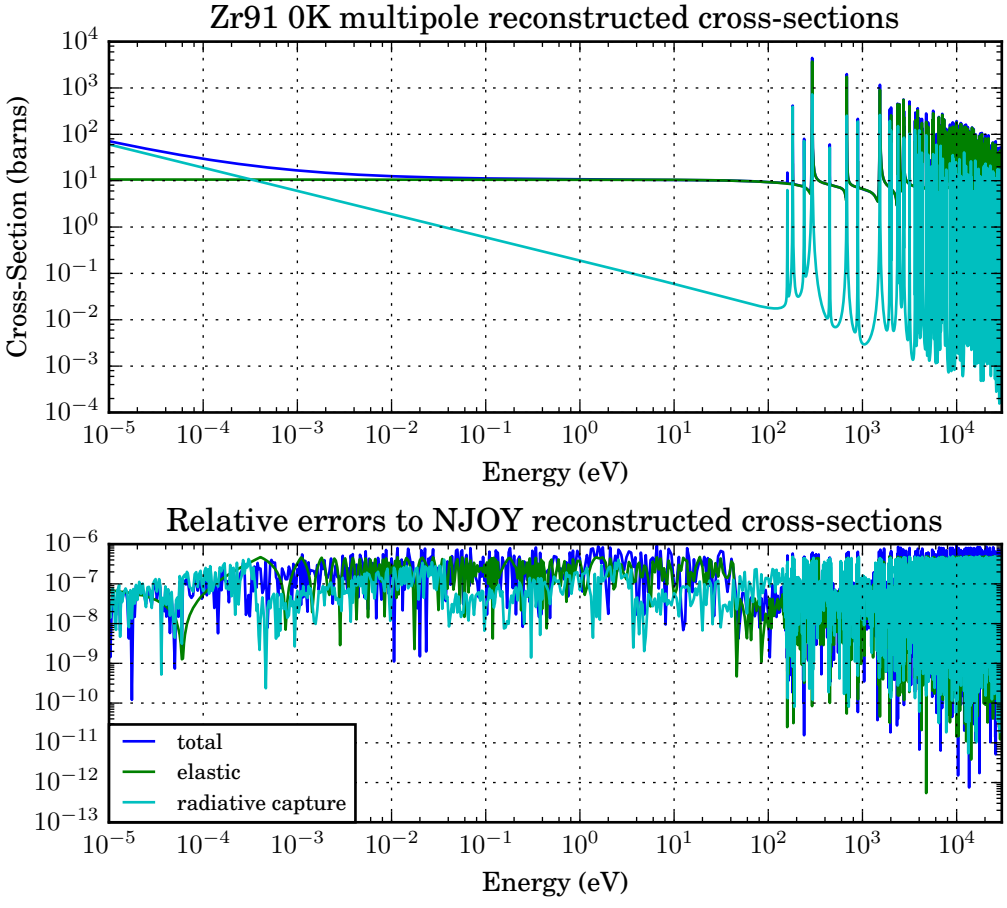

Maximum relative errors

total	elastic	fission	radiative capture
9.24E-07	4.91E-07	-	4.95E-07

Figure 1.2: Reconstruction with multipole parameters of the 0K cross-sections of the Multi-Level Breit-Wigner nucleus Zirconium 91

Figure 1.2 shows that the reconstruction is very satisfactory with the new multipole parameters. Similarly to Silver 107, the relative errors are below 10^{-6}. This confirms the results of the theoretical study concerning the possibility of lowering the number of poles required.

As I have mentioned, the number of resonances in each pack is not a particular obstacle for the Multi-Level Breit-Wigner formalism multipole representation. For that reason I did not focus on this aspect when presenting these two successful reconstructions. I also did not present fissile nuclei as the fission cross-section formula is almost identical to that the radiative capture cross-section. As a result, there are no numerical difficulties associated with the former that would not appear for the latter.

1.1.2 Reich-Moore nuclei

For the Reich-Moore nuclei, I identified three possible issues for the implementation of the conversion of standard resonance parameters to multipole parameters.

The first issue I perceived as an obstacle was again the energy dependency of the penetration and level-shift factors. This quickly appeared to be less of a problem for the Reich-Moore formalism. On one hand, there is no level-shift of the resonance energies. On the other hand, while there still is a penetration factor, the number of poles per resonance does not grow with the quantum number l of the pack they belong to. Compared to previous results on the multipole representation, we go from $(2l + 2)$ poles per resonance (as initially in the Multi-Level Breit-Wigner case) to 2 poles per resonance whatever the value of l of the pack of resonances. This is at the cost of $2l$ poles for the whole pack. Numerical applications were necessary to prove that this is indeed a limited source of problems.

Second, the analytical formulae of the cross-sections involve the inversion of a reduced R-matrix. This poses a major problem for deriving the multipole representation as it implies the use of formal calculus tools to manipulate determinant and rational functions. One of my theoretical results was to show that additional steps allow reducing the complexity of this problem to that of a scalar inversion. At this stage, however, it still remained unclear whether this would impact the numerical accuracy of the values input in the root-finding algorithm that follows.

Third, the root-finding problem itself is vastly more complicated than in the Multi-Level Breit-Wigner case. Resonances cannot be treated separately for multipole representation. The algorithmic challenge consists in finding the roots of polynomials of very high degree (higher than 50) for many Reich-Moore nuclei.

Non-fissile Reich-Moore nuclei

I will begin with the case of non-fissile Reich-Moore nuclei, which skips the second point and avoids the possible numerical inaccuracies it could introduce. This allows focusing on the two other points. For the first point, I will present the reconstructed cross-sections of the

nucleus Aluminium 27. It possesses a large number of packs, some with quantum number up to $l = 2$. This will validate my approach to treat the corresponding energy dependency of the penetration factor and to reduce the number of poles. For the third point, I will present those of the nucleus Chromium 53, whose resonance packs are larger. This will indicate the validity of the root-finding algorithm I have adopted.

A coincidental advantage of Aluminium 27 is that each of its packs contain few resonances. It allows separating the complexity coming from the penetration factor energy dependency (that we are trying to convince ourselves can be overcome easily for the Reich-Moore case) from the complexity of solving high degree polynomials. Table 1.3 displays the relevant pack and pole properties. The theoretical reduction of the total number of poles is of 30%, which is quite significant. The resolved resonance range extends from 10^{-5} eV to 845000 eV.

l	s	J	Number of resonances	Previous number of poles	New number of poles
0	2	2	10	20	20
	3	3	14	28	28
1	2	1	10	40	22
		2	9	36	20
		3	8	32	18
	3	2	3	12	8
		3	0	0	0
		4	3	12	8
2	2	0	2	12	8
		1	3	18	10
		2	1	6	6
		3	4	24	12
		4	0	0	0
	3	1	2	12	8
		2	3	18	10
		3	1	6	6
		4	4	24	12
		5	2	12	8
total			78	312	204

Table 1.3: Number of resonances and poles for Aluminium 27

As a remark, one may notice lines with zero resonances in Table 1.3. My result concerning the number of poles needed for such packs may suggest that we would need $2N + 2l = 2l \neq 0$ poles. However, since there are no resonances, there are no associated widths and no resonant contributions of these packs to the cross-sections (there still is a contribution to the so-called scattering potential, but this is irrelevant as far as the poles are concerned).

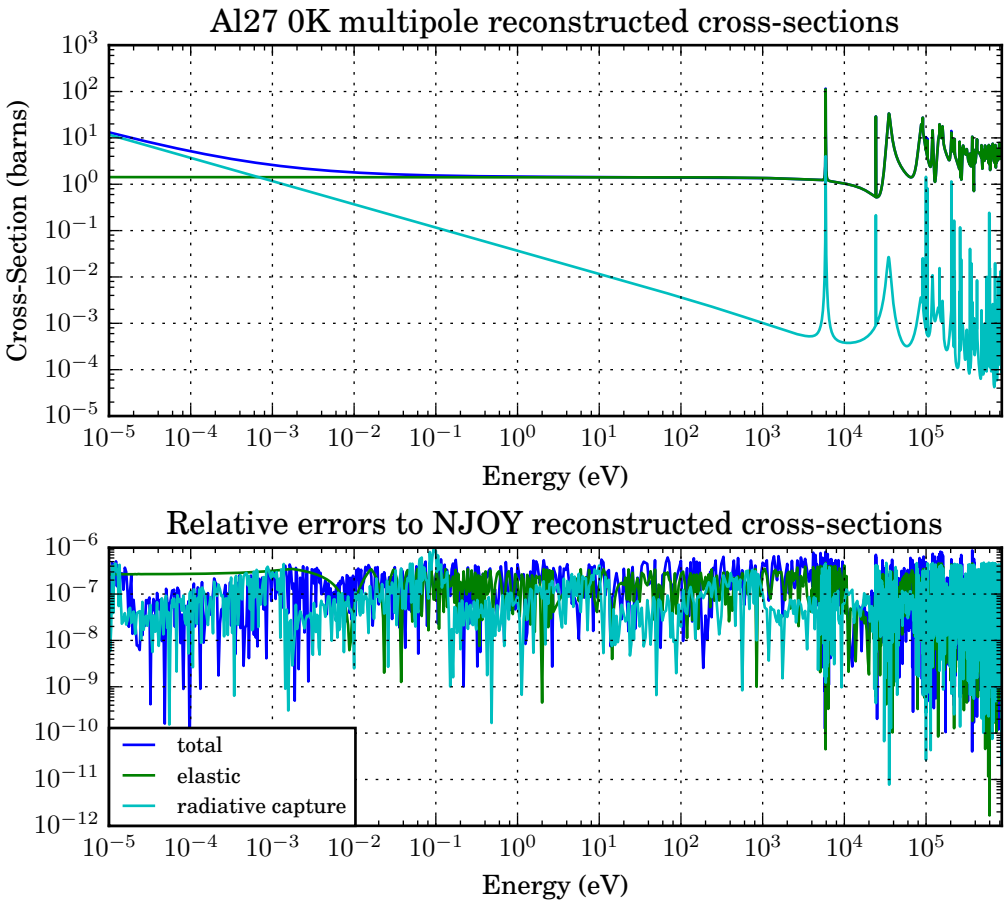

Maximum relative errors

total	elastic	fission	radiative capture
8.73E-07	4.70E-07	-	9.19E-07

Figure 1.3: Reconstruction with multipole parameters of the 0K cross-sections of the non-fissile Reich-Moore nucleus Aluminium 27

Figure 1.3 shows the reconstructed 0K cross-sections with the newly computed multipole parameters. The maximum relative errors are all below 10^{-6}. Interestingly, the maximum error on the elastic cross-section is lower than for the radiative capture cross-section. I expected the opposite considering that the formulae for the former are more complicated and involve phase-shifts. However, for Reich-Moore nuclei, the radiative capture cross-section is obtained by a perturbative treatment, which might well be an adequate explanation. In any case, this required quite a lot of coding work to get the implementation right and particularly for the choice of the mass of the nucleus (which is prescribed slightly differently in various parts of the ENDF files).

The second example of a non-fissile nucleus is that of Chromium 53. It contains packs of

resonances with quantum number up to $l = 1$. The previous results concerning Aluminum 27 shows that the corresponding energy dependencies can be treated accurately. This nucleus, however, possesses packs with a larger number of resonances and consequently a larger number of poles to find. Table 1.4 summarizes these properties. Considering the higher number of resonances in the packs of quantum number $l = 1$, the gain in the total number of poles is of 40%, which is even better than before. The resolved resonance range extends from 10^{-5} eV to 564000 eV

l	s	J	Number of resonances	Previous number of poles	New number of poles
0	1	1	40	80	80
	2	2	55	110	110
1	1	0	12	48	26
		1	91	364	184
		2	35	140	72
	2	1	11	44	24
		2	50	200	102
		3	56	224	114
total			350	1210	712

Table 1.4: Number of resonances and poles for Chromium 53

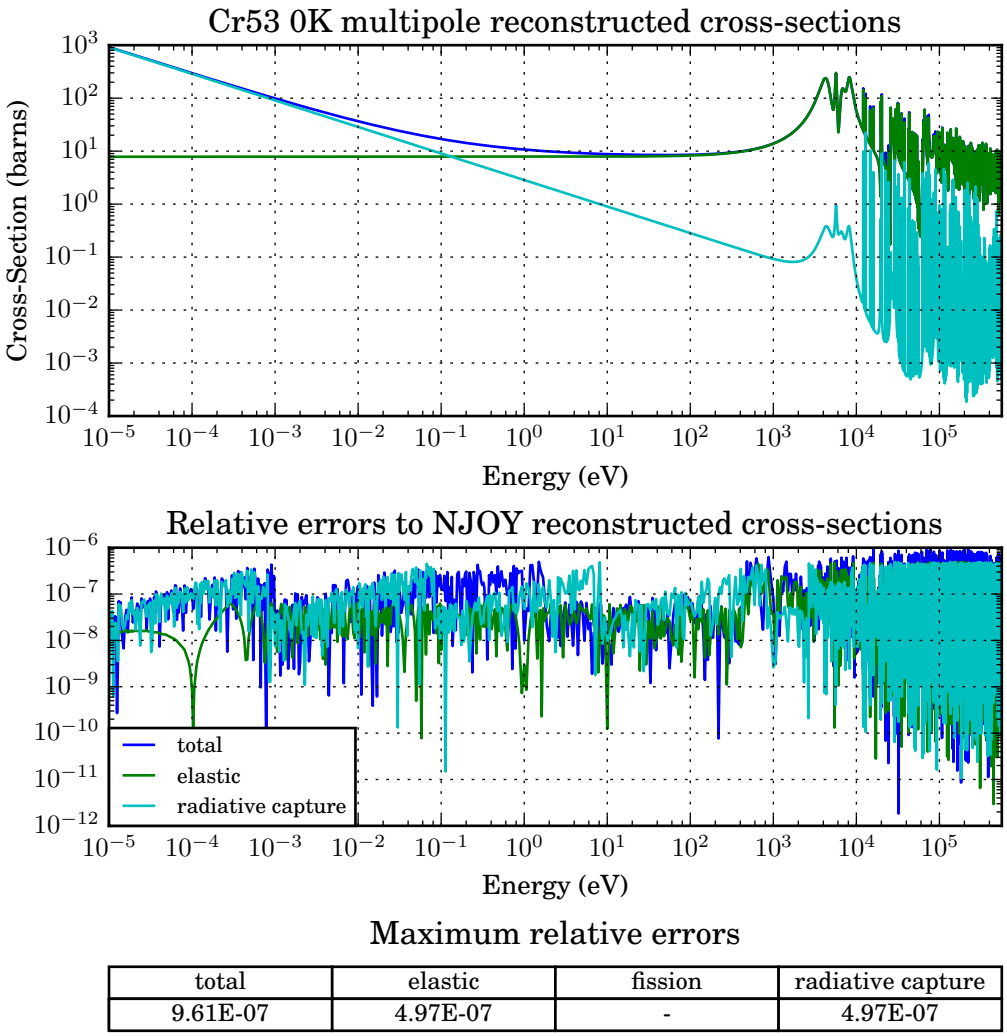

Maximum relative errors

total	elastic	fission	radiative capture
9.61E-07	4.97E-07	-	4.97E-07

Figure 1.4: Reconstruction with multipole parameters of the 0K cross-sections of the non-fissile Reich-Moore nucleus Chromium 53

Figure 1.4 shows that the reconstructed cross-sections are in excellent accordance with NJOY reconstructed ones. Let me draw attention to the fact that it required finding the roots of polynomials of degree higher than a hundred. This is in contrast to the multipole representation of Aluminium 27, which does not involve such a challenge.

Fissile Reich-Moore nuclei

The case of fissile Reich-Moore nuclei was the hardest to treat. As I mentioned before, an added computational step is needed to reduce a matrix inversion to a scalar inversion. It proved quite challenging to implement in a numerically stable way. On top of that, most fissile

nuclei are heavier and present more resonances on the resolved resonance range. The case of Chromium 53 suggested that my adapted Newton-Raphson algorithm for the root-finding was a good approach. I still needed to test cases where even higher degree polynomials were involved. I will present here three successful cases of major importance for nuclear reactor physics : Plutonium 239, Uranium 235 and Uranium 238.

Plutonium 239 has only 2 packs of resonances, both with quantum number $l = 0$. Each of them contains a very high number of resonances as presented in Table 1.5. This table also shows that, as expected, I need the same number of poles as previously established. My goal with this nucleus was to test further the accuracy of my root-finding algorithm. The resolved range extends from 10^{-5} eV to 2500 eV

l	s	J	Number of resonances	Previous number of poles	New number of poles
0	0	0	231	462	462
	1	1	812	1624	1624
total			1043	2086	2086

Table 1.5: Number of resonances and poles for Plutonium 239

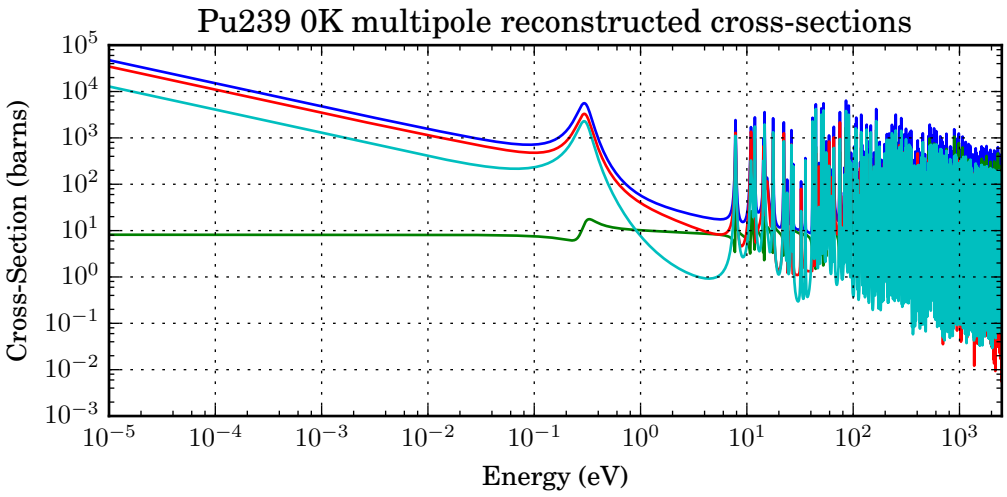

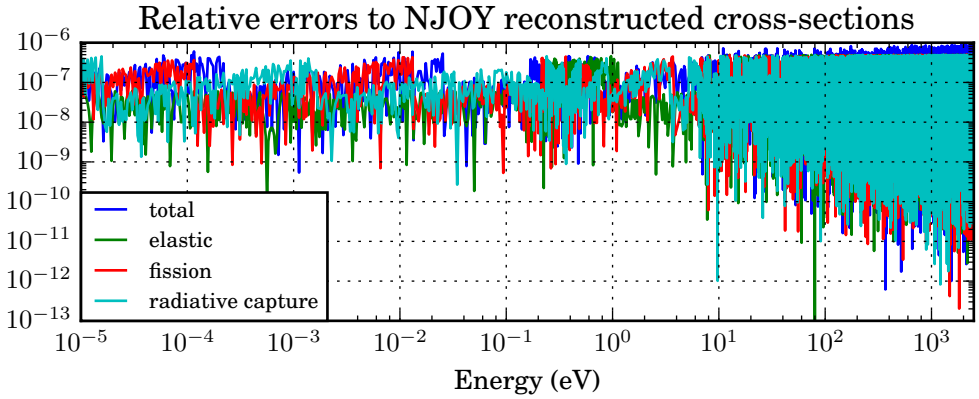

Maximum relative errors

total	elastic	fission	radiative capture
8.97E-07	4.97E-07	5.01E-07	4.97E-07

Figure 1.5: Reconstruction with multipole parameters of the 0K cross-sections of the fissile Reich-Moore nucleus Plutonium 239

Figure 1.5 shows a very satisfactory reconstruction result with all relative errors under 10^{-6}. Finding this new multipole parameters involved solving a polynomial of degree 462 and a polynomial of degree 1624. As for the case of Chrome 53, the Newton-Raphson algorithm proved to be adequate to solve this problem.

I then tried to convert the standard resonance parameters of Uranium 235 to multipole parameters. This nucleus also has 2 packs of resonances, both of quantum number $l = 0$, as presented in Table 1.6. The resolved resonance range extends from 10^{-5}eV to 2250eV.

l	s	J	Number of resonances	Previous number of poles	New number of poles
0	3	3	1449	2898	2898
	4	4	1744	3488	3488
total			3193	6386	6386

Table 1.6: Number of resonances and poles for Uranium 235

The number of resonances and the corresponding number of poles is much larger than for Plutonium 239. The degree of the polynomials we need to find the roots of goes up to the thousands.

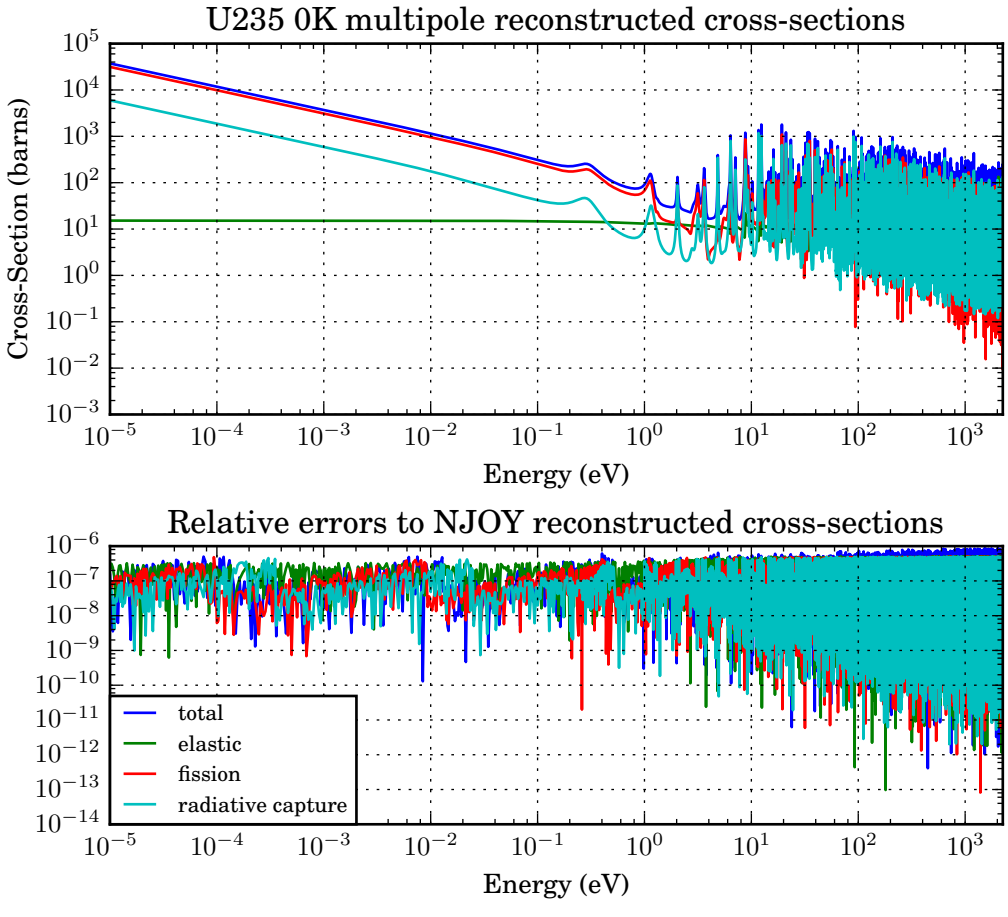

Maximum relative errors

total	elastic	fission	radiative capture
8.79E-07	4.99E-07	4.99E-07	4.99E-07

Figure 1.6: Reconstruction with multipole parameters of the 0K cross-sections of the fissile Reich-Moore nucleus Uranium 235

Figure 1.6 shows that, as for Plutonium 239, the reconstruction is very satisfactory. This was the major test of my algorithm as the number of poles to find is higher than for any other nuclei of the JEFF-3.2 library.

Having treated Plutonium 239 and Uranium 235 succesfully, I decided to try and treat Uranium 238. As I have mentioned, these first two nuclei only have packs with quantum number $l = 0$. As such, and as can be seen in Table 1.5 and Table 1.6, I have not reduced the number of needed poles. This is emphatically not the case for Uranium 238, which contains a huge pack of resonances of quantum number $l = 1$. As we can see in Table 1.7, my new multipole representation significantly reduces the number of required poles. The resolved resonance range extends from 10^{-5} eV to 20000 eV.

l	s	J	Number of resonances	Previous number of poles	New number of poles
0	1/2	1/2	929	1858	1858
1	1/2	1/2	850	3400	1702
		3/2	1566	6264	3134
total			3193	11522	6694

Table 1.7: Number of resonances and poles for Uranium 238

Figure 1.7 shows a successful reconstruction with these new multipole parameters, but less satisfactory than the previous ones I presented. First we can see larger relative errors, up to $5.27 \cdot 10^{-6}$, on the fission cross-sections above 1 keV. These are due to the very low fission cross-section of Uranium 238 in that range of energy and the limited precision of the NJOY generated file. They are printed in the same format as ENDF evaluations which only allows for 5 decimals for numbers with exponent lower than minus nine. I quickly looked up a comparison between GALILÉE-1 and NJOY, which revealed a similar situation. I am not particularly concerned about this type of error, as it is relatively specific to Uranium 238 and still quite satisfactory. The error for the elastic and fission cross-sections are below 10^{-6}, as I sought, but higher than $5 \cdot 10^{-7}$, in contrast to Plutonium 239 and Uranium 235. This is still a very good result and confirms the interest of the multipole representation for 0K cross-section reconstruction.

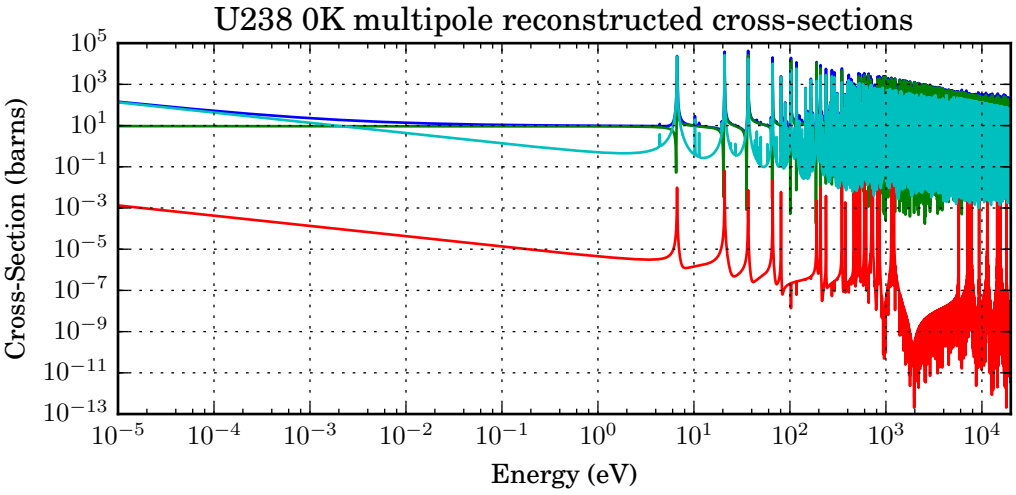

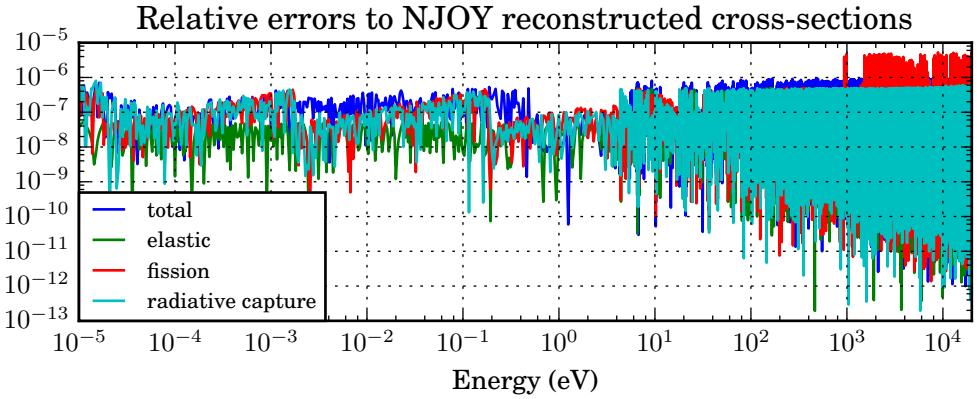

Maximum relative errors

total	elastic	fission	radiative capture
9.79E-07	6.28E-07	5.27E-06	8.05E-07

Figure 1.7: Reconstruction with multipole parameters of the 0K cross-sections of the fissile Reich-Moore nucleus Uranium 238

1.2 Contributions of the different types of poles to a reconstructed 0K cross-section profile

In the previous chapter I have proposed a qualitative classification of the poles. In the previous section I have shown that the conversion to multipole parameters and their use for reconstruction of 0K cross-sections is quite successful. I now wish to show how these two elements are mirrored in the reconstruction of cross-section profiles, and particularly how each type of pole contributes to them.

A good test-case that exhibits such properties is Plutonium 239. In Figure 1.5, we can see

that there is a resonance around 0.3 eV that is quite separated from the others. This will hopefully illustrate with clarity the contribution of an individual pole. For this same resonance, I will show how symmetric and anti-symmetric pole terms contribute to the asymmetric shape of the elastic cross-section. I will then discuss the importance of positive resonance poles compared to that of negative resonance poles and orbital poles.

1.2.1 One pole contribution

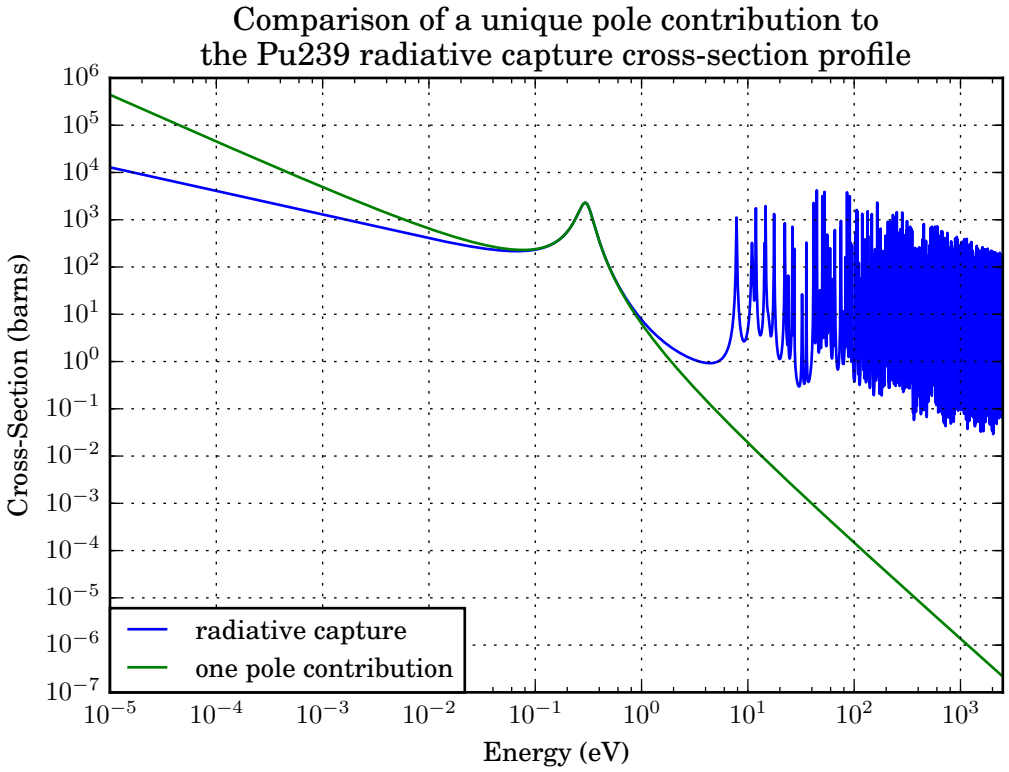

Figure 1.8: A unique pole contribution to the radiative capture cross-section profile of Plutonium 239

Figure 1.8 shows the radiative capture cross-section of Plutonium 239 and the contribution of a single positive resonance pole term. Considering that the poles are found by studying packs of resonances all together, it is not immediately apparent to which pole corresponds to which resonance, although in this case the first resonance is sufficiently isolated so that I had no trouble finding it.

It is striking on this graph that the resonance peak profile is very well captured with just one pole contribution. We can also see that the low energy profile is wrong. Other positive resonance poles are expected to give this same low energy contribution. This suggests that the other types of poles are very necessary for a correct low energy profile. Figure 1.9 presents the relative error of these two curves around the first resonance peak. We can see that the error at the peak itself is quite low, but rises rather quickly above the percent. As a remark, the inverted peak in the relative error that is not centered on the resonance corresponds to

the intersection of the pole contribution and the full radiative capture cross-section. The fact that this peak does go further down on the graph is merely a plotting artefact of the logarithmic scale.

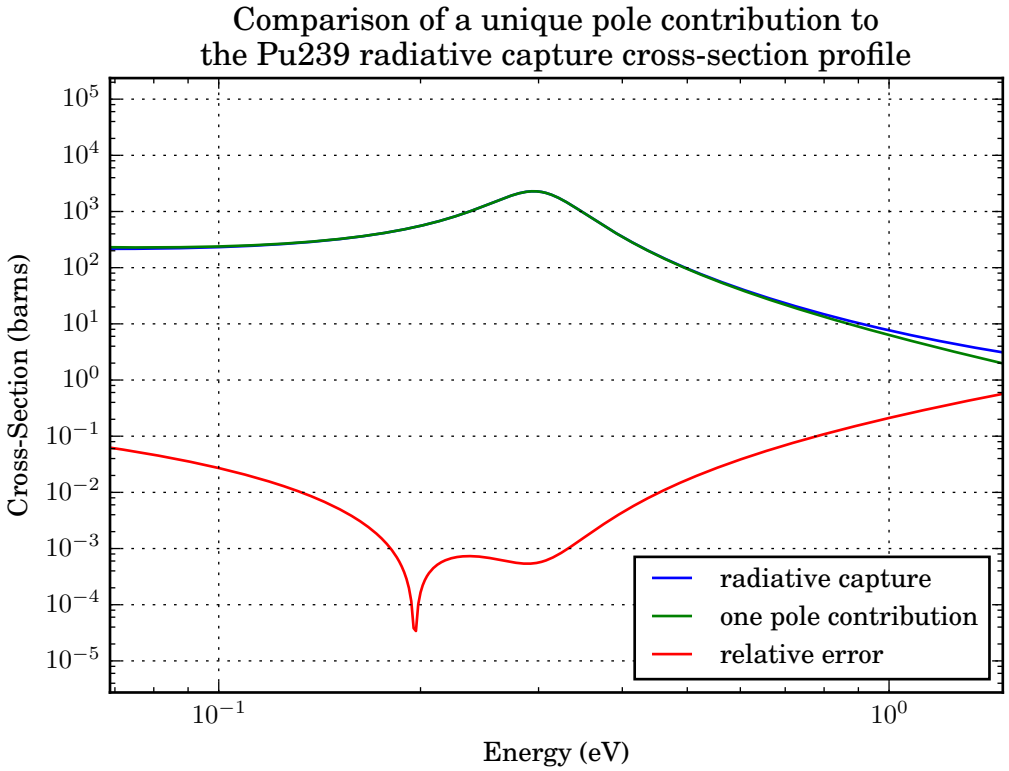

Figure 1.9: Relative error between a unique pole contribution and the complete radiative capture cross-section profile of Plutonium 239 around its first resonance peak

Figure 1.10 presents a zoom on the elastic cross-section for the same resonance. I have briefly mentioned in my qualitative study of the type of poles that the elastic cross-section resonance peaks are notoriously asymmetric. I have shown that the asymmetry of positive resonance poles contribution is related to the value of the residues. I have plotted the contribution of the same pole as for the radiative capture. The two other curves on this plot correspond to the symmetric and anti-symmetric parts of pole contribution. As for the radiative capture cross-section profile, a one-pole contribution captures very well the elastic cross-section resonance shape. The contribution of the other poles is necessary to provide the background that would align vertically the cross-section and the pole contribution. This was interestingly not the case for the radiative capture cross-section.

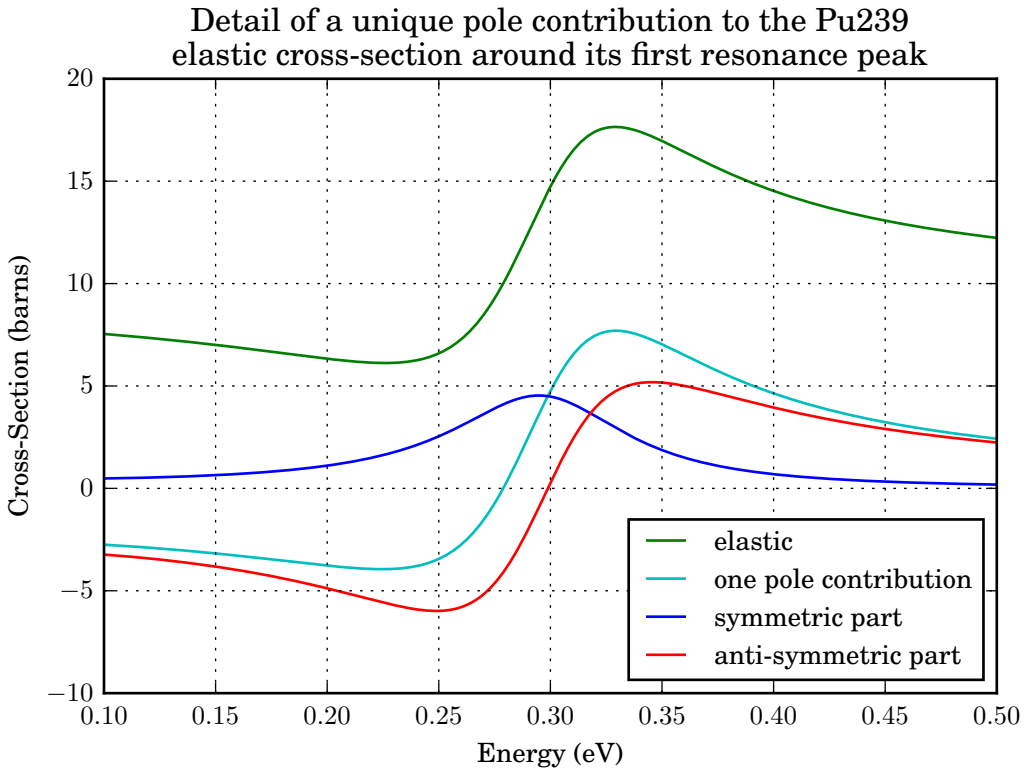

Figure 1.10: Detail of a unique pole contribution to the elastic cross-section of Plutonium 239 around its first resonance

1.2.2 All positive resonance pole contributions

Figure 1.11 presents again the radiative capture cross-section, but this time the other curve is the sum of all positive resonance pole contributions. The fit on the first few resonance peaks seems very good. A closer look at the other resonances peak proved that this was systematically the case. However, we can already see a significant difference in the two profiles at the depression between the first and the second resonance. I observed that this was also the case for the other depressions in between resonance peaks after a closer examination. As expected from the one pole contribution seen on Figure 1.8, the low energy dependency is very wrong. Both aspects confirm the need for other poles to correctly represent the non-resonant part of the cross-section profiles.

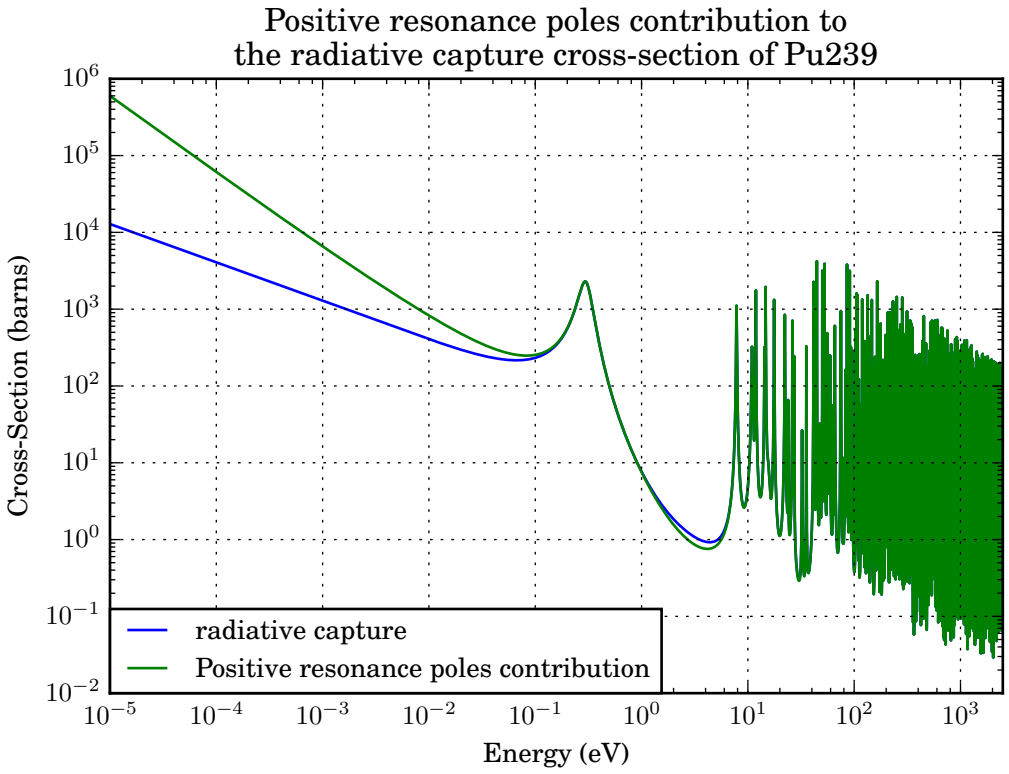

Figure 1.11: Contribution of all positive resonance poles to the profile of the radiative capture cross-section of Plutonium 239

1.2.3 Negative resonance poles and orbital poles contribution

I wished to compare the magnitude of the contribution of all other poles (orbital and negative resonance poles) to the profile of the radiative capture cross-section to visualize the missing elements in Figure 1.11. Figure 1.12 displays both the plot of the profile and the total contribution of these other poles. This contribution is not always positive. In order to still be able to use the logarithmic scale, I plotted the absolute value. The two peaks on the green curve are plotting artefacts due to this choice of scale. They correspond to a change of sign which is not well captured graphically and is of little importance for the magnitude comparison.

First, we can see that the low energy profile is similar to that of the positive resonance pole contributions. Since the sum of all pole contributions yield the correct profile as seen in Figure 1.5 of the previous section, we can surmise that the wrong low energy profile of Figure 1.11 and Figure 1.12 will compensate exactly to yield the correct one. Second, and more critically, we can see that the contribution compared to the complete cross-section is far from insignificant up until 10^2 eV. This suggests that, although the contribution of each individual negative resonance pole and orbital pole is rather non-fluctuating, their combination can have a more complicated shape. Admittedly, it is not as subtle as a positive resonant pole contribution and an approximation of this contribution with few pseudo-poles seems reasonable and possible.

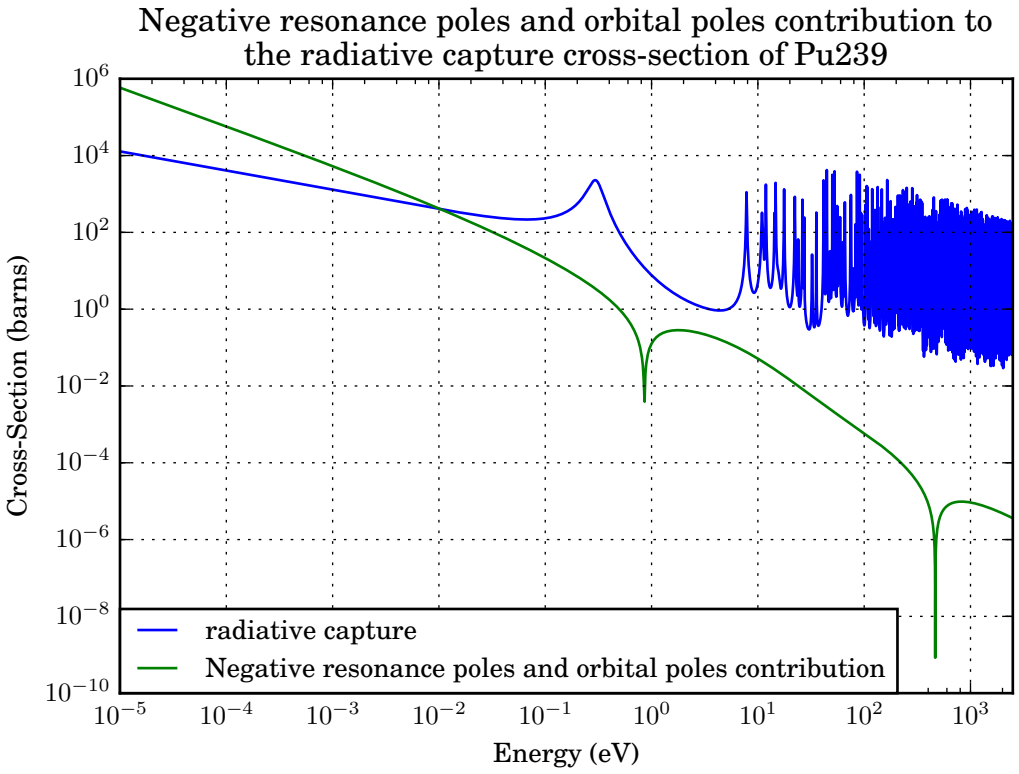

Figure 1.12: Contribution of all non positive resonance poles to the profile of the radiative capture cross-section of Plutonium 239

1.3 Scope of the application to the ENDF libraries

The examples that I have presented are mostly successful reconstructions. They demonstrate the validity of my theoretical study and its code implementation. The next logical step is to try and convert the standard resonance parameters to multipole parameters for all available nuclei. I have worked mainly with the ENDF library JEFF-3.2 [64]. The numbers presented thereafter may vary slightly between libraries but the general orders of magnitude are the same for libraries published at similar time.

JEFF-3.2 proposes nuclear data for some 472 nuclei. Among those, 65 do not have resonance data. Of those which do have resonance data, 11 do not have resonance data in the resolved resonance range. This leaves us with 392 nuclei with resonance data in the resolved resonance range. I have extensively discussed the Multi-Level Breit-Wigner and Reich-Moore formalisms. This is motivated by the fact that the vast majority of the 392 nuclei previously mentioned fall under one of these two categories. Namely, 175 nuclei have resonance data under the Multi-Level Breit-Wigner formalism and 209 under the Reich-Moore formalism. This leaves aside 12 nuclei. Ten of them have resonance data under the Single-Level Breit-Wigner formalism. I have not discussed their treatment, as it is very close to that of the Multi-Level Breit-Wigner case. Two of them have resonance data under the upcoming R-matrix limited format formalism.

The application of my work is constrained to the 175 Multi-Level Breit-Wigner nuclei and the 209 Reich-Moore nuclei. The cases I have previously presented suggested that aiming at a 10^{-6} maximum relative error for the elastic, fission (when relevant), and radiative capture cross-sections was not unreasonable. This error threshold also appeared to be reasonable for the total-cross-section. With these criteria, approximately two third of the nuclei passed the validation test.

I started, but did not complete, a review of the nuclei that failed the test. A lot of issues I encountered could be solved somewhat globally but some of them will require individual work. For the former I can cite the addition of background terms to the cross-sections. For the total cross-section this can correspond to other reactions which are not treated with resonance parameters but rather tabulated and provided in conjoint data files to the resonance data files. For the elastic, fission and radiative capture cross-section, this corresponds to background terms that are required to get the correct profile. This, among other issues, posed implementation challenges that, while not particularly complicated, were rather time consuming. With hindsight, I could have solved them by working with reconstruction codes such as GALILÉE-1, that already tackle such problems. I am hopeful that my implementation of the conversion to multipole parameters will benefit tremendously from an integration in such codes.

Regarding individual problems, this mainly concerns errors or discrepancies in the ENDF resonance data file. Sometimes two resonances are listed with the same energy. Sometimes the presented triplet (l, s, J) of the pack of resonance of a nucleus is not in accordance with its spin. There are many other pathological cases that would require individual attention outside the scope of this work. Thankfully, they only concern a handful of nuclei and is not necessarily an obstacle to the use of the multipole representation.

All things considered, the reconstruction of the cross-sections of nuclei such as Plutonium 239, Uranium 235 and Uranium 238 is quite encouraging. The treatment of a complete library will require more time.

Chapter 2

Doppler broadening of the cross-sections with the multipole representation

In this chapter, I will give a brief summary of the formulae and approximations used to broaden the cross-sections. I will detail how the multipole representation can be used to perform this broadening. Notably, I will describe the analytical tools that are required for this computation. Finally, I will present some numerical results of the Doppler broadening for a few nuclei of interest.

2.1 Short theoretical framework

2.1.1 Free-gas model and the Solbrig kernel

The cross-sections formulae that I have presented before model interactions between moving neutrons and motionless target nuclei. To obtain cross-sections at a given temperature, one must first describe the corresponding distribution of velocities of the nuclei. Under the commonly adopted free-gas model, this velocity distribution is known as the Maxwell-Boltzmann distribution. I note it $p(\boldsymbol{w})d\boldsymbol{w}$ where $\boldsymbol{w}$ is the velocity. It is defined by :

$$p(\boldsymbol{w})d\boldsymbol{w} = \frac{1}{\pi^{3/2}w_T^3}\exp\left(-\frac{\|\boldsymbol{w}\|^2}{w_T^2}\right)d\boldsymbol{w}, \tag{2.1}$$

$$\frac{Mw_T^2}{2} = k_B T \tag{2.2}$$

where the quantity M is the mass of an individual nucleus, the quantity k_B is the Boltzmann constant and the quantity T is the absolute temperature of the medium expressed in Kelvin (K).

In presence of temperature effects, the reaction rates of the interactions of the neutron

with the medium have to be averaged with respect to the velocity distribution of the nuclei. The corresponding formula is

$$\|\boldsymbol{v}\|\sigma\left(m\|\boldsymbol{v}\|^2/2,T\right)=\int\|\boldsymbol{v}-\boldsymbol{w}\|\sigma\left(\frac{m\|\boldsymbol{v}-\boldsymbol{w}\|^2}{2},0\right)p(\boldsymbol{w})d\boldsymbol{w} \tag{2.3}$$

where the vector $\boldsymbol{v}$ is the velocity of the considered neutron and the quantity m its mass.

In the particular case of the Maxwell-Boltzmann distribution, by substituting (2.1), we get

$$\begin{aligned}\|\boldsymbol{v}\|\sigma\left(\frac{m\|\boldsymbol{v}\|^2}{2},T\right)&=\frac{1}{\pi^{3/2}w_T^3}\int\|\boldsymbol{v}-\boldsymbol{w}\|\sigma\left(\frac{m\|\boldsymbol{v}-\boldsymbol{w}\|^2}{2},0\right)\exp\left(-\frac{\|\boldsymbol{w}\|^2}{w_T^2}\right)d\boldsymbol{w}\\&=\frac{1}{\pi^{3/2}w_T^3}\int\|\boldsymbol{w}\|\sigma\left(\frac{m\|\boldsymbol{w}\|^2}{2},0\right)\exp\left(-\frac{\|\boldsymbol{v}-\boldsymbol{w}\|^2}{w_T^2}\right)d\boldsymbol{w}.\end{aligned} \tag{2.4}$$

The particular form of the Maxwell-Boltzmann distribution allows us to rewrite this integral, initially over all the velocity space, as an integral on the norm of the velocity. The details can be found in [65]. We note $v=\|\boldsymbol{v}\|$ and $w=\|\boldsymbol{w}\|$. Equation (2.4) becomes

$$\begin{aligned}\sigma\left(\frac{mv^2}{2},T\right)=&+\frac{1}{\sqrt{\pi}w_Tv^2}\int_{w=0}^{\infty}w^2\sigma\left(\frac{mw^2}{2},0\right)\exp\left(-\frac{(v-w)^2}{w_T^2}\right)dw\\&-\frac{1}{\sqrt{\pi}w_Tv^2}\int_{w=0}^{\infty}w^2\sigma\left(\frac{mw^2}{2},0\right)\exp\left(-\frac{(v+w)^2}{w_T^2}\right)dw.\end{aligned} \tag{2.5}$$

In this formula, I have split the integral in two parts for clarity. Furthermore, it is sometimes written in terms of the energy of the neutron instead of its velocity. We note

$$E=\frac{mv^2}{2}\text{ and }E'=\frac{mw^2}{2}. \tag{2.6}$$

Then, after a change of variable in the integrals :

$$\begin{aligned}\sigma\left(E,T\right)=&+\frac{1}{\sqrt{4\pi}E}\int_{E'=0}^{\infty}\frac{\sqrt{E'}}{\sqrt{E_T}}\sigma\left(E',0\right)\exp\left(-\frac{(\sqrt{E}-\sqrt{E'})^2}{E_T}\right)dE'\\&-\frac{1}{\sqrt{4\pi}E}\int_{E'=0}^{\infty}\frac{\sqrt{E'}}{\sqrt{E_T}}\sigma\left(E',0\right)\exp\left(-\frac{(\sqrt{E}+\sqrt{E'})^2}{E_T}\right)dE'\end{aligned} \tag{2.7}$$

with the Doppler width defined by $E_T:=\frac{mw_T^2}{2}=\frac{m}{M}k_BT$.

The main result is that the computation of cross-sections at temperature T is a linear operation on the $0K$ cross-sections. This is what is generally called a kernel operator in mathematics. Gathering the two integrals, we would have a product of the cross-section with the difference of the two exponential terms. This function is called the Solbrig kernel [23]. I will now discuss the approximations of formula (2.7) to effectively broaden the cross-sections.

2.1.2 Approximations on the Doppler broadening energy range

The cross-sections models are only valid on a certain range of energies. The ones that we have studied in this manuscript are concerned with the so-called resolved resonance range. A priori, the integrals in expression (2.7) are to be computed on the whole real positive axis. As such, many different descriptions of the cross-sections would be required in the computation of a single energy cross-section. This does not make much physical sense and I am going to present the classical approximation to solve this problem.

The broadening is somewhat restrained to a small energy range centered around the energy of interest noted E in expression (2.7). The commonly accepted argument is that the exponential terms are strongly decaying, so that we can restrain the range of the integrals to smaller intervals. This argument is central to many approximations of the Doppler broadening. I am going to develop the semi-quantitative approach that describes this interval for each integral. In the following, we will consider that the exponential term is vanishingly small if its argument is larger than 100. This is a rather conservative choice compared to the literature [26]. However, the general ideas presented here are well suited for a change to a lesser strict condition if need be.

I will first discuss how we can reduce the range of each of these integrals depending on the energy we are broadening the cross-sections around. Then I will discuss the appropriate modelling of the cross-sections on these reduced ranges of integration.

Second integral

We will treat the two integrals of expression (2.7) separately to examine the impact of this approximation. We began with the second integral, whose treatment is simpler. The exponential term is small if

$$\sqrt{E} + \sqrt{E'} < 10\sqrt{E_T} \tag{2.8}$$

$$\sqrt{E'} < 10\sqrt{E_T} - \sqrt{E}. \tag{2.9}$$

First case, if $E > 100E_T$, this second integral can be considered null as there is no value of $\sqrt{E'}$ in the range of integration. This threshold depends on the value of E_T, which itself depends on the temperature and the mass of the target nucleus considered. Its lowest value is reached for heavy nuclei and low temperature. For Plutonium 239 and a temperature of 300K, it evaluates to approximately 10^{-2} eV. On the contrary, for light nuclei and high temperature it reaches its highest values. For Aluminium 27 and a temperature of 3000K, it evaluates to approximately 2 eV.

Second case, namely $E < 100E_T$, the integral range is bounded by $\left(10\sqrt{E_T} - \sqrt{E}\right)^2$, which is itself bounded by $100E_T$.

First integral

The impact of the approximation for the first integral is more complicated. With the vanishing exponential argument, the reduced range of integration is defined by

$$-10\sqrt{E_T} < (\sqrt{E} - \sqrt{E'}) < 10\sqrt{E_T} \tag{2.10}$$

$$\sqrt{E} - 10\sqrt{E_T} < \sqrt{E'} < \sqrt{E} + 10\sqrt{E_T}. \tag{2.11}$$

First case, if $\sqrt{E} < 10\sqrt{E_T}$, or equivalently, $E < 100E_T$, then the left hand-side is negative, so the reduced range of integration becomes

$$0 < E' < (\sqrt{E} + 10\sqrt{E_T})^2. \tag{2.12}$$

In the worst case, namely $E = 100E_T$, this upper bound is equal to $400E_T$. This is similar to the case of the second integral, to the difference that the reduced range of integration is slightly larger.

Second case, if $\sqrt{E} > 10\sqrt{E_T}$, or equivalently, $E > 100E_T$. The range of integration becomes

$$(\sqrt{E} - 10\sqrt{E_T})^2 < E' < (\sqrt{E} + 10\sqrt{E_T})^2. \tag{2.13}$$

Whereas the second integral vanishes for $E > 100E_T$, the first one will be solely responsible for the computation of the Doppler broadening.

Choice of cross-section modelling on each range

For both integrals, the vanishing exponential argument implies the definition of a low-energy threshold of $100E_T$. Below this threshold, the Doppler broadening formula (2.7) can be approximated by

$$\begin{aligned}\sigma(E,T) \approx &+ \frac{1}{\sqrt{4\pi}E}\int_{E'=0}^{400E_T} \frac{\sqrt{E'}}{\sqrt{E_T}}\sigma(E',0)\exp\left(-\frac{(\sqrt{E}-\sqrt{E'})^2}{E_T}\right)dE' \\ &- \frac{1}{\sqrt{4\pi}E}\int_{E'=0}^{100E_T} \frac{\sqrt{E'}}{\sqrt{E_T}}\sigma(E',0)\exp\left(-\frac{(\sqrt{E}+\sqrt{E'})^2}{E_T}\right)dE'.\end{aligned} \tag{2.14}$$

The multipole representation is valid at these energies, but replacing the cross-sections by the sum of the pole terms does not allow for an easy computation of the integrals. Moreover, there exists a much simpler representation of the cross-sections below $400E_T$. At low energy, most cross-sections can be approximated by simple $1/\sqrt{E}$ laws. The elastic and total cross-sections require the addition of a constant to be accurately described. Replacing the cross-sections by these simple, yet accurate models, the integrals of expression (2.14) can be computed rather easily. This is done with the use of analytical tools such as the error function. Details can be found in [65].

Above this low-energy threshold of $100E_T$, the second integral is considered null and the Doppler broadening formula is approximated by

$$\sigma(E,T) \approx \frac{1}{\sqrt{4\pi}E} \int_{(\sqrt{E}-10\sqrt{E_T})^2}^{(\sqrt{E}+10\sqrt{E_T})^2} \frac{\sqrt{E'}}{\sqrt{E_T}} \sigma(E',0) \exp\left(-\frac{(\sqrt{E}-\sqrt{E'})^2}{E_T}\right) dE'. \tag{2.15}$$

If we take an energy E in the resolved resonance range, the cross-section profile is well represented by the multipole representation. However, the range of integration can reach outside the resolved resonance range, notably in the unresolved resonance range. The cross-sections do not admit a multipole representation there. This means that even if it is well suited to describe 0K cross-sections up to a certain energy E_{upper}, we can only use it in the integral of expression (2.15) for broadening cross-sections up to

$$(\sqrt{E}+10\sqrt{E_T})^2 < E_{upper} \tag{2.16}$$

$$\sqrt{E} < \sqrt{E_{upper}} - 10\sqrt{E_T} \tag{2.17}$$

$$E < (\sqrt{E_{upper}} - 10\sqrt{E_T})^2. \tag{2.18}$$

For heavy nuclei with a resolved resonance range upper limit around 10^4 eV and a temperature of 300K, this means that we cannot use the multipole representation of the cross-sections on the last 50 eV of this range. For light nuclei with a resolved energy range upper limit around 10^6 eV and temperature of 3000K, this concerns the last 1000 eV. In any case, this upper part of the range typically contains resonances and the multipole representation, which is useful to describe them at 0K, is not sufficient for the Doppler broadening.

To conclude, if we need to broaden cross-sections at energies below $100E_T$, we will use simple power laws and perform the broadening according to expression (2.14). If we need to broaden cross-sections at energies above $100E_T$, we will use the multipole representation of the cross-sections. Finally, we assume that we broaden cross-sections below $\left(\sqrt{E_{upper}}-10\sqrt{E_T}\right)^2$ to avoid the problematic of representing the cross-section in the unresolved resonance range. I will now detail the use of the multipole representation and the mathematical aspects of the computation of (2.15) with it.

2.2 Doppler broadening of the different multipole terms

On the reduced range of energies defined previously, we broaden the cross-sections with formula (2.15). Let us do a change of variable in the integral of this expression. We pose $u_T := \sqrt{E_T}$ and $u = \sqrt{E'}$:

$$\sigma(E,T) \approx \frac{1}{\sqrt{4\pi}E} \int_{\sqrt{E}-10u_T}^{\sqrt{E}+10u_T} \frac{2u^2}{u_T} \sigma(u,0) \exp\left(-\frac{(u-\sqrt{E})^2}{u_T^2}\right) du. \tag{2.19}$$

The multipole representation of the cross-section is a set of analytical formulae that coincides with the 0K cross-sections on the resolved resonance range. However, the formulae

are well defined for any value of u, provided that it is a real number. The idea is to extend the range of the integrals so as to be able to use well known analytical tools to compute them. With the argument on the vanishing exponential, this range can be formally extended to the entire real axis :

$$\sigma\left(E,T\right) \approx \frac{1}{\sqrt{4\pi}E}\int_{-\infty}^{+\infty}\frac{2u^2}{u_T}\sigma\left(u,0\right)\exp\left(-\frac{(u-\sqrt{E})^2}{u_T^2}\right)du. \tag{2.20}$$

One of the particular interest of the multipole representation is that the cross-sections are described by a sum of independent terms. The linearity of the operation on the cross-section of expression (2.20) allows treating the broadening of these terms separately. To each of them will correspond a different type of integral to compute, which I will now describe.

There are various types of terms that occur additively in the multipole representation of the cross-sections. We note a general pole z and one of its residue a. The quantity k is related to the energy E at which we consider the cross-section by $k = \alpha\sqrt{E}$. The definition of α is that of expression (2.24) of Part 1. We note again $u = \sqrt{E}$. The multipole representation of the cross-sections is a sum of terms that can all be split in 4 different categories :

- Simple pole terms of the form $\frac{4\pi}{k^2}\Re\left(\frac{a}{u-z}\right)$.
  These are the main type of terms of the multipole representation. Their Doppler broadening is done with the Faddeeva function.
- Phase-shifted pole terms of the form $\frac{4\pi}{k^2}\Re\left(\frac{a\exp(-2i\phi_l(\beta u)}{u-z}\right)$.
  These appear conjointly with the first type of terms for the elastic and total cross-sections. The treatment of the ϕ_l term necessitates further approximations that I will discuss.
- The so-called potential scattering terms of the form $\frac{4\pi}{k^2}\sin^2(\phi_l(\beta u))$.
  There are only few such terms but they are important nonetheless for the elastic and total cross-sections. We will see that their broadening is rather simple.
- Background terms and other tabulated cross-sections.
  These are not peculiar to the multipole representation and are present for several cross-sections. I will briefly hint at some ideas to treat them.

2.2.1 Simple pole terms

We replace $\sigma(u,0)$ by $\frac{4\pi}{k^2}\Re\left(\frac{a}{u-z}\right)$ in equation (2.20) :

$$\begin{aligned}\sigma\left(E,T\right) &= \frac{1}{\sqrt{4\pi}E}\int_{-\infty}^{+\infty}\frac{2u^2}{u_T}\frac{4\pi}{k^2}\Re\left(\frac{a}{u-z}\right)\exp\left(-\frac{(u-\sqrt{E})^2}{u_T^2}\right)du \\ &= \frac{1}{\sqrt{4\pi}E}\Re\left(a\int_{-\infty}^{+\infty}\frac{2u^2}{u_T}\frac{4\pi}{\alpha^2u^2}\frac{1}{u-z}\exp\left(-\frac{(u-\sqrt{E})^2}{u_T^2}\right)du\right)\end{aligned}$$

$$= \frac{4\pi}{\alpha^2 E}\Re\left(a\frac{1}{\sqrt{\pi}u_T}\int_{-\infty}^{+\infty}\frac{1}{u-z}\exp\left(-\frac{(u-\sqrt{E})^2}{u_T^2}\right)du\right). \tag{2.21}$$

We make a change of variable to get an adimensioned integral. For this purpose, we pose $x = (u - \sqrt{E})/u_T$. Then we have

$$\begin{aligned}\sigma(E,T) &= \frac{4\pi}{\alpha^2 E}\Re\left(a\frac{1}{\sqrt{\pi}u_T}\int_{-\infty}^{+\infty}\frac{1}{u_T x + \sqrt{E} - z}\exp\left(-x^2\right)u_T dx\right)\\ &= \frac{4\pi}{\alpha^2 E}\Re\left(a\frac{1}{\sqrt{\pi}u_T}\int_{-\infty}^{+\infty}\frac{1}{x - \dfrac{z-\sqrt{E}}{u_T}}\exp\left(-x^2\right)dx\right).\end{aligned} \tag{2.22}$$

The integral can be computed with the help of the Faddeeva function. Formally, it is defined by

$$w(z) := \exp(-z^2)\left(1 + \frac{2i}{\sqrt{\pi}}\int_0^z \exp(t^2)dt\right). \tag{2.23}$$

One demonstrable property of the Faddeeva function for a complex number z with positive imaginary part is

$$w(z) = \frac{i}{\pi}\int_{-\infty}^{+\infty}\frac{\exp(-x^2)}{z-x}dx. \tag{2.24}$$

Using this expression, we can further rewrite expression (2.22) :

$$\sigma(E,T) = \begin{cases}\dfrac{4\pi}{\alpha^2 E}\Re\left(a\dfrac{1}{\sqrt{\pi}u_T}(+i\pi)w\left(+\dfrac{z-\sqrt{E}}{u_T}\right)\right) & \text{if } \Im(z) > 0\\ \dfrac{4\pi}{\alpha^2 E}\Re\left(a\dfrac{1}{\sqrt{\pi}u_T}(-i\pi)w\left(-\dfrac{z-\sqrt{E}}{u_T}\right)\right) & \text{if } \Im(z) < 0\end{cases}. \tag{2.25}$$

The case of $\Im(z) = 0$ is not taken into account because poles never have a null imaginary part. The interest of this formulation is that the Faddeeva function is a well known special function that can be evaluated in many different ways [39]. However, its evaluation can be somewhat costly compared to more usual special functions such as the error function.

Interestingly, the integral depends on the pole value but not on the residue. Since the four partial cross-sections that are described with the multipole representation have a common set of poles, we only need one evaluation of the Faddeeva function to compute the Doppler broadening of a pole term for the different concerned cross-sections. An additional step in the form of a multiplication by their corresponding residue, noted a here, must then be performed.

2.2.2 Phase-shifted pole terms

The pole terms with a phase-shift look more complicated at first sight. The form of the energy dependency of ϕ_l depends on the value of l.

For $l > 0$, $\exp(-2i\phi_l(\beta u))$ is numerically very close to 1 on the whole resolved resonance range. We do not need to adopt such a strong approximation but rather, we assume that it does not vary much around the energy E. Rather, we compute the same integral as for the simple pole term case with an additional multiplicative term in front of the integral :

$$\sigma\left(E,T\right) \approx \frac{4\pi}{\alpha^2 E}\Re\left(a\frac{\exp\left(-2i\phi_l(\beta\sqrt{E})\right)}{\sqrt{\pi}u_T}\int_{-\infty}^{+\infty}\frac{1}{x-\dfrac{z-\sqrt{E}}{u_T}}\exp\left(-x^2\right)dx\right) \tag{2.26}$$

$$= \begin{cases} \dfrac{4\pi}{\alpha^2 E}\Re\left(a\dfrac{\exp\left(-2i\phi_l(\beta\sqrt{E})\right)}{\sqrt{\pi}u_T}(+i\pi)w\left(+\dfrac{z-\sqrt{E}}{u_T}\right)\right) & \text{if } \Im(z) > 0 \\ \dfrac{4\pi}{\alpha^2 E}\Re\left(a\dfrac{\exp\left(-2i\phi_l(\beta\sqrt{E})\right)}{\sqrt{\pi}u_T}(-i\pi)w\left(-\dfrac{z-\sqrt{E}}{u_T}\right)\right) & \text{if } \Im(z) < 0 \end{cases} . \tag{2.27}$$

For $l = 0$, the phase-shift $\phi_l(\beta u) = \beta u$ is no longer such that $\exp(-2i\phi_l(\beta u))$ is close to 1. However, its variations are of the order of βu_T, which is somewhat negligible. I have found an analytical treatment of this dependency with the Faddeeva function. We start back from an expression as (2.21) with a phase-shift :

$$\sigma\left(E,T\right) = \frac{4\pi}{\alpha^2 E}\Re\left(a\frac{1}{\sqrt{\pi}u_T}\int_{-\infty}^{+\infty}\frac{\exp(-2i\beta u)}{u-z}\exp\left(-\frac{(u-\sqrt{E})^2}{u_T^2}\right)du\right) \tag{2.28}$$

$$= \frac{4\pi}{\alpha^2 E}\Re\left(a\frac{\exp(-2i\beta\sqrt{E})}{\sqrt{\pi}u_T}\int_{-\infty}^{+\infty}\frac{\exp(-2i\beta u_T x)}{x-\dfrac{z-\sqrt{E}}{u_T}}\exp\left(-x^2\right)dx\right). \tag{2.29}$$

We are going to work a bit on this integral, so we first note $\omega = \beta u_T$ and $y = (z-\sqrt{E})/u_T$. We assume that $\Im(y) > 0$. We define

$$F_y(\omega) = \int_{-\infty}^{+\infty}\frac{\exp(-2i\omega x)}{x-y}\exp\left(-x^2\right)dx. \tag{2.30}$$

We derive in terms of ω :

$$\begin{aligned}\frac{\partial F_y}{\partial \omega} &= \int_{-\infty}^{+\infty}\frac{-2ix\exp(-2i\omega x)}{x-y}\exp\left(-x^2\right)dx \\ &= \int_{-\infty}^{+\infty}\frac{((-2ix+2iy)-2iy)\exp(-2i\omega x)}{x-y}\exp\left(-x^2\right)dx \\ &= -2i\int_{-\infty}^{+\infty}\exp(-2i\omega x)\exp\left(-x^2\right)dx - 2iyF_y(\omega) \\ &= -2i\sqrt{\pi}\exp(-\omega^2) - 2iyF_y(\omega).\end{aligned} \tag{2.31}$$

We can see that F_y verifies a first-order linear differential equation. By the Picard-Lindelöf theorem [66], if we find a solution of this equation that is equal to F_y for any value of ω

then these functions will be equal for all values of ω. We consider the function $G(\omega) := i\pi \exp(-\omega^2) w(y + i\omega)$, where w denotes again the Faddeeva function. Let us show that G is the solution that we are looking for :

$$\frac{\partial G}{\partial \omega} = i\pi \exp(-\omega^2) \left(-2\omega w(y + i\omega) + i w'(y + i\omega)\right). \tag{2.32}$$

The Faddeeva function verifies the following differential equation on the whole complex plan :

$$w'(z) = -2zw(z) + \frac{2i}{\sqrt{\pi}}. \tag{2.33}$$

We can then replace $w'(y + i\omega)$ in expression (2.32) with the help of this relation :

$$\begin{aligned}
\frac{\partial G}{\partial \omega} &= i\pi \exp(-\omega^2) \left(-2\omega w(y + i\omega) - 2i(y + i\omega) w(y - i\omega) + i\frac{2i}{\sqrt{\pi}}\right) && (2.34)\\
&= i\pi \exp(-\omega^2) \left(-2iy w(y + i\omega) - \frac{2}{\sqrt{\pi}}\right) && (2.35)\\
&= -2iy(i\pi \exp(-\omega^2) w(y + i\omega)) - 2i\sqrt{\pi} \exp(-\omega^2) && (2.36)\\
&= -2i\sqrt{\pi} \exp(-\omega^2) - 2iy G(\omega). && (2.37)
\end{aligned}$$

Hence G and F_y verify the exact same differential equation. The final argument relies on their evaluation at $\omega = 0$:

$$\begin{aligned}
F_y(0) &= \int_{-\infty}^{+\infty} \frac{1}{x - y} \exp\left(-x^2\right) dx = i\pi w(y), && (2.38)\\
G(0) &= i\pi w(y). && (2.39)
\end{aligned}$$

Their equality at $\omega = 0$ implies equality for any value of ω. Finally, we have

$$\begin{aligned}
\sigma(E, T) &= \frac{4\pi}{\alpha^2 E} \Re \left(a \frac{\exp(-2i\beta\sqrt{E})}{\sqrt{\pi} u_T} \int_{-\infty}^{+\infty} \frac{\exp(-2i\beta u_T x)}{x - \dfrac{z - \sqrt{E}}{u_T}} \exp\left(-x^2\right) dx \right) && (2.40)\\
&= \frac{4\pi}{\alpha^2 E} \Re \left(a \frac{\exp(-2i\beta\sqrt{E})}{\sqrt{\pi} u_T} i\pi \exp(-(\beta u_T)^2) w\left(\frac{z - \sqrt{E}}{u_T} + i\beta u_T\right)\right). && (2.41)
\end{aligned}$$

I have made no further approximations here. However, we now need to compute a second evaluation of the Faddeeva function for each pole.

We have assumed that $\Im(y) > 0$. There is again a split case on the sign of the imaginary part of the pole. If $\Im(y) < 0$, the whole reasoning presented here is still valid by considering $G = -i\pi \exp(-\omega^2) w(-y - i\omega)$. Then, we compute the broadening of a term with

$$\sigma(E, T) = \frac{4\pi}{\alpha^2 E} \Re \left(a \frac{\exp(-2i\beta\sqrt{E})}{\sqrt{\pi} u_T} (-i\pi) \exp(-(\beta u_T)^2) w\left(-\frac{z - \sqrt{E}}{u_T} - i\beta u_T\right)\right). \tag{2.42}$$

This point appeared to be particularly important for the correct Doppler broadening of the depression part of the elastic cross-sections. As I have mentioned previously, the resonance peaks for this particular cross-section present a strong asymmetry. Not doing the procedure I presented here for the phase-shifted pole terms with $l = 0$ produced major discrepancies with other codes for Doppler broadening. This was up to 50% error for the first resonance of Plutonium 240, which has a significant elastic depression.

2.2.3 Potential scattering

For the elastic and total cross-sections we need to broaden terms of the form

$$\frac{4\pi}{k^2}\sin^2\big(\phi_l(\beta u)\big). \tag{2.43}$$

For $l > 0$, we consider that this term is slowly fluctuating on the Doppler broadening range so that we just compute

$$\begin{aligned}
\sigma\left(E,T\right) &= \frac{1}{\sqrt{4\pi}E}\int_{-\infty}^{+\infty}\frac{2u^2}{u_T}\frac{4\pi}{k^2}\sin^2\big(\phi_l(\beta u)\big)\exp\left(-\frac{(u-\sqrt{E})^2}{u_T^2}\right)du \\
&= \frac{1}{\sqrt{4\pi}E}\int_{-\infty}^{+\infty}\frac{2u^2}{u_T}\frac{4\pi}{\alpha^2u^2}\sin^2\big(\phi_l(\beta u)\big)\exp\left(-\frac{(u-\sqrt{E})^2}{u_T^2}\right)du \\
&= \frac{4\pi}{\alpha^2E}\frac{1}{\sqrt{\pi}u_T}\int_{-\infty}^{+\infty}\sin^2\big(\phi_l(\beta u)\big)\exp\left(-\frac{(u-\sqrt{E})^2}{u_T^2}\right)du \\
&\approx \frac{4\pi}{\alpha^2E}\sin^2\left(\phi_l\big(\beta\sqrt{E}\big)\right).
\end{aligned} \tag{2.44}$$

For $l = 0$, we have $\phi_l(\beta u) = \beta u$. We can give an analytical expression of integral (2.44) :

$$\begin{aligned}
\sigma\left(E,T\right) &= \frac{4\pi}{\alpha^2E}\frac{1}{\sqrt{\pi}u_T}\int_{-\infty}^{+\infty}\sin^2(\beta u)\exp\left(-\frac{(u-\sqrt{E})^2}{u_T^2}\right)du \\
&= \frac{4\pi}{\alpha^2E}\frac{1}{2\sqrt{\pi}u_T}\int_{-\infty}^{+\infty}(1-\cos(2\beta u))\exp\left(-\frac{(u-\sqrt{E})^2}{u_T^2}\right)du \\
&= \frac{2\pi}{\alpha^2E} - \frac{4\pi}{\alpha^2E}\frac{1}{2\sqrt{\pi}u_T}\Re\left(\int_{-\infty}^{+\infty}\exp(2i\beta u)\exp\left(-\frac{(u-\sqrt{E})^2}{u_T^2}\right)du\right) \\
&= \frac{2\pi}{\alpha^2E}\left[1-\exp\big(-(\beta u_T)^2\big)\cos\big(2\beta\sqrt{E}\big)\right].
\end{aligned} \tag{2.45}$$

When u_T goes to 0, we get back the original non broadened potential term.

2.2.4 Other partial cross-sections and background terms

In addition to the resonant terms described in the three previous subsections, there are interpolated values to add to the cross-sections. For the elastic, fission and radiative capture

cross-sections, they correspond to the background terms needed because the cross-sections are not accurately described by the resonance formalisms alone. For the total cross-sections, not only these partial background terms have to be added, but also other tabulated cross-sections not described with resonance parameters have to be taken into account.

All those additional terms are provided as a set of energy points, corresponding values to add, and interpolation schemes to apply to obtain the values in between the tabulated points. The ENDF format proposes mainly 5 interpolation schemes on the interval [14] :

- Histogram. The background is a constant on the interval $\sigma(E) = b$
- Linear-Linear interpolation. The background on the interval is given by $\sigma(E) = aE+b$. From a mathematical standpoint, the histogram scheme is a subset of this case.
- Logarithmic-Linear interpolation. The background on the interval is given by $\log(\sigma(E)) = aE + b$
- Linear-Logarithmic interpolation. The background on the interval is given by $\sigma(E) = a\log(E) + b$
- Logarithmic-Logarithmic interpolation. The background on the interval is given by $\log(\sigma(E)) = a\log(E) + b$

I will not detail here the different way to broaden these terms. I simply wish to say that Linear-Linear and Logarithmic-Linear can be treated analytically with the use of the error function. As far as I know, the last two are not suitable for such a treatment. On one hand, the use of Linear-Logarithmic interpolation is somewhat anecdotal in the latest ENDF libraries. On the other hand, the Logarithmic-Logarithmic interpolation scheme is widely used. As of today, the Doppler broadening of such terms necessitates other approaches such as the sigma-1 method.

This is outside of the scope of my work but I have to mention that such terms appear for many nuclei cross-sections. In addition to the nuclei with no resonance parameters on the resolved resonance range (whose cross-sections have therefore no analytical description), this is one of the biggest limitation to the multipole approach for the Doppler broadening of the cross-sections.

2.3 First numerical applications and results of the Doppler broadening with the multipole representation

In the previous chapter I have presented the reconstruction of the cross-sections with multipole parameters. The very good accuracy of these results, with respect to reconstruction with reference codes such as NJOY, suggests that the multipole parameters I have computed are correct. In this section I will present the Doppler broadening of the cross-sections with these multipole parameters following the procedure I have described in the previous sections.

In contrast to the 0K reconstruction, we do not expect to obtain exactly the same cross-sections as NJOY. The reference codes use the sigma-1 algorithm. The main approximations introduced by this approach are the linearization of the cross-sections on an energy grid. The

precision of the broadening is tightly related to the accuracy of this operation. The default tolerance displayed for this process has been set to 10^{-3}. It is important to keep in mind that it is not a guaranteed point-wise precision criterion. We aim at reconstructing the elastic, radiative capture and fission cross-sections at $5 \cdot 10^{-3}$. The total cross-section that I present is always computed as the sum of these three partial cross-sections and must respect this same criterion.

In all figures of broadened cross-section that I will present, there will be a discontinuity in the error at low energy. This corresponds to a switch between the models that I use for the broadening. Namely, before this discontinuity I approximate the elastic cross-section by the sum of a $1/\sqrt{E}$ law and a constant. This solves the problems of very low energy Doppler broadening at the cost of a numerical fit to obtain this law. This fit is done between the lowest energy of the resolved resonance range and 100 times this energy. This is typically 10^{-5} eV and 10^{-3} eV. It is possible that a more accurate choice should be made by taking into account specificities of the nucleus cross-section profile but I have not done such a study.

I then use the multipole representation with the Faddeeva function to broaden each pole term. This is a straightforward implementation of the results of the previous section. I did not implement myself the computation of the Faddeeva function : I used two separate implementations, one from ABINIT [43] and one from the numerical recipes [41]. Their source code is substantially different but the results I obtained were virtually identical so that I will not comment more on such a choice.

Finally, I have cut the resolved energy range according to the choice of the upper threshold that I have presented in the first section of this chapter. This cut varies for each of the presented nuclei with respect to its resolved resonance range and its mass. It is worth keeping in mind that in any case the broadened cross-sections are displayed on a slightly smaller energy range than the total resolved resonance energy range. The results that I present here are mostly those of the nuclei presented in the 0K case for which I am confident the multipole parameters are correct.

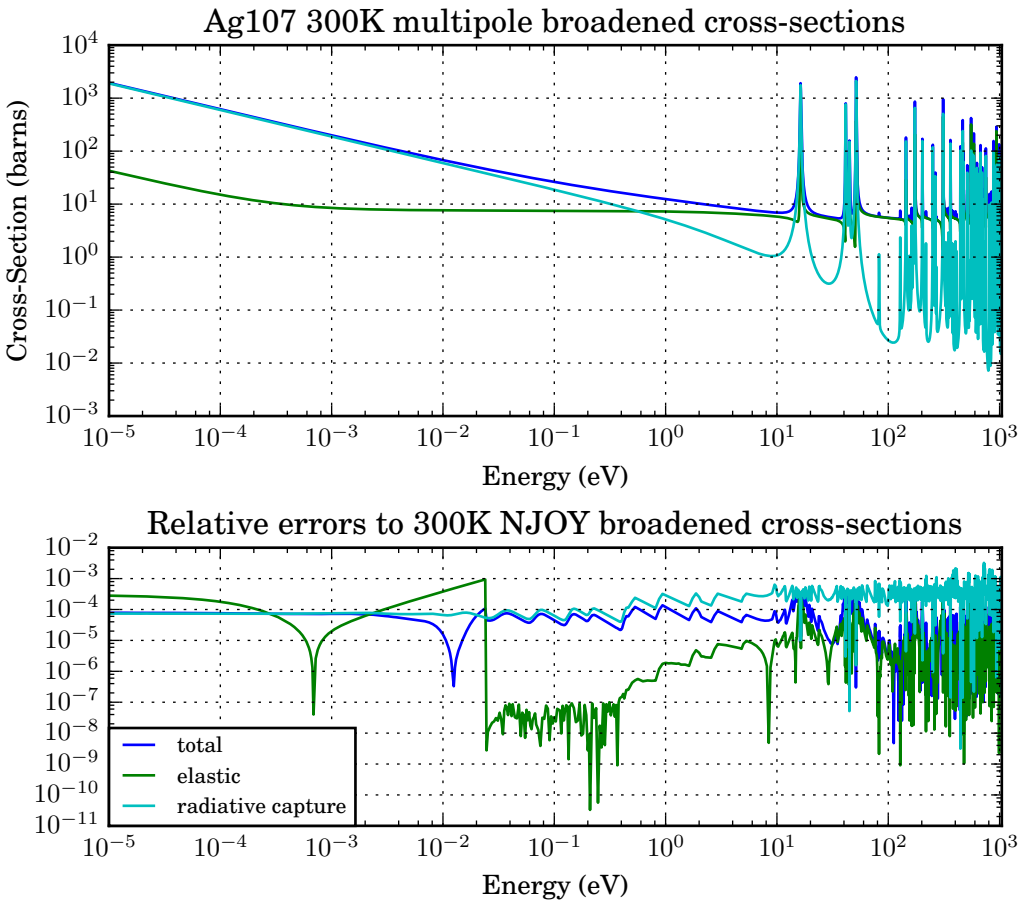

Maximum relative errors

total	elastic	fission	radiative capture
4.19E-04	9.41E-04	-	3.23E-03

Figure 2.1: Silver 107 300K cross-sections broadened with the multipole representation

Figure 2.1 displays the broadened cross-sections of the nucleus Silver 107 at 300K. We can see that the maximum relative errors are below $5 \cdot 10^{-3}$, which I consider satisfactory. Interestingly, the maximum relative error on the elastic cross-section happens at the discontinuity between the low energy approximation and the multipole representation. The fact that the jump at the discontinuity is very high suggests that moving the low-energy threshold to the left, or improving the power law that models the cross-section below this threshold, would be beneficial.

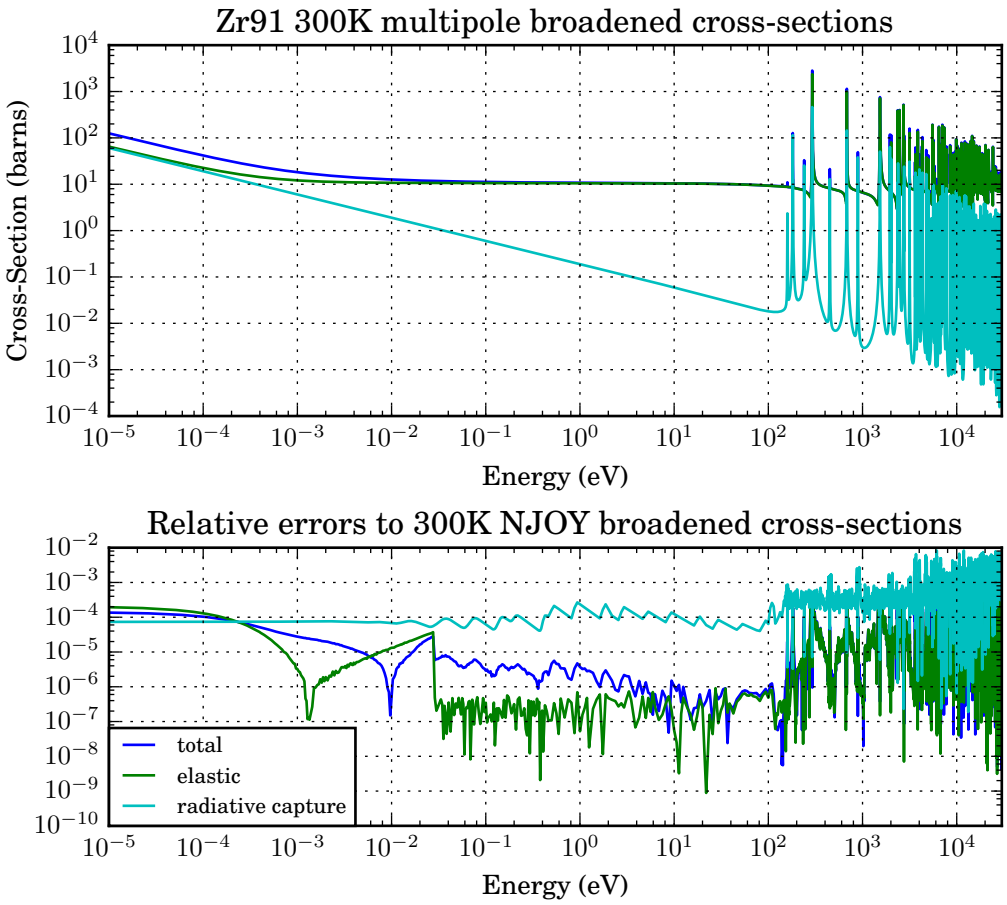

Maximum relative errors

total	elastic	fission	radiative capture
5.94E-04	5.95E-04	-	8.30E-03

Figure 2.2: Zirconium 91 300K cross-sections broadened with the multipole representation

Figure 2.2 displays the broadened cross-sections of the nucleus Zirconium 91 at 300K. The jump at the low energy threshold is smaller here. Moving it to the left again would probably lower it, although it is more acceptable than before and the relative error on the elastic cross-section is not bounded by its choice. I must admit that I have not found a correct heuristic that could apply to all nuclei. I recall that this threshold is computed as $100E_T$. Given that Silver 107 and Zirconium 91 have a similar mass and that we work at the same temperature, it does not seem obvious why the threshold performed well the latter and not the former. A closer look at the resonance structure of the nuclei could help improve this choice. The relative error on the radiative capture reaches higher values close to the percent, which is a bit worrying. We will discuss it shortly there after as it is a recurring hurdle in my comparison to NJOY Doppler broadened cross-sections.

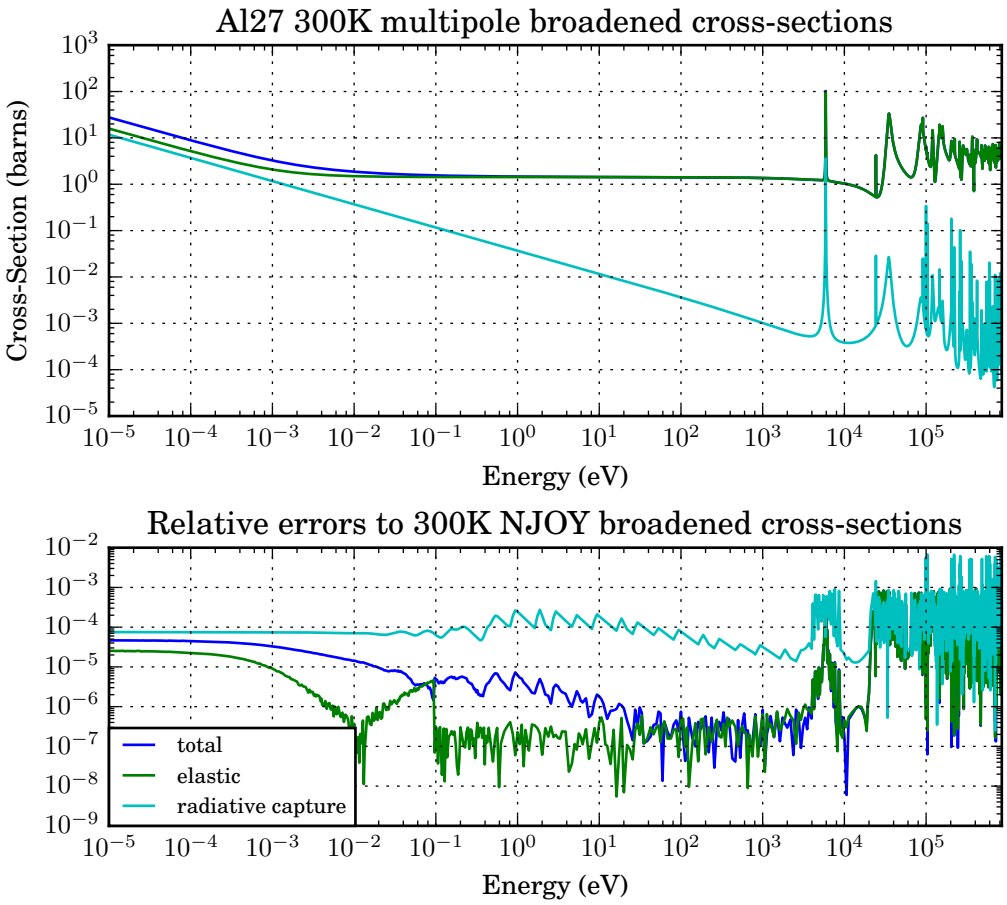

Maximum relative errors

total	elastic	fission	radiative capture
9.36E-04	9.36E-04	-	6.85E-03

Figure 2.3: Aluminium 27 300K cross-sections broadened with the multipole representation

Figure 2.3 displays the broadened cross-sections of the nucleus Aluminium 27 at 300K. The choice of the low energy threshold is relatively good here, too. The situation is also similar to that of the nucleus Zirconium 91 for the elastic cross-section (satisfactory) and the radiative capture (localized error peaks). I zoomed on the cross-section profile where these higher relative errors happen. It revealed that they are not localized on resonance peaks themselves but rather on their sides. Let us recall that the multipole representation of the radiative capture only requires simple pole terms and no phase-shift occur whatsoever. This suggests that this problem cannot be attributed to the added approximation choices on the treatment of these phase-shifts. This encouraged me to try a different implementation of the Faddeeva function but, as I mentioned previously, this did not have any impact of the obtained Doppler broadened cross-section.

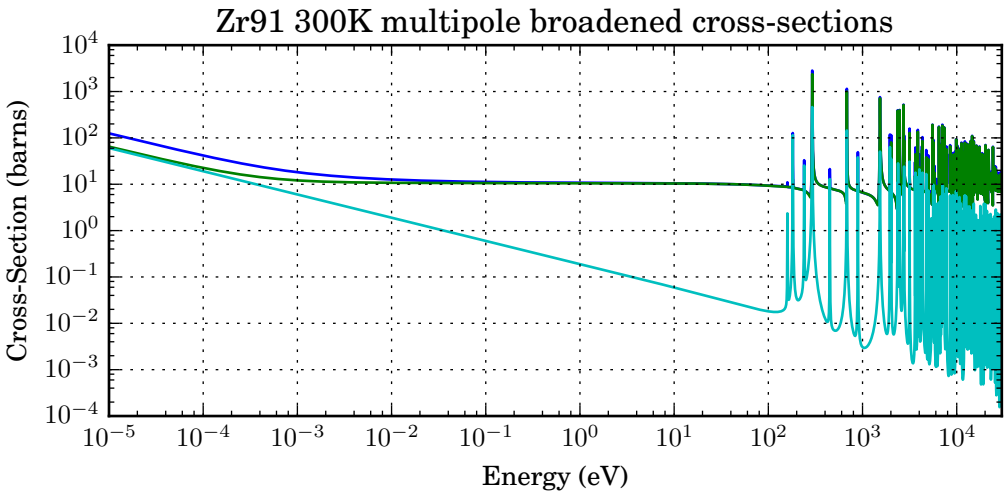

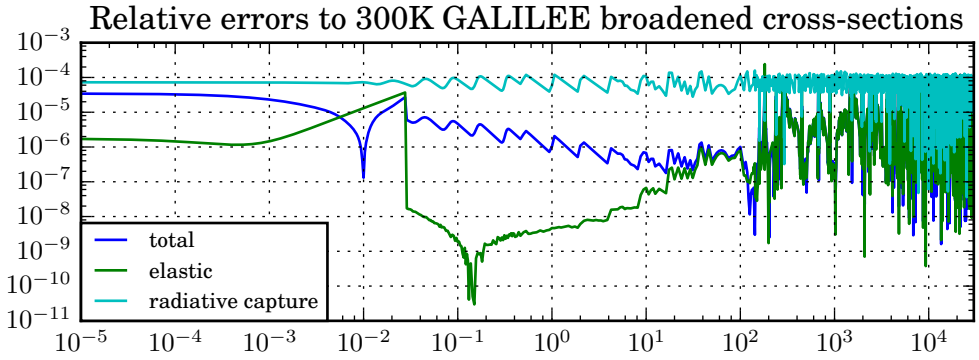

Maximum relative errors

total	elastic	fission	radiative capture
1.19E-04	2.42E-04	-	1.58E-04

Figure 2.4: Zirconium 91 300K cross-sections compared to GALILÉE-1

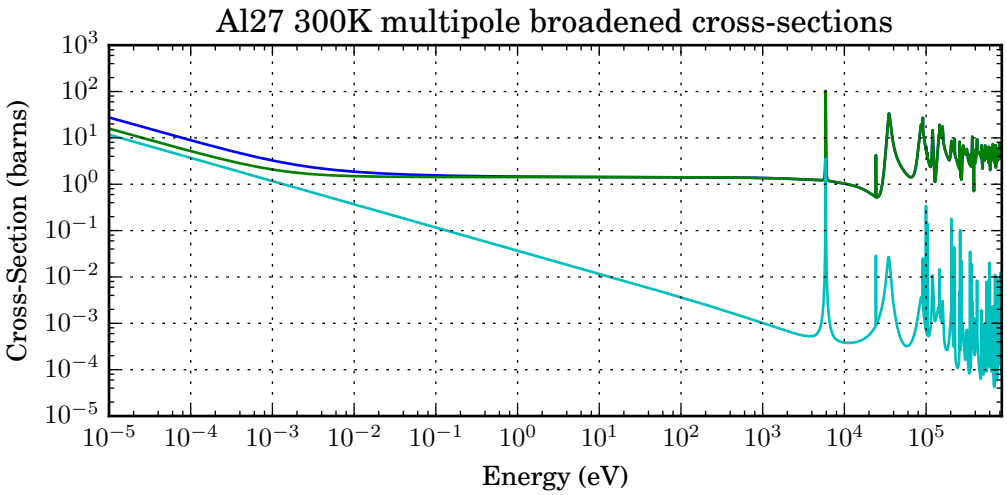

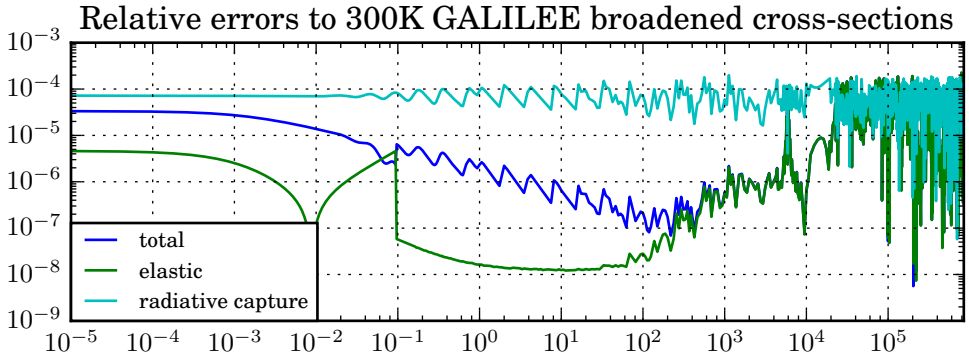

Maximum relative errors

total	elastic	fission	radiative capture
2.25E-04	2.25E-04	-	1.99E-04

Figure 2.5: Aluminium 27 300K cross-sections compared to GALILÉE-1

To investigate this issue I decided to also do a comparison to GALILÉE-1. As NJOY, this code uses the sigma-1 algorithm to broaden the cross-sections. The choice of precision to generate these cross-sections was set to $2 \cdot 10^{-4}$. Figure 2.4 and Figure 2.5 display the relative errors of multipole broadened 300K cross-sections to that of GALILÉE-1 for, respectively, Zirconium 91 and Aluminium 27. We can see that my Doppler broadening is in very good agreement with GALILÉE-1 and that the localized error peaks have disappeared.

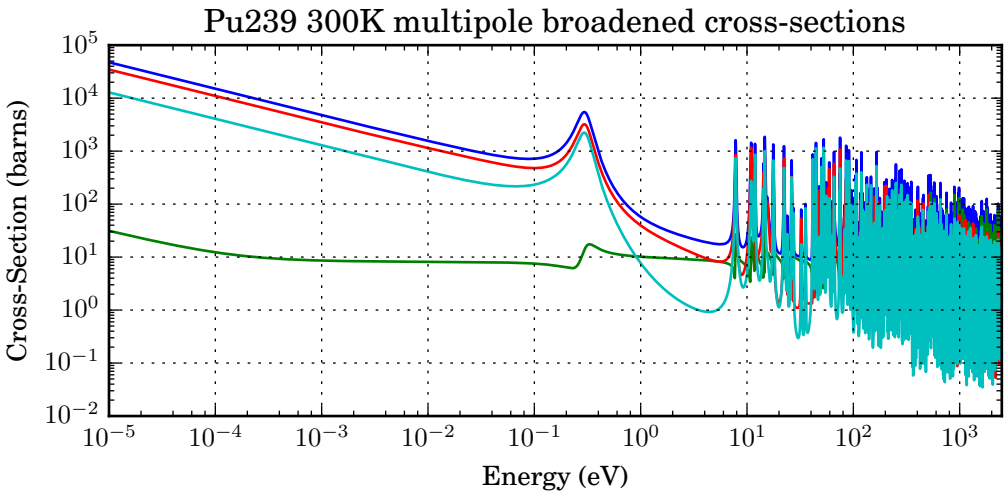

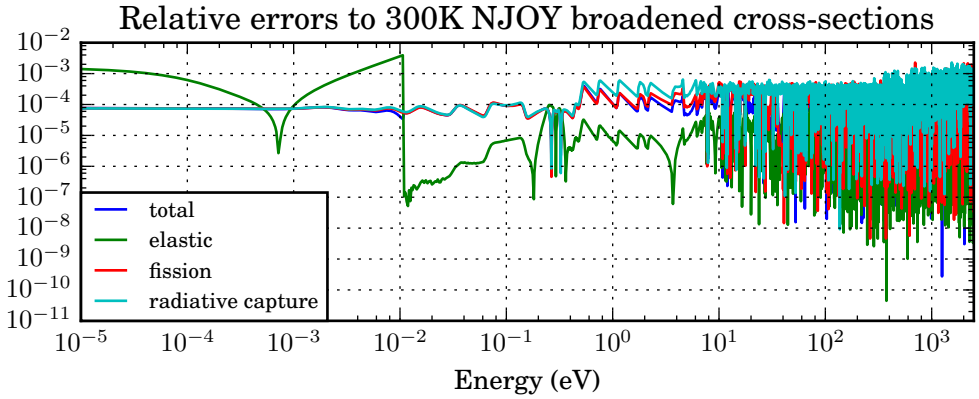

Maximum relative errors

total	elastic	fission	radiative capture
4.73E-04	3.92E-03	2.27E-03	2.28E-03

Figure 2.6: Plutonium 239 300K cross-sections broadened with the multipole representation

Figure 2.6 displays the broadened cross-sections of the nucleus Plutonium 239 at 300K. The choice of the low energy threshold is as bad as for Silver 107. Namely, the relative error on the elastic cross-section is bounded by the value at the gap. This suggests that moving the threshold left would have a positive impact. Nonetheless the broadening is satisfactory with the $5 \cdot 10^{-3}$ accuracy goal. The relative error is even lower than $5 \cdot 10^{-4}$ for the total cross-section.

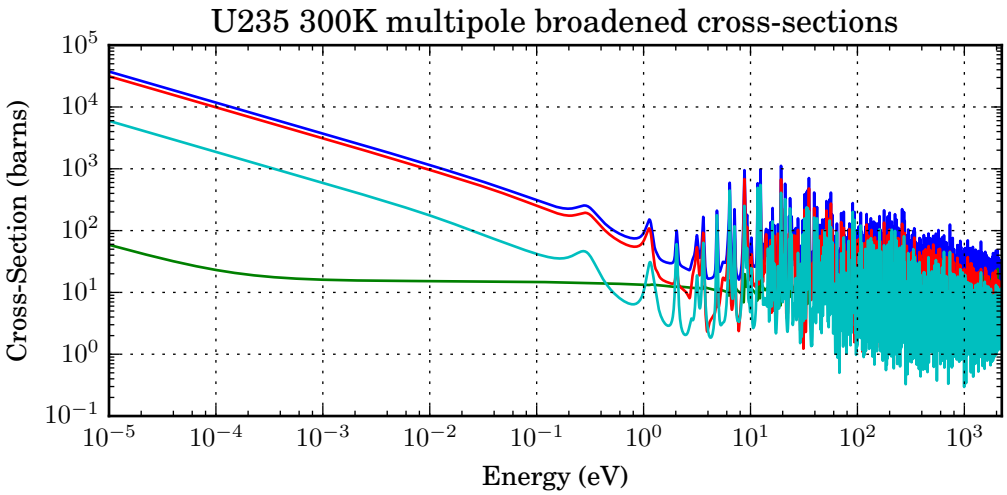

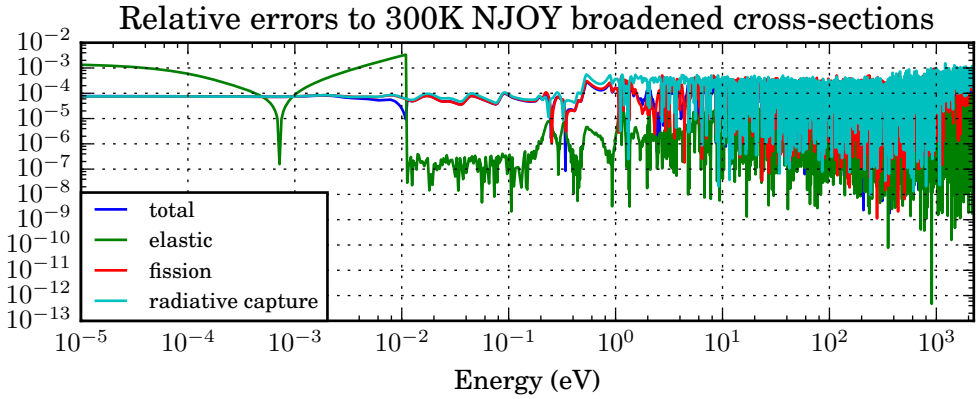

Maximum relative errors

total	elastic	fission	radiative capture
4.48E-04	3.36E-03	1.17E-03	1.53E-03

Figure 2.7: Uranium 235 300K cross-sections broadened with the multipole representation

Figure 2.7 displays the broadened cross-sections of the nucleus Uranium 235 at 300K. The results are comparable to those of Plutonium 239 and are very satisfactory. Consequently, I did not perform a comparison to GALILÉE-1 for these two nuclei.

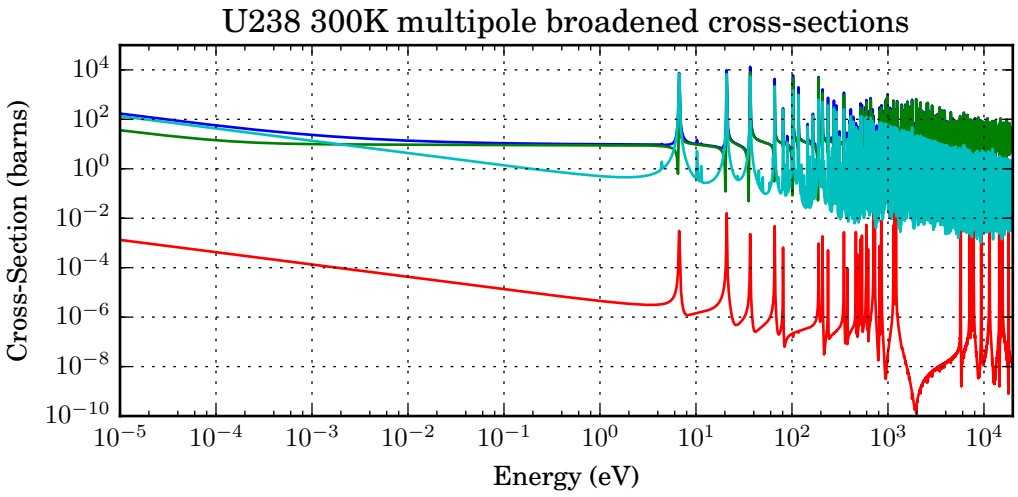

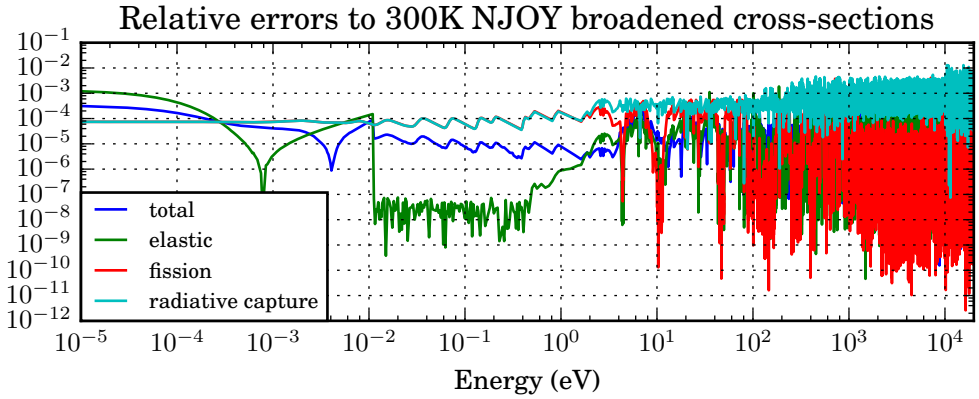

Maximum relative errors

total	elastic	fission	radiative capture
3.71E-03	1.90E-03	4.10E-03	1.30E-02

Figure 2.8: Uranium 238 300K cross-sections broadened with the multipole representation

Figure 2.8 displays the broadened cross-sections of the nucleus Uranium 238 at 300K. The results are significantly less satisfactory than previously and the error on the radiative capture cross-section cannot be ignored. Interestingly, the relative error peaks (that reach the order of the percent) are not particularly on the side of the resonances as they were for Aluminium 27. A closer look reveals that there are non physical results in the NJOY broadening. Comparison studies between NJOY and GALILÉE-1 that already revealed such anomalies can be found in [67]. I must admit that I have not examined each of the hundreds of error peaks on the radiative capture cross-section to prove that they are of this nature, but a look at a random dozen of them showed it to be the case. A more systematic approach to that issue should be done.

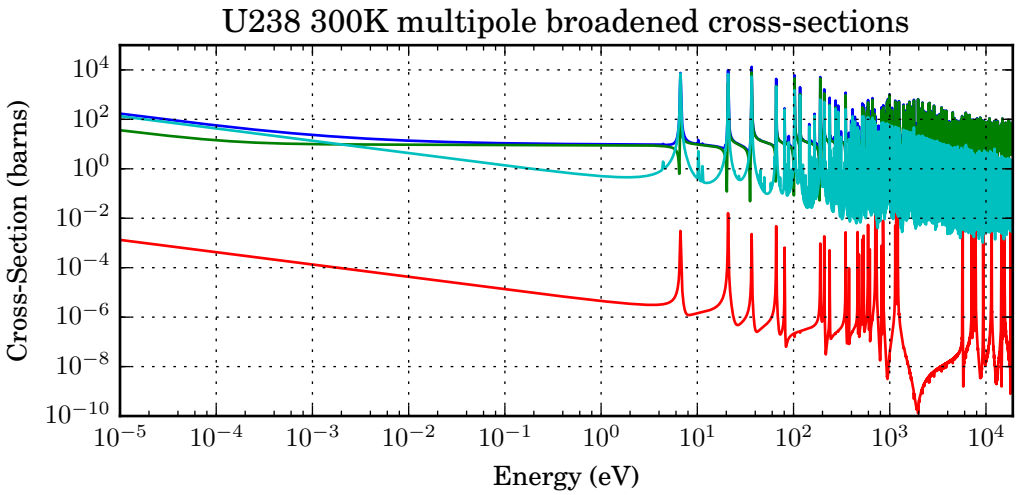

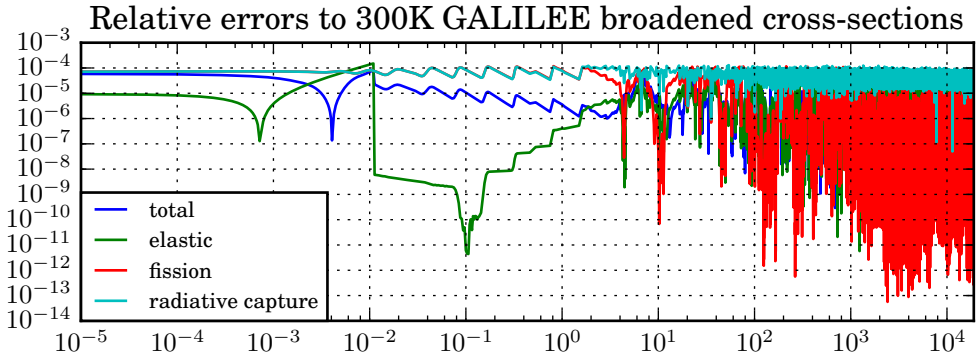

Maximum relative errors

total	elastic	fission	radiative capture
8.44E-05	1.51E-04	1.19E-04	1.29E-04

Figure 2.9: Uranium 238 300K cross-sections compared to GALILÉE-1

I tried to use GALILÉE-1 again to see if such discrepancies disappeared. Figure 2.9 displays the cross-sections broadened with it. The results are very satisfactory as the maximum relative errors are all well below the limit of $5 \cdot 10^{-3}$ I have fixed.

I have not performed a systematic study of the errors to NJOY or GALILÉE-1 but these first results are very encouraging. More work needs to be done particularly concerning the treatment of background piece-wise terms and the upper part of the resolved resonance range.

Conclusions and perspectives

Main results of this thesis

In my thesis, I was concerned with the development of original tools allowing us to find a multipole representation of the resonant cross-sections for neutron-nucleus interactions. Although the investigations carried out in this work were mainly focused on theoretical aspects, the findings of my thesis lend themselves to a forthcoming use for on-the-fly Doppler-broadening schemes in the Monte Carlo particle transport code(s) developed at SERMA. These approaches to the computation of the temperature dependency of the cross-sections allow a considerable breakthrough for the issue of memory occupation and are thus central for the development of next-generation codes oriented towards multi-physics and massively parallel simulations.

The first part of this thesis presented an overview of the context of my work, as well as the tools I would later use in the study of the multipole representation. This included a short description of the R-matrix theory to represent resonant cross-sections, its implementation in the ENDF format, and some mathematical elements pertaining to the study of polynomials and rational functions.

In the second part of this thesis, I have presented a new mathematical investigation of the multipole representation of the cross-sections at zero temperature (0 K) :

- Chapter 1 was devoted to the study of the multipole representation of the Multi-Level Breit-Wigner formalism. I have shown that such a representation is possible with less poles than previously established [19]. Namely, resonances pertaining to a pack of quantum number l can be represented with only $l + 2$ poles (down from $2l + 2$). This is at the cost of l additional poles per pack. This also explained the numerical observation presented in [19] concerning some poles with null residues. These results involved a carefull mathematical study of penetration and level-shift factors in section 2 of this chapter. These will be useful in further investigations of the cross-section formulae properties.
- Chapter 2 was devoted to the study of the multipole representation of the Reich-Moore formalism. Again, I have shown that such a representation is possible with less poles than previously established [18]. Namely, resonances pertaining to a pack of quantum number l can be represented with only 2 poles (down from $2l + 2$). This is at the cost of $2l$ additional poles per pack. For this formalism, the obtention of the multipole

representation requires finding the roots of polynomials of high degree (superior to 50). Hence, reducing the number of poles needed also reduces the complexity of this root-finding step. I have also provided a way of simplifying the matrix treatment involved in the fissile case to get back to the simpler non-fissile case.
- Chapter 3 was aimed at describing some qualitative properties of the poles and their respective contributions to the resulting cross-section profiles. Admittedly this did not provide new results but served as a framework for the applications of the multipole representation.

Finally, in the third part of this thesis, I have presented two relevant applications of the multipole representation :

- Chapter 1 gathered reconstruction results of 0K cross-sections with multipole parameters. These results were achieved by implementing the theoretical formulae presented in Part II of this manuscript into an ad-hoc computer code developed during this thesis. The newly computed multipole parameters were then used to obtain cross-section profiles for several nuclei. These profiles were compared to NJOY reconstructed cross-sections with standard resonance parameters and formulae, used as a reference. The findings for these comparisons were very satisfactory and proved the correctness of both the theoretical results and their code implementation.
- Chapter 2 gathered results concerning the Doppler broadening of the cross-sections with the multipole approach. This first involved describing the theoretical tools used both for a general Doppler broadening and the ones specific to the multipole method. In particular, I provided a few theoretical elements that had not been previously addressed in the literature, and that might improve the accuracy of the Doppler broadening. Then, I performed a comparison of the multipole Doppler broadening with the classical sigma-1 approach implemented in the NJOY code. Some results were immediately satisfactory, whereas a few displayed numerical inaccuracies and required further investigation. For the latter, comparisons were also made with the GALILÉE-1 code, developed at CEA. These new comparisons were entirely satisfactory, which suggests that the few discrepancies of the multipole Doppler broadening with respect to NJOY might actually be due to underlying choices in the implementation of the sigma-1 method in NJOY.

Challenges and perspectives

Short-term goals

The theoretical findings obtained in this thesis might rapidly benefit to the nuclear data treatment code GALILÉE-1. In particular, the following items should be considered :

- the conversion of standard resonance parameters into multipole parameters. Although the application of the theoretical results was rather successful for the cases considered in this manuscript, some nuclei that are reconstructed under the Multi-Level Breit-Wigner formalism still elude a theoretical treatment. This is due to pathological numerical

values of the resonance parameters that are found in the nuclear data libraries (for the JEFF-3.2 library, for instance, this issue concerns a dozen nuclei). Furthermore, I did not provide results for the Single-Level Breit-Wigner formalism, which concerns a comparable number of nuclei. These issues might be solved with relatively small implementation efforts.

- the reconstruction of zero-temperature cross-sections with multipole parameters. The results I have presented in this thesis are quite satisfactory, but concern cross-sections with no background terms. The addition of these terms in the framework of GALILÉE-1 should be quite natural and will allow verifying the reconstruction with multipole parameters of the resonant part of the cross-sections for nuclei whose cross-sections have such background terms.
- the Doppler broadening of cross-sections with multipole parameters. First, the definition of the low-energy threshold for the Doppler broadening still needs adjustments. Second, the background terms needed at zero-temperature must also be Doppler-broadened. An exact treatment could be very difficult for some backgrounds, particularly those described with logarithmic-logarithmic interpolation scheme. An idea to circumvent both issues would be to use a sigma-1 approach for the broadening of both low energy cross-sections and background terms (the resonant part being broadened quite accurately with the help of the Faddeeva function).

Challenges for the use of the multipole representation

Two main concerns about the use of the multipole representation seem to emerge from the considerations presented in this manuscript.

First, concerning the theoretical aspects of the multipole representation, the use of a new formalism is now encouraged for cross-section evaluations. The so-called R-matrix limited format includes interactions with emitted charged particles (proton and alpha particles, for instance) and inelastic scattering. Moreover, the size of the reduced R-matrices involved in the formulae can be significantly larger than for the Reich-Moore formalism (for which these are at most 3 by 3). Concerning the inclusion of new reactions, this poses serious challenges to the derivation of a multipole representation as the cross-sections formulae will not readily be rational functions of the square root of the energy. Concerning the size of the reduced R-matrices, the determinant study I have provided in the Reich-Moore multipole representation chapter might prove useful.

Second, I have not studied the on-the-fly aspect of the temperature dependency calculation in this thesis. I hope that the results presented in the last chapter will be the stepping stone of future work. Admittedly, the requirement of efficiency related to on-the-fly computation are somewhat in opposition to the search for precision I concentrated upon. Hence, significant work will be needed to find a good compromise between accuracy (that I have at least partially achieved) and computing speed. The pseudo-poles method which aims at reducing the number of poles to take into account at a given energy, and its application to on-the-fly Doppler broadening, constitutes a key element of such a work. The windowed multipole method [45] developed at MIT applies these ideas and should serve as a basis for

future studies.

It must also be underlined that the MIT has already proposed a method to circumvent the lack of theoretical foundation for the multipole representation of some cross-sections. As I briefly outlined in the introduction of this manuscript, they have applied vector-fitting techniques to cross-section profiles [47]. This allows treating entire libraries under the multipole representation, at the expense of a more limited accuracy than the one achieved in this thesis.

Perspectives

In addition to the previous elements, I would like to propose a few perspectives that might stem from the present work.

This first concerns the use of the multipole representation as an analytical description of the 0K cross-sections. From its simple form, it is possible to differentiate analytically, and accurately, the cross-sections with respect to their energy dependency. This could allow computing important points of the cross-section profiles such as extrema and inflexion points. These could be used to, for instance, improve the linearization of these profiles. Further, this idea of using analytical formulae could also be applied to the computation of the moments of the cross-sections, that could in turn be used to compute probability tables. Finally, in combination with the Faddeeva function, the multipole representation might also provide an original way of obtaining the derivative of the cross-sections with respect to the temperature for extended sensitivity and perturbation studies.

These personal perspectives and the investigation of the methods concurrently and independently developed at MIT concerning the multipole representation should provide inspiration for future work. The implementation of the results presented in this manuscript in the CEA code GALILÉE-1, and its potential application in TRIPOLI-4®, will serve as a first step in this direction.

List of Figures

List of Tables

Résumé en français

Introduction

Les simulations numériques ont un rôle prépondérant dans la conception et l'utilisation des réacteurs nucléaires. Ces études impliquent de multiples disciplines dont la mécanique, la thermohydraulique et la neutronique. Le Commissariat à l'Énergie atomique (CEA) s'intéresse à ces multiples aspects et, plus particulièrement, le Service d'Études des Réacteurs et de Mathématiques Appliquées (SERMA) se concentre sur le développement de codes simulant le transport des neutrons dans ces réacteurs.

Ce dernier est modélisé par l'équation du transport de Boltzmann dans laquelle les interactions des neutrons avec le milieu qu'ils traversent sont décrites par des quantités appelées sections efficaces macroscopiques. A leur tour, celles-ci dépendent d'une part de la concentration locale des différents noyaux et d'autre part de quantités physiques appelées sections efficaces microscopiques. Ces dernières décrivent des interactions entre un neutron et un noyau individuel immobile. Pour tenir compte de l'agitation thermique des noyaux, les sections microscopiques, qui ne dépendent a priori que de l'énergie du neutron incident, doivent être élargies par effet Doppler et ont donc une dépendance supplémentaire en température.

La nature des simulations par méthode Monte-Carlo implique une description continue en énergie et température de ces sections. Cela correspond aujourd'hui d'un point de vue informatique au stockage en mémoire de tabulations fines des sections efficaces. Celles-ci ont une empreinte mémoire conséquente ce qui limite la précision des études pouvant être effectuées. Une idée consiste à calculer au vol la dépendance en température des sections efficaces, permettant de réduire de manière conséquente leur occupation de la mémoire au prix de calculs supplémentaires durant les simulations.

Différentes méthodes pour effectuer ce calcul au vol peuvent être envisagées. L'idée générale est de ne stocker un profil en énergie des sections qu'à un nombre limité de températures. Cette thèse est consacrée à l'étude de la représentation multipôle des sections à température nulle en vue de son utilisation pour une approche au vol. Ce manuscrit est divisé en trois grandes parties. La première contient différents rappels concernant les modèles physiques décrivant les sections efficaces, une description de leur utilisation dans le format ENDF et une liste de quelques outils mathématiques utiles dans le reste du manuscrit. La seconde partie est consacrée à l'étude théorique de la représentation multipôle dans deux cas d'importance majeure. Enfin, la troisième partie expose quelques applications de la représentation multipôle.

Partie I : Rappels et contexte

Le premier chapitre est un sommaire de la théorie de la matrice R dont sont dérivés les formalismes de représentation des sections efficaces nucléaires. Ce sont des modèles physiques permettant de décrire les sections efficaces nucléaires résonnantes par des formules analytiques et des ensembles de paramètres. L'obtention théorique des deux formalismes principalement utilisés aujourd'hui y est décrite : le formalisme Multi-Level Breit-Wigner et le formalisme Reich-Moore.

Le second chapitre décrit l'utilisation particulière qui est faite des formalismes dans le cadre du format ENDF. Il s'agit de présenter les approximations additionnelles qui sont faites aux deux formalismes précédemment cités. On fixe notamment les formules de sections efficaces et les paramètres de résonance qui sont le point de départ de l'étude théorique faite par la suite.

Le troisième chapitre rassemble les notions mathématiques qui sont utilisées pour l'étude théorique et sa mise en oeuvre informatique. D'une part, il propose quelques rappels concernant les fractions rationnelles et le théorème de décomposition en éléments simples. D'autre part, on y décrit quelques algorithmes de recherche de racines de polynômes, et plus particulièrement celui qui est adopté par la suite.

Partie II : Étude théorique de la représentation multipôle

L'étude théorique repose sur les travaux de R.N. Hwang [17, 18] qui a proposé le premier la représentation multipôle. En utilisant certaines particularités du format ENDF et en étudiant les propriétés mathématiques des formules des sections, on propose une réduction du nombre de pôles nécessaires pour obtenir cette représentation.

Le premier chapitre est consacré à l'étude de la représentation multipôle des sections efficaces reconstruites sous le formalisme Multi-Level Breit-Wigner. Les contributions des résonances peuvent être étudiées séparément ce qui permet d'obtenir de façon relativement simple la représentation recherchée. Un résultat original de cette thèse consiste en une étude mathématique de ces termes de résonance individuels permettant de réduire le nombre de pôles nécessaires par rapport aux résultats précédemment établis. La démonstration implique l'étude des propriétés des facteurs de pénétrabilité et de décalage de niveau. Ceux-ci ont des expressions bien connues et il s'agit ici de mettre en lumière certaines propriétés de divisibilité.

Le deuxième chapitre est consacré à l'étude du formalisme Reich-Moore. Les contributions des résonances ne peuvent pas être étudiées séparément ce qui complique significativement l'obtention de la représentation multipôle. On propose une méthode de résolution du cas des noyaux non-fissiles pour lequel le problème apparaît plus simple de prime abord. Cela nécessite tout de même la résolution de polynômes de très haut degré (supérieur à 50 et pouvant atteindre plusieurs milliers). Un algorithme de Newton-Raphson adapté décrit dans

la partie I de ce manuscrit permet de résoudre ce problème. On propose ensuite une méthode pour obtenir la représentation multipôle pour le cas plus général des noyaux fissiles. Une contribution originale de ces travaux est de ramener l'étude du cas fissile à celui du cas non-fissile dont on a maîtrisé la résolution. Il convient de souligner qu'on obtient ici aussi une réduction théorique du nombre de pôles nécessaire, ce qui a un fort intérêt algorithmique pour la recherche des racines de polynômes.

Cette partie est complétée par un court troisième chapitre décrivant les contributions qualitatives de différent pôles de la représentation multipôle. On y rappelle notamment une classification de ces pôles qui ne dépend pas du formalisme initial à partir duquel ils ont été obtenus.

Partie III : Applications de la représentation multipôle

La partie III rassemble des applications de la représentation multipôle. Il fait suite à une mise en oeuvre informatique personnelle des résultats théoriques qui permet d'obtenir un ensemble de paramètres multipôles à partir de paramètres de résonance classiques.

Le premier chapitre est consacré à la reconstruction des sections efficaces à température nulle par la représentation multipôle. On compare ici la reconstruction des sections par la représentation multipôle (avec l'ensemble de paramètres nouvellement calculés) et la reconstruction des sections par un code de traitement de données nucléaires de référence NJOY. On présente successivement des résultats de reconstruction pour des noyaux dont les sections sont reconstruites sous le formalisme Multi-Level Brei-Wigner, puis sous le formalisme Reich-Moore pour des noyaux non-fissiles et enfin sous le formalisme Reich-Moore pour des noyaux fissiles. Les résultats obtenus et présentés sont excellents et suggèrent donc que les nouveaux paramètres multipôles sont corrects. Ceci inclut notamment certains noyaux fissiles de première importance : Uranium 235, Uranium 238 et Plutonium 239. Cela valide notamment l'approche de résolution des polynômes adoptée, dont le degré atteint plusieurs milliers pour les noyaux précédemment cités. Il convient cependant de souligner certaines limites liées à la mise en oeuvre informatique de la reconstruction. Le traitement de la partie non-analytique des sections efficaces n'est pas pris en compte ce qui limite la comparaison à deux tiers des noyaux reconstruits aux formalismes Multi-Level Breit-Wigner et Reich-Moore. Une inclusion dans un code de traitement de données nucléaires tel GALILÉE-1 (qui effectue déjà de telles opérations) permettrait vraisemblablement de résoudre ce problème.

Le second chapitre rassemble des résultats concernant l'élargissement Doppler des sections efficaces par l'approche multipôle. Dans un premier temps, on décrit des outils théoriques classiques utilisés pour cet élargissement puis ceux spécifiquement associés à la méthode multipôle. Le principe remarquable déjà proposé par le passé est d'utiliser la nature additive de la représentation multipôle et la linéarité de l'opération d'élargissement Doppler par le noyau de Solbrig. On se ramène alors à l'étude de l'élargissement des termes de pôle individuels, effectué notamment par la fonction de Faddeeva. On décrit aussi ici un ajout théorique original qui améliore la précision de l'élargissement des termes de pôle avec décalage de phase. Dans un second temps, une comparaison est faite à l'élargissement Doppler par NJOY qui

utilise la méthode classique sigma-1. Certains des résultats s'avèrent immédiatement satisfaisants tandis que d'autres présentent des imprécisions numériques et suggèrent le besoin d'une étude plus approfondie. Pour une partie de ces derniers, des comparaisons additionnelles et complémentaires au code GALILÉE-1 ont été effectuées. Elles se révèlent être très bonnes ce qui laisse penser que les écarts précédemment observés pourraient être dus à des choix de mise en oeuvre informatique de la méthode sigma-1 dans NJOY.

Conclusion

Ce manuscrit présente des résultats théoriques originaux permettant de réduire le nombre de pôles nécessaires pour obtenir une représentation multipôle des sections efficaces nucléaires résonnantes. Cela concerne les formalismes de représentation Multi-Level Breit-Wigner et Reich-Moore. Des applications numériques confirment la validité de l'étude théorique et la possibilité d'effectuer un élargissement Doppler via cette représentation. La généralisation des résultats théoriques au formalisme "R matrix limited" à venir nécessitera des travaux supplémentaires. Des études plus avant seront aussi requises concernant l'utilisation de la méthode pour des calculs au vol. L'intégration du code de conversion des paramètres de résonance classiques en paramètres multipôles dans un code tel GALILÉE-1 pourrait faciliter de telles études. Enfin, pour une perspective plus personnelle, on pourra envisager d'utiliser la forme analytique relativement simple de la représentation multipôle pour calculer avec précision les dérivées des sections efficaces en énergie et en température.

Bibliography

[1] M. Coste-Delclaux, C. Diop, A. Nicolas, and B. Bonin. Neutronique, 2013.

[2] E.E. Lewis and W.F. Miller. Computational methods of neutron transport, 1984.

[3] I. Lux and L. Koblinger. Monte Carlo particle transport methods: Neutron and photon calculations, 1991.

[4] J. von Neumann and S. Ulam. Monte Carlo method. *National Bureau of Standards Applied Mathematics Series*, 12(1951):36, 1951.

[5] E.P. Wigner. Resonance reactions and anomalous scattering. *Physical Review*, 70(1-2):15, 1946.

[6] E. P. Wigner and L. Eisenbud. Higher angular momenta and long range interaction in resonance reactions. *Phys. Rev.*, 72:29–41, Jul 1947.

[7] A.M. Lane and R.G. Thomas. R-matrix theory of nuclear reactions. *Rev. Mod. Phys.*, 30:257–353, Apr 1958.

[8] D.L. Hill and J.A. Wheeler. Nuclear constitution and the interpretation of fission phenomena. *Phys. Rev.*, 89:1102–1145, Mar 1953.

[9] J.E. Lynn. *The Theory of Neutron Resonance Reactions.* 1968.

[10] F.H. Fröhner. Applied neutron resonance theory. Technical report, Karlsruhe Institute of Technology, Germany, 1978. KFK–2669.

[11] F.H. Fröhner. New techniques for multi-level cross section calculation and fitting. Technical report, Karlsruhe Institute of Technology, Germany, 1980. KFK–3081.

[12] G. Breit and E.P. Wigner. Capture of slow neutrons. *Physical review*, 49(7):519, 1936.

[13] C.W. Reich and M.S. Moore. Multilevel formula for the fission process. *Phys. Rev.*, 111:929–933, Aug 1958.

[14] M.W. Herman and A. Trkov. *ENDF-6, Formats Manual, Data Formats and Procedures for the Evaluated Nuclear Data File ENDF/B-VI and ENDF/B-VII.* Cross Section Evaluation Working Group, Brookhaven National Laboratory, 2012.

[15] G. de Saussure and R.B. Perez. POLLA: A fortran program to convert R-matrix-type multilevel resonance parameters for fissile nuclei into equivalent Kapur-Peierls-type parameters. Technical report, Oak Ridge National Lab., Tenn., 1969.

[16] D.B. Adler and F.T. Adler. Proc. conf. breeding, economics, and safety in large fast reactors. page 695. Argonne National Laboratory, 1963.

[17] R.N. Hwang. A rigorous pole representation of multilevel cross sections and its practical applications. *Nuclear Science and Engineering*, 96(3):192–209, 1987.

[18] R.N. Hwang. An extension of the rigorous pole representation of cross sections for reactor applications. *Nuclear Science and Engineering*, 111(2):113–131, 1992.

[19] C. Jammes and R.N. Hwang. Conversion of Single and Multilevel Breit-Wigner resonance parameters to pole representation parameters. *Nuclear Science and Engineering*, 134(1):37–49, 2000.

[20] B. Forget, S. Xu, and K. Smith. Direct Doppler broadening in monte carlo simulations using the multipole representation. *Annals of Nuclear Energy*, 64:78–85, 2014.

[21] D.E. Cullen and C.R. Weisbin. Exact Doppler broadening of tabulated cross sections. *Nuclear Science and Engineering*, 60(3):199–229, 1976.

[22] F. Mandl. Statistical Physics, Manchester Physics, 2008.

[23] A.W. Solbrig. Doppler broadening of low-energy neutron resonances. *Nuclear Science and Engineering*, 10(2):167–168, 1961.

[24] N. Larson. *Updated Users Guide For SAMMY: Multilevel R-Matrix Fits to Neutron Data Using Bayes Equations*, 2008.

[25] P. Archier, C. De Saint Jean, O. Litaize, G. Noguère, L. Berge, E. Privas, and P. Tamagno. CONRAD evaluation code: development status and perspectives. *Nuclear Data Sheets*, 118:488–490, 2014.

[26] R.E. MacFarlane and D.W. Muir. The NJOY nuclear data processing system Version 91. Technical report, Los Alamos National Laboratory, United States, 1994. LA–12740-M.

[27] D.E. Cullen. *The 1996 ENDF pre-processing codes*, 1996.

[28] M. Coste-Delclaux. *GALILEE: A nuclear data processing system for transport, depletion and shielding codes*. 2008.

[29] G. Ferran, W. Haeck, and M. Gonin. A new method for the Doppler broadening of the Solbrig's kernel using a fourier transform. *Nuclear Science and Engineering*, 179(3):285–301, 2015.

[30] C.L. Dunford and E.T. Bramblett. Doppler broadening of resonance data for Monte Carlo calculations. *AI-CE-MEMO-21*, 1966.

[31] L.C. Leal and R.N. Hwang. Finite difference method for treating the Doppler broadening of neutron cross sections. *Transactions of the American Nuclear Society*, 55, 1987.

[32] J. Leppänen. Two practical methods for unionized energy grid construction in continuous-energy monte carlo neutron transport calculation. *Annals of Nuclear Energy*, 36(7):878–885, 2009.

[33] P.K. Romano and B. Forget. The OpenMC monte carlo particle transport code. *Annals of Nuclear Energy*, 51:274–281, 2013.

[34] Y. Wang, E. Brun, F. Malvagi, and C. Calvin. Competing energy lookup algorithms in Monte Carlo neutron transport calculations and their optimization on CPU and Intel MIC architectures. *Journal of Computational Science*, 20:94–102, 2017.

[35] G. Yesilyurt, W.R. Martin, and F.B. Brown. On-the-fly Doppler broadening for monte carlo codes. *Nuclear Science and Engineering*, 171(3):239–257, 2012.

[36] T. Viitanen and J. Leppänen. Explicit treatment of thermal motion in continuous energy monte carlo tracking routines. *Nuclear Science and Engineering*, 171(2):165–173, 2012.

[37] T. Viitanen and J. Leppänen. Optimizing the implementation of the explicit treatment of thermal motion - How fast can it get? *Proc. M&C 2013*, pages 5–9, 2013.

[38] P. Ducru, C. Josey, K. Dibert, V. Sobes, B. Forget, and K. Smith. Kernel reconstruction methods for Doppler broadening—temperature interpolation by linear combination of reference cross sections at optimally chosen temperatures. *Journal of Computational Physics*, 335:535–557, 2017.

[39] V.N. Faddeyeva and N.M. Terentev. *Tables of the probability integral for complex argument*. Pergamon Press, 1961.

[40] M. Abramowitz and I.A. Stegun. *Handbook of mathematical functions: with formulas, graphs, and mathematical tables*, volume 55. Courier Corporation, 1965.

[41] B.P. Flannery, W.H. Press, S.A. Teukolsky, and W. Vetterling. Numerical recipes in C. *Press Syndicate of the University of Cambridge, New York*, 24:78, 1992.

[42] A. Oeftiger, S. Hegglin, E. McIntosh, L. Moneta, R. De Maria, L. Deniau, K. Li, and A. Aviral. Review of CPU and GPU Faddeeva implementations. Technical report, CERN, 2016.

[43] X. Gonze, JM. Beuken, R. Caracas, F. Detraux, M. Fuchs, GM. Rignanese, L. Sindic, M. Verstraete, G. Zerah, F. Jollet, et al. First-principles computation of material properties : the ABINIT software project. *Computational Materials Science*, 25(3):478–492, 2002.

[44] C. Josey, B. Forget, and K. Smith. Windowed multipole sensitivity to target accuracy of the optimization procedure: Physor2014. *Journal of Nuclear Science and Technology*, 52(7-8):987–992, 2015.

[45] C. Josey, P. Ducru, B. Forget, and K. Smith. Windowed multipole for cross section Doppler broadening. *Journal of Computational Physics*, 307:715–727, 2016.

[46] X. Peng, P. Ducru, S. Liu, B. Forget, J. Liang, and K. Smith. Converting point-wise nuclear cross sections to pole representation using regularized vector fitting. *Computer Physics Communications*, 224:52–62, 2018.

[47] S. Liu, X. Peng, C. Josey, J. Liang, B. Forget, K. Smith, and K. Wang. Generation of the windowed multipole resonance data using vector fitting technique. *Annals of Nuclear Energy*, 112:30–41, 2018.

[48] J. Liang, X. Peng, S. Liu, C. Josey, B. Forget, and K. Smith. Processing of a comprehensive windowed multipole library via vector fitting. PHYSOR, 2018.

[49] TRIPOLI-4 Project Team, E. Brun, F. Damian, C.M. Diop, E. Dumonteil, FX. Hugot, C. Jouanne, Y.K. Lee, F. Malvagi, A. Mazzolo, O. Petit, J.C. Trama, T. Visonneau, and A. Zoia. TRIPOLI-4®, CEA, EDF and AREVA Reference Monte Carlo Code. In *SNA + MC 2013 - Joint International Conference on Supercomputing in Nuclear Applications + Monte Carlo*, page 06023, 2014.

[50] E. Brun, S. Chauveau, and F. Malvagi. PATMOS : A prototype monte carlo transport code to test high performance architectures. In *Proceedings of International Conference on Mathematics & Computational Methods Applied to Nuclear Science & Engineering, Jeju, Korea*, 2017.

[51] Monte Carlo Team, MCNP - A general purpose Monte Carlo N-Particle transport code, version 5. Technical report, LA-UR-03 1987, Los Alamos National Laboratory, 2003.

[52] Ghislain Ferran. *Nouvelles méthodes numériques pour le traitement des sections efficaces nucléaires*. PhD thesis, Palaiseau, Ecole polytechnique, 2014.

[53] P. Descouvemont and D. Baye. The R-matrix theory. *Reports on progress in physics*, 73(3):036301, 2010.

[54] J. Lelong-Ferrand. *Cours de mathématiques*. Dunod, 1971.

[55] G. Golub and F. Uhlig. The QR algorithm: 50 years later its genesis by John Francis and Vera Kublanovskaya and subsequent developments. *IMA Journal of Numerical Analysis*, 29(3):467–485, 2009.

[56] J. Francis. The QR transformation a unitary analogue to the LR transformation—part 1. *The Computer Journal*, 4(3):265–271, 1961.

[57] J. Francis. The QR transformation—part 2. *The Computer Journal*, 4(4):332–345, 1962.

[58] E. Durand. Solutions numériques des équations algébriques, 1960.

[59] I.O. Kerner. Ein gesamtschrittverfahren zur berechnung der nullstellen von polynomen. *Numerische Mathematik*, 8(3):290–294, 1966.

[60] T.J. Ypma. Historical development of the Newton–Raphson method. *SIAM review*, 37(4):531–551, 1995.

[61] H.J. Maehly. Zur iterativen auflösung algebraischer gleichungen. *Zeitschrift für angewandte Mathematik und Physik ZAMP*, 5(3):260–263, 1954.

[62] F.L. Bauer and J. Stoer. Algorithm 105 : Newton-Maehly. *Communications of the ACM*, 5(7):387–388, 1962.

[63] W. Kahan. Pracniques: further remarks on reducing truncation errors. *Communications of the ACM*, 8(1):40, 1965.

[64] A. Koning, E. Bauge, C. Dean, E. Dupont, U. Fischer, R. Forrest, R. Jacqmin, H. Leeb, M. Kellett, R. Mills, et al. Status of the JEFF nuclear data library. *J. Korean Phys. Soc*, 59(2):1057–1062, 2011.

[65] L.C. Leal. Brief review of the R-Matrix theory. *MIT OpenCourseWare*, 2010.

[66] E.A. Coddington and N. Levinson. *Theory of ordinary differential equations*. Tata McGraw-Hill Education, 1955.

[67] M. Coste-Delclaux, C. Jouanne, F. Moreau, C. Mounier, T. Visonneau, and F. Malouch. Current status of the verification and processing system GALILÉE-1 for Evaluated Data. In *EPJ Web of Conferences*, volume 211. EDP Sciences, 2019.

université PARIS-SACLAY

ECOLE DOCTORALE N°576
Particules, Hadrons, Énérgie, Noyau, Instrumentation, Image, Cosmos et Simulation (PHENIICS)

Titre : Méthode multipôle pour l'évaluation au vol de la dépendance en température des sections efficaces nucléaires

Mots clés : section efficace, multipôle, élargissement Doppler

Résumé : Dans le contexte de la physique des réacteurs nucléaires, la connaissance des sections efficaces décrivant les interactions des neutrons avec le milieu traversé est primordiale. Ces sections dépendent à la fois de l'énergie du neutron et de la température du milieu. Concernant la dépendance en énergie, les profils des sections efficaces présentent en général de nombreuses résonances résolues sur le domaine d'énergie d'intérêt. La représentation multipôle est une description additive et exacte des sections efficaces résonantes à température nulle. La dépendance en température est ensuite calculée par une opération linéaire faisant intervenir des outils analytiques tels que la fonction de Faddeeva.
Cette thèse se concentre sur les aspects théoriques de la représentation multipôle ainsi que sur deux applications principales. Concernant l'étude théorique, on démontre que le nombre de pôles nécessaires pour la représentation des sections aux formalismes Multi-Level Breit-Wigner et Reich-Moore peut être réduit par rapport aux résultats précédemment établis en littérature. Cela nécessite notamment une étude formelle de fractions rationnelles et la résolution de polynômes de très haut degré (supérieur à 50 et pouvant atteindre plusieurs milliers).
Concernant les applications, la première se concentre sur la mise en œuvre informatique des éléments théoriques originaux trouvés durant les travaux de thèse. Une reconstruction des sections à température nulle et une comparaison à des résultats de référence est présentée afin de démontrer la pertinence et l'exactitude des paramètres multipôles nouvellement calculés. Les résultats sont extrêmement satisfaisants quoique limités par nature aux sections résonantes. La seconde application est l'utilisation de la représentation multipôle pour l'élargissement Doppler des sections efficaces : une comparaison à des sections élargies par la méthode classique (dite « sigma-1 ») est présentée. Les résultats de cette comparaison sont aussi très satisfaisants mais des efforts sont encore nécessaires aux frontières du domaine d'énergie des résonances résolues.
Dans le cadre des simulations de transport par méthode de Monte-Carlo, la linéarité de l'élargissement et la nature additive de la représentation multipôle suggèrent la possibilité de calculer la section efficace « au vol » à chaque collision du neutron, ce qui permettrait de réduire très fortement l'encombrement mémoire par rapport à l'approche actuelle (tabulation de ces profils à de multiples températures).

Title : The multipole method for the on-the-fly computation of the temperature dependency of nuclear cross-sections

Keywords : cross-section, multipole, Doppler broadening

Abstract : In nuclear reactor physics, the knowledge of the cross-sections describing interactions of neutrons with the medium through which they diffuse is of paramount importance. These sections depend both on the energy of the neutron and the temperature of the medium. Concerning the energy dependency, cross-section profiles display, in general, numerous resolved resonances on the energy range of interest. The multipole representation is an additive and exact description of the resonant cross-sections at zero temperature. The temperature dependency is then computed by a linear operation using analytical tools such as the Faddeeva function.
This thesis is devoted to the theoretical aspects of the multipole representation as well as two main applications. Concerning the theoretical study, we show that the number of required poles for the representation of sections under the Multi-Level Breit-Wigner and Reich-Moore formalisms can be reduced compared to previously established results. This requires, notably, a formal study of rational functions and solving polynomials of very high degree (greater than 50 and potentially reaching the thousands).
Concerning the applications, the first one focuses on the implementation of the original theoretical elements found during the thesis. A reconstruction of sections at zero temperature and a comparison with reference results is proposed in order to prove the relevance and correctness of the newly computed multipole parameters. The results are extremely satisfying albeit limited by nature to resonant cross-sections. The second application consists in using the multipole representation for the Doppler broadening of cross-sections : a comparison to sections broadened with the usual method (so-called « sigma-1 ») is presented. The results of this comparison are also very satisfying although some efforts are still necessary on the border of the energy domain of resolved resonances.
In the context of Monte Carlo transport simulations, the linearity of the Doppler broadening and the additive nature of the multipole representation suggest that it is possible to compute cross-sections « on-the-fly », at each neutron collision, which would allow strongly reducing the memory footprint compared to current approaches (tabulation in energy of the cross-section profiles at multiple temperatures).

Université Paris-Saclay
Espace Technologique / Immeuble Discovery
Route de l'Orme aux Merisiers RD 128 / 91190 Saint-Aubin, France